PUBLISHED VERSION

G. Aad … P. Jackson … L. Lee … A. Petridis … N. Soni ... M. White ... et al. (ATLAS Collaboration)
Measurements of normalized differential cross sections for $t\bar{t}$ production in pp collisions at $\sqrt{s}$ = 7TeV using the ATLAS detector
Physical Review D - Particles, Fields, Gravitation, and Cosmology, 2014; 90(7):072004-1-072004-42

Originally published at:
http://doi.org/10.1103/PhysRevD.90.072004

Measurements of normalized differential cross sections for $t\bar{t}$ production in pp collisions at $\sqrt{(s)} = 7$ TeV using the ATLAS detector

G. Aad *et al.*[*]
(ATLAS Collaboration)

(Received 1 July 2014; revised manuscript received 3 September 2014; published 13 October 2014)

Measurements of normalized differential cross sections for top-quark pair production are presented as a function of the top-quark transverse momentum, and of the mass, transverse momentum, and rapidity of the $t\bar{t}$ system, in proton–proton collisions at a center-of-mass energy of $\sqrt{s} = 7$ TeV. The data set corresponds to an integrated luminosity of 4.6 fb^{-1}, recorded in 2011 with the ATLAS detector at the CERN Large Hadron Collider. Events are selected in the lepton + jets channel, requiring exactly one lepton and at least four jets with at least one of the jets tagged as originating from a b-quark. The measured spectra are corrected for detector efficiency and resolution effects and are compared to several Monte Carlo simulations and theory calculations. The results are in fair agreement with the predictions in a wide kinematic range. Nevertheless, data distributions are softer than predicted for higher values of the mass of the $t\bar{t}$ system and of the top-quark transverse momentum. The measurements can also discriminate among different sets of parton distribution functions.

DOI: 10.1103/PhysRevD.90.072004 PACS numbers: 13.85.-t, 12.38.Qk, 14.65.Ha

I. INTRODUCTION

Top-quark measurements have entered a high-precision era at the Large Hadron Collider (LHC) where the cross sections for single top-quark and top-quark pair ($t\bar{t}$) production at a center-of-mass energy $\sqrt{s} = 7$ TeV are factors of 40 and 20 higher than at the Tevatron. The large number of $t\bar{t}$ events makes it possible to measure precisely the $t\bar{t}$ production cross sections differentially, providing precision tests of current predictions based on perturbative quantum chromodynamics (QCD). The top quark plays an important role in many theories beyond the Standard Model (SM) [1] and differential measurements have been proposed to be sensitive to new-physics effects [2].

The inclusive cross section for $t\bar{t}$ production ($\sigma_{t\bar{t}}$) in proton–proton (pp) collisions at a center-of-mass energy $\sqrt{s} = 7$ TeV has been measured by both the ATLAS and CMS experiments with increasing precision in a variety of channels [3–9]. The CMS Collaboration has published [10] differential cross sections using the full data set collected in 2011 at $\sqrt{s} = 7$ TeV and corresponding to an integrated luminosity of 5.0 fb^{-1}. The ATLAS Collaboration has published [11] the differential cross sections as a function of the mass ($m_{t\bar{t}}$), the transverse momentum ($p_{\mathrm{T}}^{t\bar{t}}$), and the rapidity ($y_{t\bar{t}}$) of the $t\bar{t}$ system with a subset of the data collected in 2011 at $\sqrt{s} = 7$ TeV corresponding to an integrated luminosity of 2.05 fb^{-1}. The measurements shown here improve the statistical precision of the previous ATLAS results by including the full 2011 data set (4.6 fb^{-1}). Furthermore, improved reconstruction algorithms and calibrations are used, thereby significantly reducing the systematic uncertainties affecting the measurements. The rapidity distribution is symmetrized and presented as $|y_{t\bar{t}}|$ and in addition to the variables previously shown, this paper also presents a measurement of the cross section as a function of the top-quark transverse momentum (p_{T}^{t}).

In the SM, the top quark decays almost exclusively into a W boson and a b-quark. The signature of a $t\bar{t}$ decay is therefore determined by the W boson decay modes. This analysis makes use of the lepton + jets decay mode, where one W boson decays into an electron or muon and a neutrino and the other W boson decays into a pair of quarks, with the two decay modes referred to as the e + jets and μ + jets channel, respectively. Events in which the W boson decays to an electron or muon through a τ decay are also included.

Kinematic reconstruction of the $t\bar{t}$ system is performed using a likelihood fit. The results are unfolded to the parton level after QCD radiation, and the normalized differential cross-section measurements are compared to the predictions of Monte Carlo (MC) generators and next-to-leading-order (NLO) QCD calculations. The p_{T}^{t}, $m_{t\bar{t}}$, and $p_{\mathrm{T}}^{t\bar{t}}$ spectra are also compared to NLO QCD calculations including next-to-next-to-leading-logarithmic (NNLL) effects, namely Ref. [12] for p_{T}^{t}, Ref. [13] for $m_{t\bar{t}}$, and Ref. [14,15] for $p_{\mathrm{T}}^{t\bar{t}}$.

The paper is organized as follows. Section II briefly describes the ATLAS detector, while Secs. III and IV describe the data and simulation samples used in the measurements. The reconstruction of physics objects, the event selection, and the kinematic reconstruction of the events are explained in Sec. V. Section VI discusses the background processes affecting these measurements. Event yields for both the signal and background samples, as well

[*] Full author list given at the end of the article.

as distributions of measured quantities before unfolding, are shown in Sec. VII. The measurements of the cross sections, including the unfolding and combination procedures, are described in Sec. VIII. Statistical and systematic uncertainties are discussed in Sec. IX. The results are presented in Sec. X and the comparison with theoretical predictions is discussed in Sec. XI.

II. THE ATLAS DETECTOR

The ATLAS detector [16] is cylindrically symmetric and has a barrel and two endcaps [17]. The inner detector (ID) is nearest to the interaction point and contains three subsystems providing high-precision track reconstruction: a silicon pixel detector (innermost), a silicon microstrip detector, and a transition radiation tracker (outermost), which also helps to discriminate electrons from hadrons. The ID covers a range of $|\eta| < 2.5$. It is surrounded by a superconducting solenoid, which produces a 2 T axial field within the ID. Liquid argon (LAr) sampling electromagnetic (EM) calorimeters cover $|\eta| < 4.9$, while the hadronic calorimeter uses scintillator tiles within $|\eta| < 1.7$ and LAr within $1.7 < |\eta| < 4.9$. The outermost detector is the muon spectrometer, which employs three sets of air-core toroidal magnets with eight coils each and is composed of three layers of chambers for triggering ($|\eta| < 2.4$) and precision track measurements ($|\eta| < 2.7$).

The trigger is divided into three levels referred to as level 1 (L1), level 2 (L2), and event filter (EF). The L1 trigger uses custom-made hardware and low-granularity detector data. The L2 and EF triggers are implemented as software algorithms. The L2 trigger has access to the full detector granularity, but only retrieves data for regions of the detector identified by L1 as containing interesting objects, while the EF system utilizes the full detector readout to reconstruct an event.

III. DATA SAMPLE

The data set used in this analysis was recorded during pp collisions at $\sqrt{s} = 7$ TeV in 2011. It only includes data recorded with stable beam conditions and with all relevant subdetector systems operational. The number of pp collisions per bunch crossing significantly increased during the data taking, reaching mean values up to 20 in the last part of the 2011 LHC run.

Single-muon and single-electron triggers were used to select the data. The single-muon trigger required at least one muon with transverse momentum (p_{T}) of at least 18 GeV and the single-electron trigger required at least one electron with a p_{T} threshold of either 20 or 22 GeV. The p_{T} threshold increased during data taking to cope with increased luminosity. With these requirements the total integrated luminosity of the data set is 4.6 fb^{-1} with an uncertainty of 1.8% [18].

IV. SIMULATION

Simulated $t\bar{t}$ events with up to five additional light partons were generated using ALPGEN [19] (v2.13) with the leading-order (LO) CTEQ6L1 [20] parton distribution functions (PDF). HERWIG [21] (v6.520) was used for parton showering and hadronization and JIMMY [22] (v4.31) was used for the modeling of multiple parton interactions. The ATLAS AUET2 tune [23] was used for the simulation of the underlying event. The ALPGEN generator uses tree-level matrix elements with a fixed number of partons in the final state, with the MLM matching scheme [24] to avoid double counting between partons created in the hard process or in the subsequent parton shower.

Two other generators, which make use of NLO QCD matrix elements with the NLO CT10 PDF [25], are used for comparisons with the final measured results, namely MC@NLO [26] (v4.01) and POWHEG [27] (POWHEG - hvq, patch4). Both are interfaced to HERWIG and JIMMY with the ATLAS AUET2 tune. The MC@NLO generator is also used for the evaluation of systematic uncertainties along with additional generators and simulation samples discussed in Sec. IX B. As an additional comparison the POWHEG generator is also interfaced to PYTHIA 6 [28], with the Perugia 2011C tune [29].

All of the simulation samples were generated assuming a top-quark mass, m_t, equal to 172.5 GeV. The $t\bar{t}$ samples are normalized to a cross section of $\sigma_{t\bar{t}} = 167^{+17}_{-18}$ pb, obtained from approximate NNLO QCD calculations [30] for pp collisions at $\sqrt{s} = 7$ TeV, again using $m_t = 172.5$ GeV. During the completion of this analysis, a calculation of the inclusive cross section to full NNLO precision with additional NNLL corrections was published [31] and gives a cross section of $\sigma_{t\bar{t}} = 177.3^{+11.5}_{-12.0}$ pb at $\sqrt{s} = 7$ TeV for the same top-quark mass. This change would only affect the results presented here by increasing the normalization of the dilepton $t\bar{t}$ background. The corresponding effect on the final results would be at the subpercent level and is covered by the assigned systematic uncertainties.

Single top-quark events produced via electroweak interactions were simulated using the ACERMC generator [32] (v3.8) interfaced to PYTHIA 6 with the MRSTMCal PDF [33] for the t-channel process and MC@NLO for the s-channel and Wt-channel processes. The production of W/Z bosons in association with jets ($W+$ jets or $Z+$ jets) was simulated using ALPGEN+HERWIG. $W+$ jets events containing heavy-flavor quarks ($Wbb+$ jets, $Wcc+$ jets, and $Wc+$ jets) were generated separately using leading-order matrix elements with massive b-and c-quarks. An overlap-removal procedure was used to avoid double counting of heavy-flavor quarks between the matrix element and the parton shower evolution. Diboson events (WW, WZ, ZZ) were generated using HERWIG with the MRSTMCal PDF.

All the simulation samples account for multiple pp interactions per bunch crossing (pile-up), including both the in-time (additional collisions within the same bunch

crossing) and out-of-time (collisions from neighboring bunch crossings) contributions, using PYTHIA 6 and the ATLAS AMBT2B CTEQ6L1 tune [34] to simulate minimum bias events. The events were reweighted so that the distribution of the average number of interactions per bunch crossing matches that observed in the data. The samples were processed through the GEANT4 [35] simulation of the ATLAS detector [36] and the standard ATLAS reconstruction software. Simulated events were corrected so that the trigger efficiency and physics object identification efficiencies, energy scales, and energy resolutions match those determined in data control samples, with the exception of the electrons and jets, the energies of which were scaled in data to match the simulation.

V. EVENT RECONSTRUCTION

The lepton + jets $t\bar{t}$ decay mode is characterized by a high-p_{T} lepton, two jets originating from b-quarks, two jets from the hadronic W boson decay, and missing transverse momentum due to the neutrino.

A. Object reconstruction and identification

Primary vertices in the event are formed from reconstructed tracks such that they are spatially compatible with the luminous interaction region. The hard-scatter primary vertex is chosen to be the vertex with the highest $\sum p_{\mathrm{T}}^2$ where the sum extends over all associated tracks with $p_{\mathrm{T}} > 0.4$ GeV.

The same electron definition as was used in the $t\bar{t}$ cross-section measurement with 2010 data [37] is adopted in this analysis, but optimized for the higher pile-up conditions of the 2011 data [38]. Strict quality requirements are applied to the shape of the energy deposition in the EM calorimeters and to the electron track variables [39]. The resulting electron candidates are required to have transverse energy $E_{\mathrm{T}} > 25$ GeV and $|\eta_{\mathrm{cluster}}| < 2.47$, where $|\eta_{\mathrm{cluster}}|$ is the pseudorapidity of the EM cluster associated with the electron. In order to ensure high-quality reconstruction, candidates in the transition region between the barrel and endcap calorimeters, $1.37 < |\eta_{\mathrm{cluster}}| < 1.52$, and candidates matching the criteria for converted photons are rejected.

Muon candidates are reconstructed by combining track segments in different layers of the muon chambers [40,41]. Such segments are assembled starting from the outermost layer, with a procedure that takes material effects into account, and are then matched with tracks found in the ID. The candidates are then refitted using all hits from both the muon spectrometer and the ID, and are required to have $p_{\mathrm{T}} > 25$ GeV and $|\eta| < 2.5$.

Electron and muon candidates are required to be isolated in order to reduce the backgrounds from hadrons mimicking lepton signatures and leptons from heavy-flavor decays.

For electrons, the isolation requirements are similar to the ones tuned for 2010 data [42] but optimized for the 2011 running conditions. The total transverse energy deposited in the calorimeter, in a cone of size $\Delta R = 0.2$ around the electron candidate, is considered. The energy associated with the electron is subtracted, and corrections are made to account for the energy deposited by pile-up interactions. An analogous isolation requirement is applied using the sum of track p_{T} (excluding the electron track) in a cone of $\Delta R = 0.3$ around the electron direction. Isolation requirements on both the transverse energy and momentum are tuned as a function of η_{cluster} and E_{T} in order to ensure a uniform 90% efficiency for electrons from $Z \to ee$ decays satisfying the electron definition described above.

For muon candidates, after subtracting the contributions from the muon itself, the total energy deposited in the calorimeter in a cone of size $\Delta R = 0.2$ around the muon direction is required to be below 4 GeV and the sum of track transverse momenta for tracks with $p_{\mathrm{T}} > 1$ GeV in a cone of $\Delta R = 0.3$ around the muon direction is required to be below 2.5 GeV. The above set of cuts has an efficiency of 88% for simulated $t\bar{t}$ signal events in the μ + jets channel with a negligible dependence on the pile-up conditions.

Jets are reconstructed from topological clusters [43] of energy depositions using the anti-k_t algorithm [44] with a radius parameter of $R = 0.4$. The jet energy is first corrected for pile-up effects and then to the hadronic scale corresponding to the particle-level jets using energy and η-dependent correction factors derived from simulation [45]. The energies of jets in data are further corrected, using *in situ* measurements, to match simulation [46]. Only jets with $p_{\mathrm{T}} > 25$ GeV and $|\eta| < 2.5$ are considered in the analysis. To suppress jets from in-time pile-up, the jet vertex fraction, defined as the sum of the p_{T} of tracks associated with the jet and originating from the primary vertex divided by the sum of the p_{T} from all tracks associated with the jet, is required to be greater than 0.75.

The missing transverse momentum vector, $E_{\mathrm{T}}^{\mathrm{miss}}$, is derived from the vector sum of calorimeter cell energies within $|\eta| < 4.9$ and corrected on the basis of the dedicated calibrations of the associated physics objects [47], including muons. Calorimeter cells containing energy depositions above noise and not associated with high-p_{T} physics objects (referred to as the unassociated-cell term) are also included.

The identification of $t\bar{t}$ events is improved by tagging jets originating from b-quarks using a combination of three b-tagging algorithms [48]. The results of the three taggers are combined using a neural network resulting in a single discriminating variable. The combined tagger operating point chosen for this analysis corresponds to a tagging efficiency of 70% for b-jets in simulated $t\bar{t}$ events, while c-jets are suppressed by a factor of 5 and light-flavor- and gluon-initiated jets are suppressed by a factor of about 100.

B. Event selection

Events are first required to pass either a single-electron or single-muon trigger and the hard-scatter primary vertex is required to be constructed from at least five tracks with $p_{\mathrm{T}} > 0.4$ GeV.

Leptons and jets are required to be well separated from each other to minimize ambiguities, background, and systematic uncertainties. First, jets within $\Delta R = 0.2$ of an electron satisfying the requirements described in Sec. V A, but with the p_{T} threshold lowered to 15 GeV, are removed. If there is another jet found within $\Delta R = 0.4$, the electron is discarded. Finally muons within $\Delta R = 0.4$ of the axis of a jet are removed.

Events are required to contain exactly one isolated lepton and this lepton is required to have fired the trigger. Four or more jets where at least one jet is b-tagged are also required. In addition, events must satisfy $E_{\mathrm{T}}^{\mathrm{miss}} > 30$ GeV and $m_{\mathrm{T}}^{W} > 35$ GeV, where $E_{\mathrm{T}}^{\mathrm{miss}}$ is the magnitude of the missing transverse momentum vector $E_{\mathrm{T}}^{\mathrm{miss}}$ and the W boson transverse mass, m_{T}^{W}, is defined as

$$m_{\mathrm{T}}^{W} = \sqrt{2p_{\mathrm{T}}^{\ell}p_{\mathrm{T}}^{\nu}(1-\cos(\phi^{\ell}-\phi^{\nu}))}, \tag{1}$$

where p_{T}^{ℓ} and ϕ^{ℓ} are, respectively, the transverse momentum and the azimuthal angle of the lepton, p_{T}^{ν} is identified at the reconstruction level with $E_{\mathrm{T}}^{\mathrm{miss}}$, and ϕ^{ν} is the azimuthal angle of $E_{\mathrm{T}}^{\mathrm{miss}}$.

C. Kinematic reconstruction of the $t\bar{t}$ system

A kinematic likelihood fit [49] is used to fully reconstruct the $t\bar{t}$ kinematics. The algorithm relates the measured kinematics of the reconstructed objects (lepton, jets and $E_{\mathrm{T}}^{\mathrm{miss}}$) to the leading-order representation of the $t\bar{t}$ system decay. The event likelihood ($\mathscr{L}$) is constructed as the product of Breit-Wigner (BW) distributions and transfer functions (TF)

$$\begin{aligned}\mathscr{L} \equiv & \mathrm{TF}(\tilde{E}^{\ell}, E^{\ell}) \cdot \left(\prod_{i=1}^{4} \mathrm{TF}(\tilde{E}_{\mathrm{jet}\,i}, E_{\mathrm{quark}\,i})\right) \\ & \cdot \mathrm{TF}(E_x^{\mathrm{miss}}|p_x^{\nu}) \cdot \mathrm{TF}(E_y^{\mathrm{miss}}|p_y^{\nu}) \\ & \cdot \mathrm{BW}(m_{jj}|m_W) \cdot \mathrm{BW}(m_{\ell\nu}|m_W) \\ & \cdot \mathrm{BW}(m_{jjj}|m_t) \cdot \mathrm{BW}(m_{\ell\nu j}|m_t), \end{aligned} \tag{2}$$

where the Breit-Wigner distributions associate the $E_{\mathrm{T}}^{\mathrm{miss}}$, lepton, and jets with W bosons and top quarks, making use of their known widths and masses. The top-quark mass used is 172.5 GeV. The transfer functions, derived from the MC@NLO+HERWIG simulation of the $t\bar{t}$ signal, represent the experimental resolutions in terms of the probability that the observed energy at reconstruction level ($\tilde{E}$) is produced by a parton-level object with a certain energy E. Transverse energy is used to parametrize the muon momentum resolution while lepton energy is used in the electron channel.

The missing transverse momentum is used as a starting value for the neutrino p_{T}, with its longitudinal component (p_z^{ν}) as a free parameter in the kinematic likelihood fit. Its starting value is computed from the W mass constraint. If there are no real solutions for p_z^{ν} then zero is used as a starting value. Otherwise, if there are two real solutions, the one giving the larger likelihood is used. The five highest-p_{T} jets (or four if there are only four jets in the event) are used as input to the likelihood fit and the best four-jet combination is selected.

The likelihood is maximized as a function of the energies of the b-quarks, the quarks from the hadronic W boson decay, the charged lepton, and the components of the neutrino three-momentum. The maximization is performed

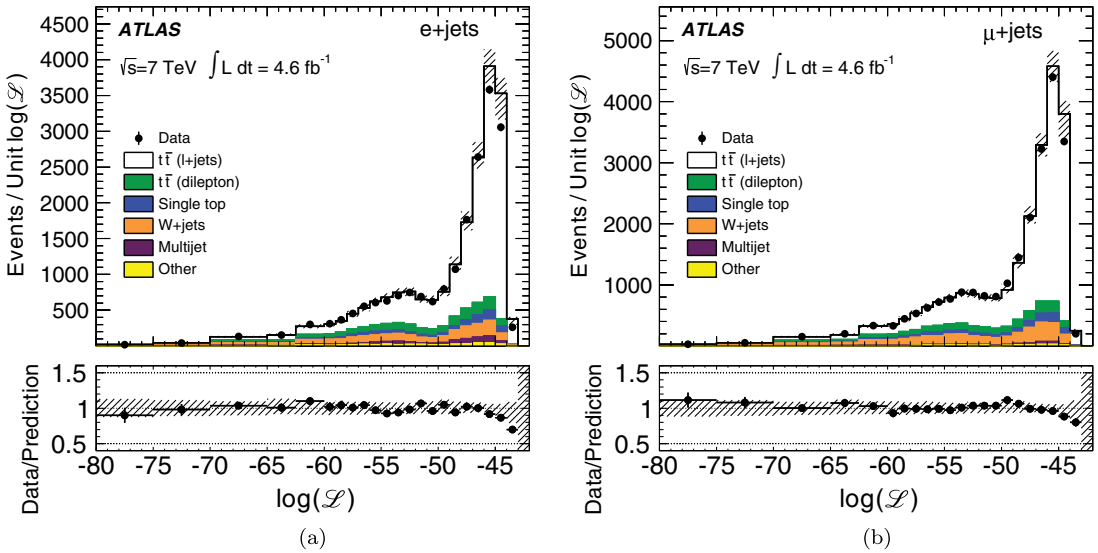

FIG. 1 (color online). Distribution of the logarithm of the likelihood [$\log(\mathscr{L})$] obtained from the kinematic fit in the (a) $e+$jets and (b) $\mu+$jets channels. Data distributions are compared to predictions, using ALPGEN+HERWIG as the $t\bar{t}$ signal model. The hashed area indicates the combined statistical and systematic uncertainties in the prediction, excluding systematic uncertainties related to the modeling of the $t\bar{t}$ system. Signal and background processes are shown in different colors, with "Other" including the small backgrounds from diboson and $Z+$jets production. The lower parts of the figures show the ratios of data to the predictions.

TABLE I. Summary of all requirements included in the event selection.

Event selection	
Trigger	Single lepton
Primary vertex	≥ 5 tracks with $p_{\mathrm{T}} > 0.4$ GeV
Exactly one	Muons: $p_{\mathrm{T}} > 25$ GeV, $\lvert\eta\rvert < 2.5$
isolated lepton	Electrons: $p_{\mathrm{T}} > 25$ GeV
	$\lvert\eta\rvert < 2.47$, excluding $1.37 < \lvert\eta\rvert < 1.52$
≥ 4 jets	$p_{\mathrm{T}} > 25$ GeV, $\lvert\eta\rvert < 2.5$
b-tagging	≥ 1 b-tagged jet at $\epsilon_b = 70\%$
$E_{\mathrm{T}}^{\mathrm{miss}}$	$E_{\mathrm{T}}^{\mathrm{miss}} > 30$ GeV
m_{T}^{W}	$m_{\mathrm{T}}^{W} > 35$ GeV
Kinematic fit	$\log(\mathscr{L}) > -50$

by testing all possible permutations, assigning jets to partons. The likelihood is combined with the probability for a jet to be b-tagged, given the parton from the top-quark decay it is associated with, to construct an event probability. The b-tagging efficiencies and rejection factors are used to promote permutations for which a b-tagged jet is assigned to a b-quark and penalize those where a b-tagged jet is assigned to a light quark. The permutation of jets with the highest event probability is retained.

The event likelihood must satisfy $\log(\mathscr{L}) > -50$. This requirement provides a good separation between properly and poorly reconstructed events. Distributions of $\log(\mathscr{L})$ for data and simulation events are shown in Fig. 1 separately for the $e+$jets and $\mu+$jets channels. The data-to-MC ratio of the efficiency of the likelihood requirement is found to be 0.98 and the simulation is corrected for this difference. The full event selection, including this final requirement on the likelihood, is summarized in Table I.

Once the best likelihood is found, the four-momenta of both top quarks in the event are formed from their decay products as determined by the kinematic likelihood fit. One top quark is reconstructed from the fitted charged lepton, neutrino, and one of the b-partons. This is referred to as the leptonically decaying top quark. The other, referred to as the hadronically decaying top quark, is reconstructed from the other three partons. The hadronically decaying top quark is selected to represent the top-quark p_{T} because the final result for this variable has smaller systematic uncertainties than the leptonically decaying top quark. The two spectra were compared and their results are compatible. The $t\bar{t}$ system is the combination of the leptonically and hadronically decaying top quarks.

VI. BACKGROUND DETERMINATION

After the event selection is applied, the largest background process is $W+$jets. Other backgrounds are due to multijet production, single top-quark electroweak production, diboson production, $Z+$jets production, and the other decay channels associated with $t\bar{t}$ production: the dilepton channel, which gives a significant contribution, and the all-hadronic channel, which is found to be negligible. The $W+$jets and multijet backgrounds are determined using a combination of simulation and data-driven techniques. The other backgrounds are determined from simulation and normalized to higher-order theoretical predictions.

A. Simulated background contributions

The single top-quark, dilepton $t\bar{t}$, $Z+$jets, and diboson contributions are estimated from simulations and normalized to theoretical calculations of the inclusive cross sections as follows. The single top-quark cross section is normalized to the NLO + NNLL prediction: the t-channel to $64.6^{+2.6}_{-1.7}$ pb [50], the s-channel to 4.6 ± 0.2 pb [51], and the Wt-channel to 15.7 ± 1.2 pb [52]. The dilepton $t\bar{t}$ background is normalized to the same inclusive cross section given in Sec. IV for the signal $t\bar{t} \to \ell +$ jets sample. The $Z+$jets background is normalized to the NNLO QCD calculation for inclusive Z production [53] and the diboson background is normalized to the NLO QCD cross-section prediction [54].

B. $W+$jets background

At the LHC the rate of $W^+ +$jets events is larger than that of $W^- +$jets as the up-quark density in the proton is larger than the down-quark one. Exploiting the fact that the ratio of $W^+ +$jets to $W^- +$jets cross sections is predicted more precisely than the total $W+$jets cross section [55], the charge asymmetry in $W+$jets production can be used to estimate the total $W+$jets background from the data. Considering that processes other than $W+$jets give, to a good approximation, equal numbers of positively and negatively charged leptons, the total number of $W+n$-jets events before requiring a b-tagged jet (pretag sample) can be estimated as

$$N_{n_{\mathrm{jets}}}^{\mathrm{W,pretag}} = N_{n_{\mathrm{jets}}}^{W^+} + N_{n_{\mathrm{jets}}}^{W^-} = \left(\frac{r_{n_{\mathrm{jets}}}^{\mathrm{MC}} + 1}{r_{n_{\mathrm{jets}}}^{\mathrm{MC}} - 1}\right)(D_{n_{\mathrm{jets}}}^{+} - D_{n_{\mathrm{jets}}}^{-}), \quad (3)$$

where n_{jets} is the number of jets, $D_{n_{\mathrm{jets}}}^{+}$ ($D_{n_{\mathrm{jets}}}^{-}$) the total numbers of events with positively (negatively) charged leptons in data meeting the selection criteria described in Sec. V B with the appropriate n_{jets} requirement and without the b-tagging requirement, and $r_{n_{\mathrm{jets}}}^{\mathrm{MC}}$ is the ratio of $\sigma(pp \to W^+ + n\text{-jets})$ to $\sigma(pp \to W^- + n\text{-jets})$ estimated from simulation. Small additional sources of charge asymmetry in data, mainly due to the single top-quark contribution, are estimated from the simulation and subtracted from data. The largest uncertainties in the ratio come from the PDFs and the heavy-flavor fractions in $W+$jets events.

The jet flavor composition of the pretag sample is the other important element needed to estimate the number of events after the requirement of at least one b-tagged jet. It is evaluated using a combination of data- and simulation-driven approaches starting from the estimation of the flavor fractions from data for the two-jet sample,

$$N_2^{W,\mathrm{tag}} = N_2^{W,\mathrm{pretag}}(F_{bb,2}P_{bb,2} + F_{cc,2}P_{cc,2} + F_{c,2}P_{c,2} + F_{\mathrm{light},2}P_{\mathrm{light},2}), \quad (4)$$

where $N_2^{W,\mathrm{tag}}$ is the number of $W+$jets events after the b-tagging requirement in the two-jet sample, evaluated from data after subtracting all non-W events (including the multijet background, estimated using the data-driven method described in Sec. VI C, the $t\bar{t}$ signal and the other backgrounds, estimated from simulation); $N_2^{W,\mathrm{pretag}}$ is the number of events before the b-tagging requirement estimated from data using Eq. (3) for the background-dominated two-jet sample. The quantities $F_{x,2}$ (with $x = bb/cc/c/\mathrm{light}$, where light refers to $u/d/s$-quark- and gluon-initiated jets) represent the flavor fractions in the two-jet sample and the $P_{x,2}$ the respective b-tagging probabilities taken from the simulation. The flavor fractions add up to unity for each jet multiplicity

$$F_{bb,2} + k_{cc\to bb}\cdot F_{bb,2} + F_{c,2} + F_{\mathrm{light},2} = 1 \quad (5)$$

with $F_{cc,2}$ constrained by $F_{bb,2}$ using the ratio $k_{cc\to bb}$ between the two fractions taken from simulation. The $Wc+$jets events have a different charge asymmetry with respect to $Wbb/Wcc/W+$light-jets events. This is because, at leading order, the former is dominated by gluon-s and gluon-$\bar{s}$ scattering, which involve symmetric s-and $\bar{s}$-quark PDF, while the latter are dominated by u-$\bar{d}$ and d-$\bar{u}$ scattering, which are asymmetric because they involve the u-and d-valence-quark PDF. The flavor fractions can therefore be determined by applying Eq. (4) and Eq. (5) separately for events with positive and negative leptons. These flavor fractions are used to redetermine the overall normalization and the procedure is iterated until no significant changes are observed. They are then used to correct the flavor fractions in the simulation.

Finally the number of events after the b-tagging and requiring $\geq$ 4-jets is estimated using the number of pretag events, $N_{\geq 4}^{W,\mathrm{pretag}}$, measured from the charge asymmetry method of Eq. (3), as

$$N_{\geq 4}^{W,\mathrm{tag}} = N_{\geq 4}^{W,\mathrm{pretag}}\cdot f_2^{\mathrm{tag}}\cdot f_{2\to\geq 4}^{\mathrm{tag}}, \quad (6)$$

where f_2^{tag} is the fraction of events in the two-jet sample that are b-tagged and $f_{2\to\geq 4}^{\mathrm{tag}}$ the ratio between the b-tagged event fractions in the $\geq$ 4-jet and two-jet samples evaluated using simulated $W+$jets events with corrected flavor fractions. The correction factors for a selection requiring $\geq$ 4 jets are obtained from the ones of the two-jet sample by applying an overall normalization factor in order to preserve the requirement that the flavor fractions add up to unity.

This method has the advantage that f_2^{tag} is evaluated from the data in a sample dominated by the $W+$jets background and that it relies on the ratio between the tagging fractions in the two-jet and $\geq$ 4-jet samples, strongly reducing the systematic uncertainties due to the b-tagging efficiencies and the heavy-flavor components of the $W+$jets background.

C. Multijet background

The multijet background is characterized by jets that are misidentified as isolated prompt leptons, or nonprompt leptons that are misidentified as isolated leptons. These are referred to as "fake leptons."

The rate of identifying such a fake lepton as a real one is calculated from data by defining two control samples. The first sample uses the lepton definition described in Sec. V A, which is referred to as the tight selection. To define the second sample, a loose selection is used, for which the identification criteria are relaxed and the isolation requirements are removed. Using these samples, the number of fake leptons passing the tight selection is given by

$$N_{\mathrm{fake}}^{\mathrm{tight}} = \frac{\epsilon_{\mathrm{fake}}}{\epsilon_{\mathrm{real}} - \epsilon_{\mathrm{fake}}}(N^{\mathrm{loose}}\epsilon_{\mathrm{real}} - N^{\mathrm{tight}}), \quad (7)$$

where N^{tight} and N^{loose} are the numbers of events with a tight or loose lepton, respectively, and ϵ_{real} and ϵ_{fake} are the fractions of real and fake loose leptons that pass the tight selection. Decays of the Z boson to two leptons are used to measure the ϵ_{real}, while the ϵ_{fake} are measured in control regions which are dominated by contributions from fake leptons. These control regions are defined by requiring low $E_{\mathrm{T}}^{\mathrm{miss}}$, low m_{T}^{W}, or by selecting leptons with high track impact parameter. Contributions from $W+$jets and $Z+$jets production are subtracted in the control regions using simulation [5]. The resulting multijet background is larger for the $e+$jets channel than it is for the $\mu+$jets channel.

VII. RECONSTRUCTED EVENT VARIABLES

The event yields after the selection described in Sec. V are displayed in Table II, separately for the $e+$jets and

TABLE II. Event yields in the $e+$jets and $\mu+$jets channels. The signal model, denoted $t\bar{t}$ ($\ell+$jets) in the table, is generated using ALPGEN. Errors indicate the total statistical and systematic uncertainties on each subsample and the uncertainty on the signal includes the generator systematic uncertainty discussed in Sec. IX B.

	$e+$jets	$\mu+$jets
$t\bar{t}$ ($\ell+$jets)	11200 ± 1900	13100 ± 2000
$t\bar{t}$ (dilepton)	850 ± 170	930 ± 170
Single top	560 ± 120	660 ± 160
$W+$jets	920 ± 240	1300 ± 300
Multijet	400 ± 200	200 ± 40
$Z+$jets	160 ± 110	89 ± 60
Diboson	22 ± 13	25 ± 14
Prediction	14100 ± 1900	16300 ± 2000
Data	13167	15752

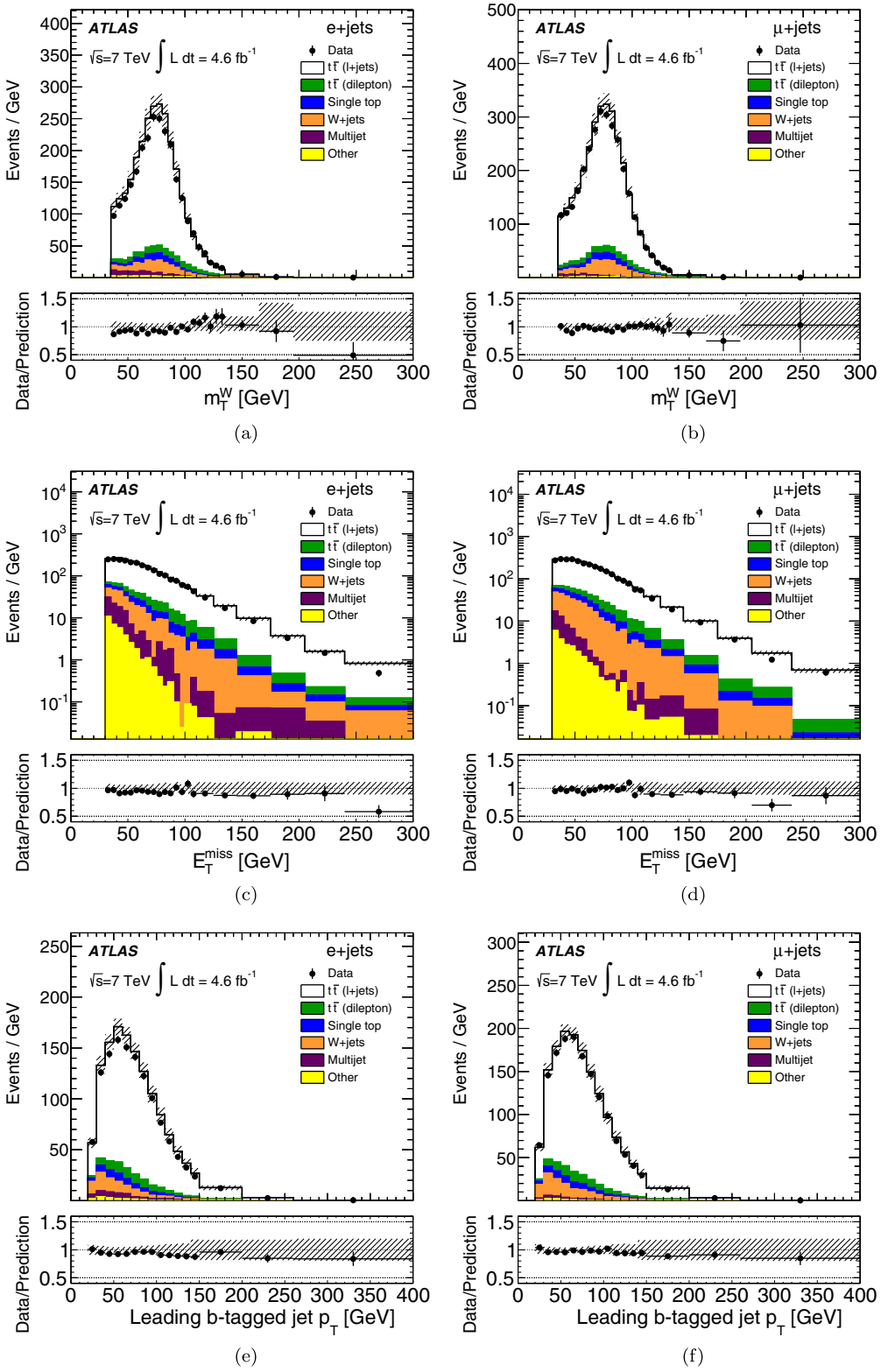

FIG. 2 (color online). Observables at the reconstruction level: W transverse mass (m_{T}^{W}) in the (a) $e+$jets and (b) $\mu+$jets channels, missing transverse momentum ($E_{\mathrm{T}}^{\mathrm{miss}}$) in the (c) $e+$jets and (d) $\mu+$jets channels, and leading b-tagged jet p_{T} in the (e) $e+$jets and (f) $\mu+$jets channels. Data distributions are compared to predictions, using ALPGEN+HERWIG as the $t\bar{t}$ signal model. The hashed area indicates the combined statistical and systematic uncertainties in the total prediction, excluding systematic uncertainties related to the modeling of the $t\bar{t}$ system. Signal and background processes are shown in different colors, with "Other" including the small backgrounds from diboson and $Z+$jets production. Events beyond the range of the horizontal axis are included in the last bin. The lower parts of the figures show the ratios of data to the predictions.

μ + jets channels, for the data, the simulated ℓ + jets signal from $t\bar{t}$ production, and for the various backgrounds discussed in Sec. VI.

A comparison of the data with the $t\bar{t}$ signal and background distributions, after all selection criteria are applied, is shown in Fig. 2 as functions of the W boson transverse mass, the missing transverse momentum, and the p_{T} of the highest-p_{T} (leading) b-tagged jet. Within the uncertainties shown, which cover the experimental and background systematic uncertainties but not the $t\bar{t}$ modeling uncertainties (discussed in Sec. IX B), the data and predictions are in agreement.

The kinematic spectra corresponding to individual top quarks as well as to the reconstructed $t\bar{t}$ system are shown in Figs. 3 and 4. Data and predictions agree within uncertainties with the exception of the high-p_{T} tails of the p_{T}^{t} and $p_{\mathrm{T}}^{t\bar{t}}$ distributions where data fall below the prediction.

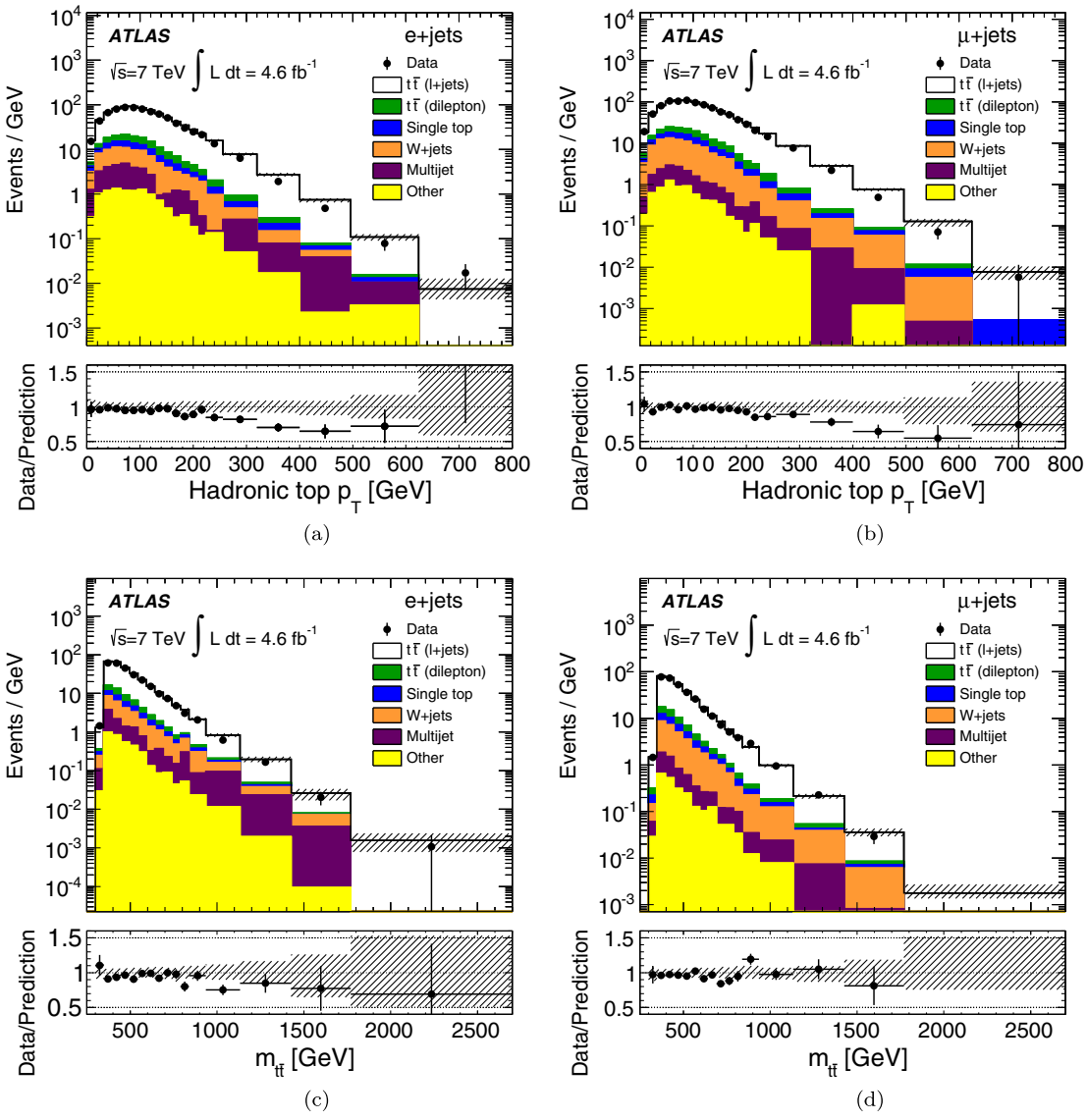

FIG. 3 (color online). Reconstructed distributions for the transverse momentum of the hadronically decaying top quark (p_{T}^{t}) in the (a) e + jets and (b) μ + jets channels and for the mass of the $t\bar{t}$ system ($m_{t\bar{t}}$) in the (c) e + jets and (d) μ + jets channels. Data distributions are compared to predictions, using ALPGEN+HERWIG as the $t\bar{t}$ signal model. The hashed area indicates the combined statistical and systematic uncertainties in the total prediction, excluding systematic uncertainties related to the modeling of the $t\bar{t}$ system. Signal and background processes are shown in different colors, with "Other" including the small backgrounds from diboson and Z + jets production. Events beyond the axis range are included in the last bin. The lower parts of the figures show the ratios of data to the predictions.

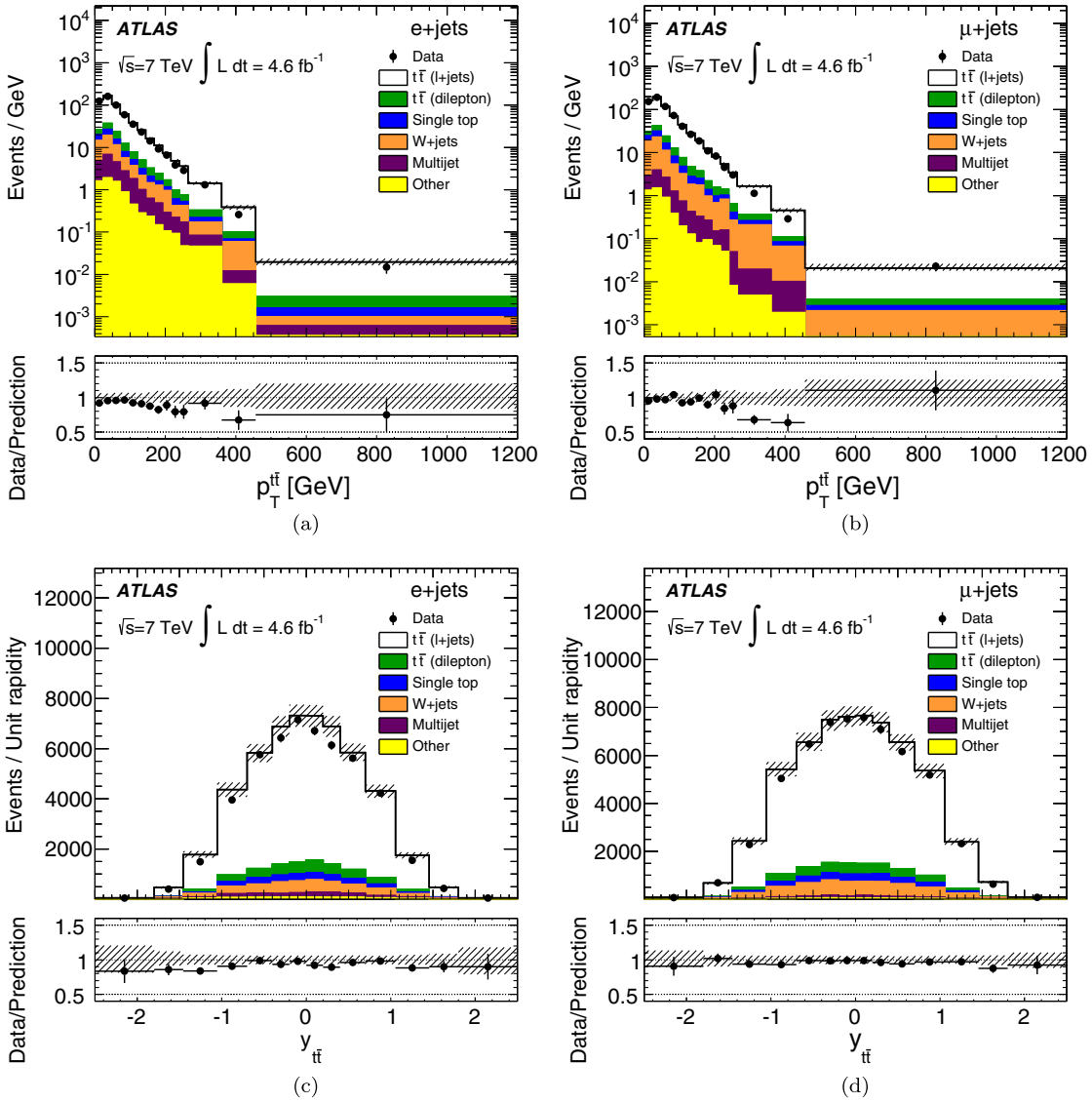

FIG. 4 (color online). Reconstructed distributions for the transverse momentum of the $t\bar{t}$ system ($p_{\mathrm{T}}^{t\bar{t}}$) in the (a) $e+$jets and (b) $\mu+$jets channels and for the rapidity of the $t\bar{t}$ system ($y_{t\bar{t}}$) in the (c) $e+$jets and (d) $\mu+$jets channels. Data distributions are compared to predictions, using ALPGEN+HERWIG as the $t\bar{t}$ signal model. The hashed area indicates the combined statistical and systematic uncertainties in the total prediction, excluding systematic uncertainties related to the modeling of the $t\bar{t}$ system. Signal and background processes are shown in different colors, with "Other" including the small backgrounds from diboson and $Z+$jets production. Events beyond the axis range are included in the last bin, or in the case of the $y_{t\bar{t}}$ spectrum the first and last bin. The lower parts of the figures show the ratios of data to the predictions.

VIII. DIFFERENTIAL CROSS-SECTION DETERMINATION

The estimated background contributions are subtracted from the measured distributions, which are then corrected for the efficiency to pass the event selection, for the detector resolution, and the branching ratio for the $t\bar{t} \to \ell + \text{jets}$ channel. To facilitate the comparison to theoretical predictions, the cross-section measurements are defined with respect to the top quarks before the decay (parton level) and after QCD radiation [56].

The efficiency (ϵ_j) to satisfy the selection criteria in bin j for each variable is evaluated as the ratio of the parton-level spectra before and after implementing the event selection at the reconstruction level. The efficiencies are displayed in Fig. 5 and are typically in the 3%–5% range. The decrease in the efficiencies at high values of p_{T}^{t}, $m_{t\bar{t}}$, and $p_{\mathrm{T}}^{t\bar{t}}$ is primarily due to the increasingly large fraction of nonisolated leptons and angularly close or merged jets in events with high top-quark p_{T}. There is also a decrease in the efficiency at high $|y_{t\bar{t}}|$ due to jets and leptons falling outside of the pseudorapidity range required for the reconstructed lepton and jets. The absolute variation of the efficiency as a function of a different choice of the top-quark mass is found to be

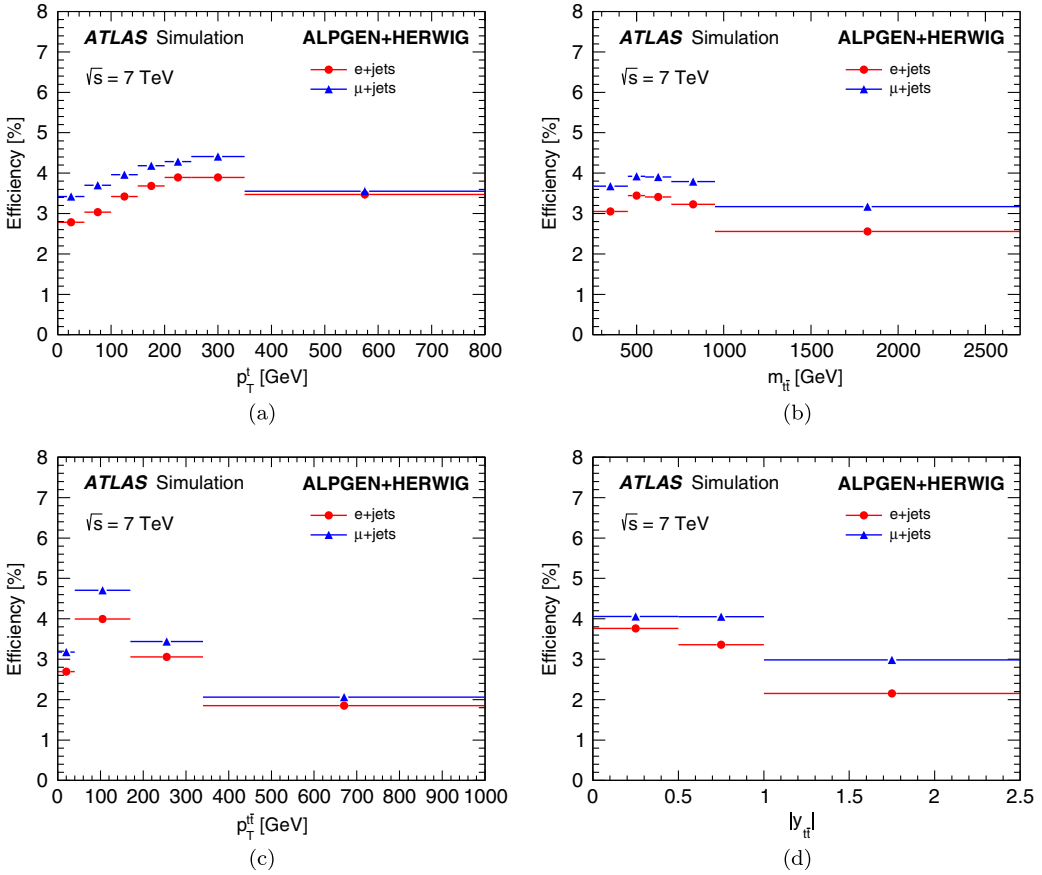

FIG. 5 (color online). The selection efficiencies binned in the (a) transverse momentum of the top-quark (p_T^t), and the (b) mass ($m_{t\bar{t}}$), (c) transverse momentum ($p_T^{t\bar{t}}$) and the (d) absolute value of the rapidity ($|y_{t\bar{t}}|$) of the $t\bar{t}$ system obtained from the ALPGEN+HERWIG simulation of the $t\bar{t}$ signal. The horizontal axes refers to parton-level variables.

$+0.025\%/\text{GeV}$, independently of the kinematic variable and bin.

The influence of detector resolution is corrected by unfolding. The measured distributions in the $e+\text{jets}$ and $\mu+\text{jets}$ channels are unfolded separately by a regularized inversion of the migration matrix (symbolized by $\mathcal{M}^{-1}$) described in Sec. VIII A and then the channels are combined as described in Sec. VIII B. The formula used to extract the cross section in each bin is

$$\frac{d\sigma}{dX_j} \equiv \frac{1}{\Delta X_j} \cdot \frac{\sum_i \mathcal{M}_{ji}^{-1}[D_i - B_i]}{\text{BR} \cdot \mathscr{L} \cdot \epsilon_j}, \tag{8}$$

where ΔX_j is the bin width, D_i (B_i) are the data (expected background) yields in each bin i of the reconstructed variable, $\mathscr{L}$ is the integrated luminosity of the data sample, ϵ_j is the event selection efficiency, and $\text{BR} = 0.438$ is the branching ratio of $t\bar{t} \to \ell + \text{jets}$ [57].

The normalized cross section $1/\sigma d\sigma/dX_j$ is computed by dividing by the measured total cross section, evaluated by integrating over all bins. The normalized distributions have substantially reduced systematic uncertainties since most of the relevant sources of uncertainty (luminosity, jet energy scale, b-tagging, and absolute normalization of the data-driven background estimate) have large bin-to-bin correlations.

A. Unfolding procedure

The binning for each of the distributions is determined by the experimental resolution of the kinematic variables, and poorly populated bins are combined with neighboring bins to reduce the uncertainty on the final result. Typical values of the fractional resolution for p_T^t and $m_{t\bar{t}}$ are 25% and 15%, respectively, while the fractional resolution for $p_T^{t\bar{t}}$ improves as a function of $p_T^{t\bar{t}}$ and is 40% at 100 GeV. For $|y_{t\bar{t}}|$, the resolution varies from 0.25 to 0.35, from central to forward rapidities.

The effect of detector resolution is taken into account by constructing the migration matrices, relating the variables of interest at the reconstructed and parton levels, using the $t\bar{t}$ signal simulation. In Figs. 6 and 7, normalized versions of the migration matrices are presented, where each column is normalized by the number of parton-level events in that bin. The probability for parton-level events to remain in the same bin is therefore shown on the diagonal, and the

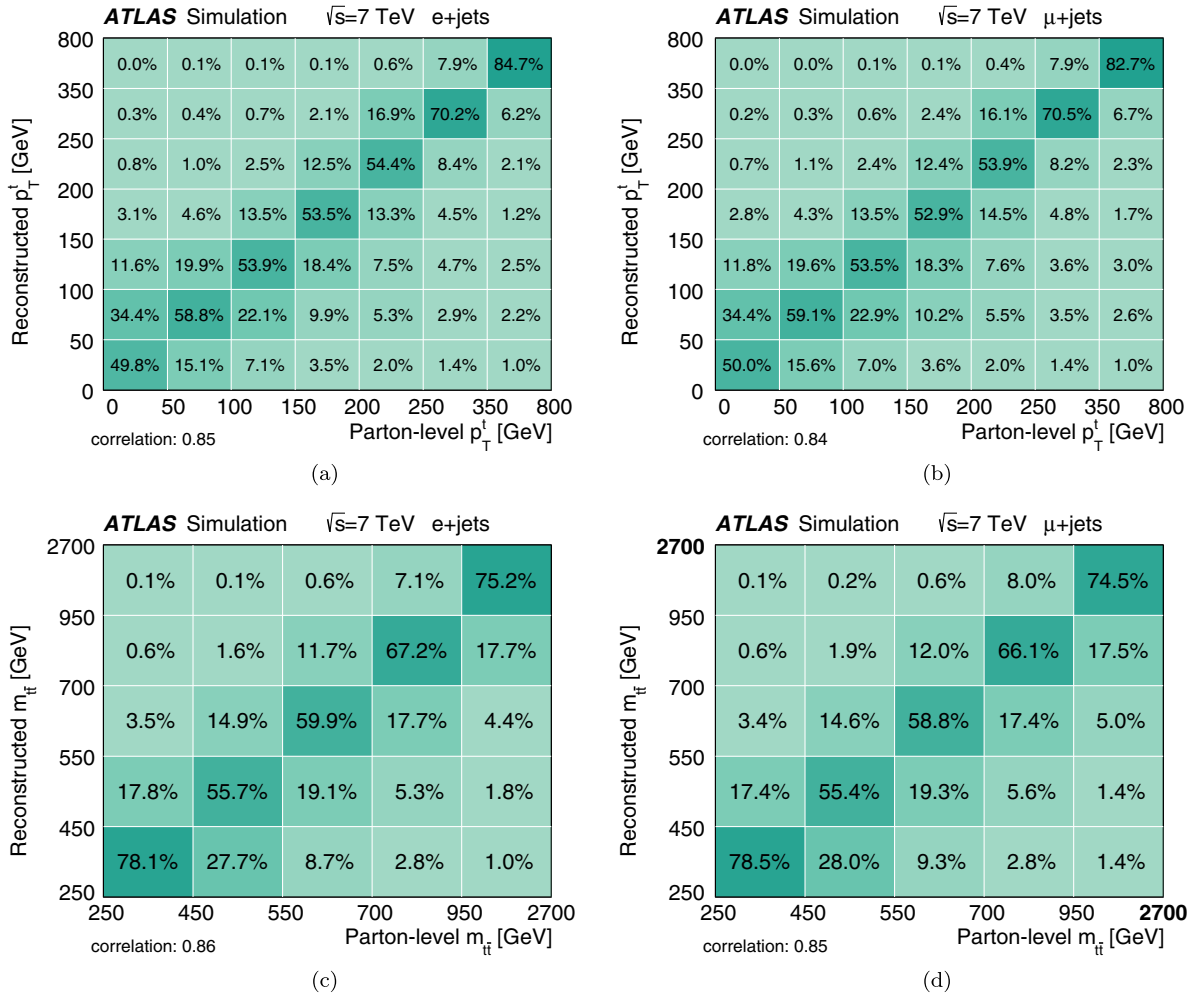

FIG. 6 (color online). The migration matrices obtained from the ALPGEN+HERWIG simulation, relating the parton and reconstructed levels for the transverse momentum of the hadronically decaying top quark (p_T^t) in the (a) $e+$jets and (b) $\mu+$jets channels, and the mass of the $t\bar{t}$ system ($m_{t\bar{t}}$) in the (c) $e+$jets and (d) $\mu+$jets channels. The linear correlation coefficient is given below each plot and all columns are normalized to unity (before rounding off).

off-diagonal elements represent the fraction of parton-level events that migrate into other bins. The fraction of events in the diagonal bins is always greater than 50%, but significant migrations are present in several bins. The regularized singular value decomposition [58] method is used for the unfolding procedure. A regularized unfolding technique is chosen in order to prevent large statistical fluctuations that can be introduced when directly inverting the migration matrix.

To ensure that the results are not biased by the MC generator used for unfolding, the parton-level spectra in simulation are altered by changing the slopes of the p_T^t and $p_T^{t\bar{t}}$ distributions by a factor of 2, while for the $m_{t\bar{t}}$ distribution the content of one bin (550–700 GeV) is increased by a factor of 2 to simulate the presence of a resonance. The shape of the rapidity of the $t\bar{t}$ system is changed by a symmetric Gaussian distribution that results in a reweighting factor of approximately 1.15 at high $|y_{t\bar{t}}|$.

The studies confirm that these altered shapes are indeed recovered within statistical uncertainties by the unfolding based on the nominal migration matrices.

B. Combination of decay channels

The individual $e+$jets and $\mu+$jets channels give consistent results: the differences observed in the corresponding bins for all variables of interest are below two standard deviations, taking into account the correlated uncertainties between the two channels.

The asymmetric BLUE method [59] is used to combine the cross sections measured in the $e+$jets and $\mu+$jets channels, where BLUE refers to the best linear unbiased estimator [60]. The covariance matrix between the two channels is constructed in each kinematic bin by assuming zero or full correlation for channel-specific or common systematic uncertainty sources, respectively.

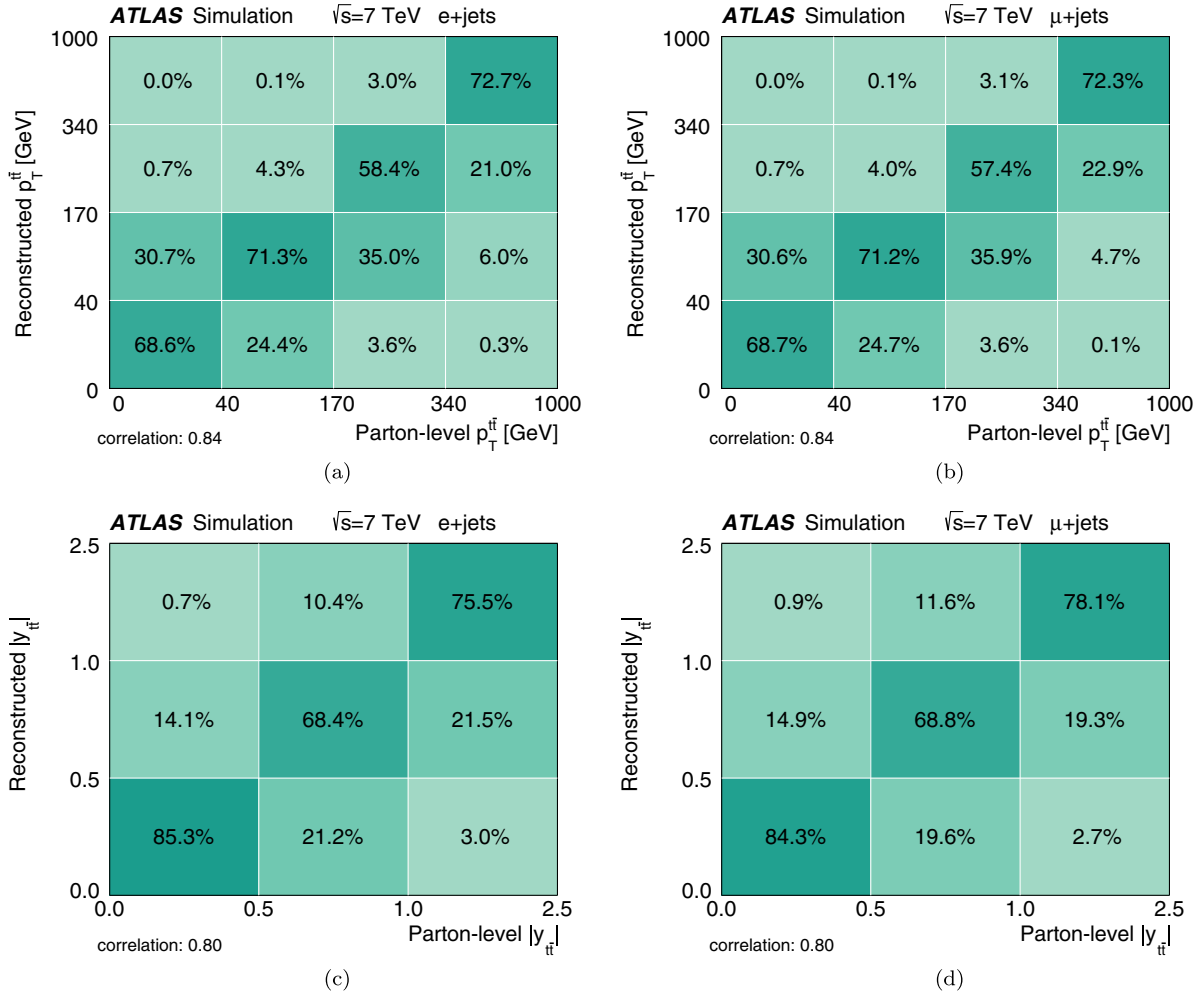

FIG. 7 (color online). The migration matrices obtained from the ALPGEN+HERWIG simulation, relating the parton and reconstructed levels for the transverse momentum of the $t\bar{t}$ system ($p_{\mathrm{T}}^{t\bar{t}}$) in the (a) $e+$jets and (b) $\mu+$jets channels, and the absolute value of the rapidity of the $t\bar{t}$ system ($|y_{t\bar{t}}|$) in the (c) $e+$jets and (d) $\mu+$jets channels. The linear correlation coefficient is given below each plot and all columns are normalized to unity (before rounding off).

The cross sections are normalized to unity after the combination. The combined results are compared and found to be in good agreement with the results of unfolding a merged data set of both the $e+$jets and $\mu+$jets channels.

IX. UNCERTAINTIES

The statistical uncertainty on the data is evaluated with pseudoexperiments by assuming Poisson fluctuations in the data event counts.

The systematic uncertainties are evaluated by varying each source of uncertainty by one standard deviation, propagating this effect through the event selection, unfolding and efficiency corrections, and then considering, for each channel, variable and bin, the variation with respect to the nominal result. This is done separately for the upward and downward variations. For one-sided uncertainties, as in the case of the comparison of two different models, the resulting variation is assumed to be of the same size in both directions and is therefore symmetrized. The combined systematic uncertainties are obtained by using the nominal BLUE weights, assigned to each channel in each bin, to linearly combine the systematic uncertainties in the individual channels, and normalizing after the combination. The total systematic uncertainty in each kinematic bin is computed as the sum in quadrature of individual systematic variations.

The systematic uncertainties and how they affect each of the variables studied are given, grouped into categories, in Tables III and IV. The individual systematic uncertainties are listed for completeness in Appendix A. The precision of the measurement is dominated by systematic uncertainties. They can be classified into three categories: systematic uncertainties affecting the detector modeling, signal modeling, and background modeling.

TABLE III. The individual systematic uncertainties in the normalized differential cross sections after combining the $e+$jets and $\mu+$jets channels for p_{T}^{t} and $m_{t\bar{t}}$, grouped into broad categories, and calculated as a percentage of the cross section in each bin. "Other backgrounds" includes the systematic uncertainties in the single top-quark, dilepton, $Z+$jets, and QCD multijet backgrounds, and IFSR refers to initial- and final-state radiation. Line dots are used when the estimated relative systematic uncertainty for that bin is below 0.1%.

$\frac{1}{\sigma}\frac{d\sigma}{dp_{\mathrm{T}}^{t}}$ Uncertainties [%]/Bins [GeV]	0–50	50–100	100–150	150–200	200–250	250–350	350–800
Jet energy scale	$^{+3.2}_{-2.9}$	$^{+1.0}_{-1.1}$	$^{+1.5}_{-1.6}$	$^{+2.4}_{-2.3}$	$^{+2.4}_{-2.1}$	±2.5	±3.6
Jet energy resolution	±0.4	±0.1	±0.5	⋯	±0.3	⋯	±0.5
Jet reconstruction efficiency	⋯	⋯	⋯	⋯	⋯	⋯	±0.1
b-quark tagging efficiency	$^{+1.1}_{-1.4}$	$^{+0.6}_{-0.8}$	±0.3	$^{+1.3}_{-1.1}$	$^{+2.1}_{-1.5}$	$^{+2.6}_{-1.6}$	$^{+3.0}_{-1.6}$
c-quark tagging efficiency	⋯	⋯	⋯	⋯	±0.1	±0.1	±0.2
Light-jet tagging efficiency	±0.3	⋯	±0.2	⋯	⋯	⋯	±0.2
Lepton selection and momentum scale	$^{+0.9}_{-0.8}$	$^{+0.2}_{-0.1}$	$^{+1.3}_{-1.2}$	±0.6	±0.9	±1.1	$^{+1.0}_{-0.8}$
$E_{\mathrm{T}}^{\mathrm{miss}}$ unassociated cells	$^{+0.4}_{-0.1}$	⋯	$^{+0.2}_{-0.4}$	⋯	$^{+0.3}_{-0.2}$	$^{+0.3}_{-0.4}$	$^{+0.3+0.3}_{\cdots\quad\cdots}$
$E_{\mathrm{T}}^{\mathrm{miss}}$ pile-up	$^{+0.6}_{-0.1}$	⋯	$^{+0.1}_{-0.6}$	$^{\cdots}_{-0.1}$	$^{+0.4}_{\cdots}$	$^{+0.6}_{\cdots}$	$^{+0.8}_{\cdots}$
MC generator	$^{+1.9}_{-1.5}$	$^{+0.5}_{-0.7}$	±0.2	$^{+1.5}_{-1.9}$	±0.1	$^{+3.5}_{-2.8}$	$^{+11}_{-8.6}$
Fragmentation	±0.6	±0.7	±0.7	$^{+0.9}_{-0.8}$	$^{+0.9}_{-1.0}$	±0.7	±1.9
IFSR	$^{+2.2}_{-2.1}$	±0.9	⋯	$^{+3.1}_{-3.2}$	$^{+3.1}_{-3.2}$	$^{+1.5}_{-1.6}$	⋯
PDF	±0.1	±0.1	⋯	±0.2	±0.5	±0.8	±0.8
MC statistics	±1.0	±0.4	±0.7	±0.9	±1.1	±1.4	±2.6
$W+$jets	±1.7	±0.3	±0.7	$^{+0.9}_{-0.8}$	$^{+1.0}_{-0.9}$	$^{+1.4}_{-1.3}$	±1.4
Other backgrounds	$^{+1.5}_{-1.6}$	±0.2	$^{+1.0}_{-0.9}$	$^{+0.7}_{-0.5}$	$^{+0.6}_{-0.4}$	±0.8	$^{+0.9}_{-1.0}$
Statistical uncertainty	±2.4	±1.2	±2.5	±2.0	±2.4	±3.5	±6.1
Total systematic uncertainty	$^{+5.3}_{-5.0}$	$^{+1.8}_{-2.0}$	$^{+2.6}_{-2.7}$	±4.8	$^{+4.9}_{-4.6}$	$^{+5.9}_{-5.1}$	$^{+12}_{-10}$

$\frac{1}{\sigma}\frac{d\sigma}{dm_{t\bar{t}}}$ Uncertainties [%]/Bins [GeV]	250–450	450–550	550–700	700–950	950–2700
Jet energy scale	$^{+1.4}_{-1.3}$	$^{+0.9}_{-0.7}$	$^{+2.1}_{-1.7}$	$^{+3.0}_{-3.1}$	$^{+3.6}_{-4.4}$
Jet energy resolution	±0.6	±0.9	±0.2	±0.2	⋯
Jet reconstruction efficiency	⋯	⋯	⋯	⋯	±0.2
b-quark tagging efficiency	$^{+0.8}_{-1.0}$	±0.4	$^{+1.6}_{-1.3}$	$^{+2.0}_{-1.3}$	$^{+2.2}_{-1.2}$
c-quark tagging efficiency	⋯	⋯	±0.2	⋯	±0.1
Light-jet tagging efficiency	⋯	±0.1	⋯	⋯	±0.1
Lepton selection and momentum scale	±0.5	±0.8	±0.9	±1.7	$^{+1.9}_{-1.8}$
$E_{\mathrm{T}}^{\mathrm{miss}}$ unassociated cells	⋯	$^{+0.1}_{\cdots}$	⋯	$^{\cdots}_{-0.2}$	$^{+0.5}_{-0.4}$
$E_{\mathrm{T}}^{\mathrm{miss}}$ pile-up	$^{\cdots}_{-0.1}$	⋯	$^{+0.2}_{\cdots}$	$^{+0.2}_{\cdots}$	$^{+0.6}_{-0.3}$
MC generator	$^{+2.7}_{-2.2}$	$^{+1.9}_{-2.3}$	$^{+2.6}_{-3.2}$	$^{+3.0}_{-3.7}$	$^{+2.5}_{-3.1}$
Fragmentation	±0.2	±0.2	±0.5	±1.7	$^{+2.1}_{-2.2}$
IFSR	$^{+0.6}_{-0.5}$	±0.2	±0.9	$^{+1.4}_{-1.5}$	±0.4
PDF	⋯	⋯	⋯	$^{+0.5}_{-0.6}$	$^{+2.2}_{-2.3}$
MC statistics	±0.4	±0.4	±0.6	±1.0	±1.6
$W+$jets	±0.2	$^{+0.3}_{-0.2}$	$^{+0.5}_{-0.4}$	$^{+1.2}_{-1.0}$	$^{+1.9}_{-1.7}$
Other backgrounds	±0.3	±0.7	$^{+0.8}_{-0.9}$	$^{+2.3}_{-2.6}$	$^{+4.5}_{-5.4}$
Statistical uncertainty	±1.2	±1.5	±2.7	±3.2	±5.5
Total systematic uncertainty	$^{+3.4}_{-2.9}$	$^{+2.6}_{-2.9}$	$^{+4.1}_{-4.3}$	$^{+6.1}_{-6.5}$	$^{+8.0}_{-8.9}$

TABLE IV. The individual systematic uncertainties in the normalized differential cross sections after combining the $e+$jets and $\mu+$jets channels for $p_{\mathrm{T}}^{t\bar{t}}$ and $|y_{t\bar{t}}|$, grouped into broad categories, and calculated as a percentage of the cross section in each bin. "Other backgrounds" includes the systematic uncertainties in the single top-quark, dilepton, $Z+$jets, and QCD multijet backgrounds, and IFSR refers to initial- and final-state radiation. Line dots are used when the estimated relative systematic uncertainty for that bin is below 0.1%.

$\frac{1}{\sigma}\frac{d\sigma}{dp_{\mathrm{T}}^{t\bar{t}}}$ Uncertainties [%]/Bins [GeV]	0–40	40–170	170–340	340–1000
Jet energy scale	$^{+1.9}_{-2.0}$	$^{+2.2}_{-2.3}$	±4.9	$^{+6.2}_{-6.5}$
Jet energy resolution	$^{+3.4}_{-3.5}$	$^{+4.2}_{-4.1}$	$^{+7.2}_{-7.1}$	$^{+8.2}_{-8.0}$
Jet reconstruction efficiency	...	...	±0.1	±0.3
b-quark tagging efficiency	$^{...}_{-0.1}$	$^{+0.1}_{...}$	$^{+0.4}_{...}$	$^{+1.0}_{-0.1}$
c-quark tagging efficiency	...	...	±0.2	$^{+0.3}_{-0.2}$
Light-jet tagging efficiency	...	...	...	$^{+0.1}_{-0.2}$
Lepton selection and momentum scale	±0.9	$^{+1.3}_{-1.2}$	±0.8	±1.0
$E_{\mathrm{T}}^{\mathrm{miss}}$ unassociated cells	$^{+1.7}_{-1.6}$	$^{+2.0}_{-2.1}$	±2.1	±1.8
$E_{\mathrm{T}}^{\mathrm{miss}}$ pile-up	$^{+1.0}_{-1.2}$	$^{+1.5}_{-1.3}$	$^{+1.6}_{-1.4}$	$^{+1.5}_{-1.6}$
MC generator	$^{+4.2}_{-3.5}$	$^{+4.2}_{-5.1}$	$^{+8.0}_{-9.8}$	$^{+1.5}_{-1.2}$
Fragmentation	±0.6	±0.1	$^{+6.8}_{-6.9}$	$^{+2.6}_{-2.7}$
IFSR	$^{+1.2}_{-1.3}$	±1.0	$^{+6.2}_{-5.8}$	$^{+10}_{-9.5}$
PDF	...	...	±0.2	±1.3
MC statistics	±0.6	±0.8	±1.7	±2.8
$W+$jets	$^{+0.6}_{-0.8}$	$^{+0.7}_{-0.9}$	$^{+1.8}_{-2.4}$	$^{+3.1}_{-3.7}$
Other backgrounds	±0.8	±1.1	±0.9	±1.1
Statistical uncertainty	±1.5	±1.8	±4.5	±7.7
Total systematic uncertainty	$^{+6.4}_{-6.0}$	$^{+7.1}_{-7.7}$	$^{+15}_{-16}$	$^{+16}_{-15}$

$\frac{1}{\sigma}\frac{d\sigma}{d\lvert y_{t\bar{t}}\rvert}$ Uncertainties [%]	0.0–0.5	0.5–1.0	1.0–2.5
Jet energy scale	$^{+0.6}_{-0.5}$	...	$^{+1.1}_{-0.9}$
Jet energy resolution	±0.1	±0.1	±0.4
Jet reconstruction efficiency	...	...	...
b-quark tagging efficiency	...	...	...
c-quark tagging efficiency	...	...	...
Light-jet tagging efficiency	...	...	...
Lepton selection and momentum scale	±0.4	±0.1	$^{+0.9}_{-0.8}$
$E_{\mathrm{T}}^{\mathrm{miss}}$ unassociated cells	±0.1	...	$^{...}_{-0.2}$
$E_{\mathrm{T}}^{\mathrm{miss}}$ pile-up	...	...	$^{...}_{-0.1}$
MC generator	$^{+2.5}_{-2.0}$	$^{+1.5}_{-1.2}$	$^{+5.0}_{-6.2}$
Fragmentation	$^{+1.8}_{-1.9}$	±0.8	$^{+4.3}_{-4.1}$
IFSR	±0.1	...	...
PDF	±1.1	...	$^{+1.9}_{-2.0}$
MC statistics	±0.2	...	±0.3
$W+$jets	±0.3	...	$^{+0.5}_{-0.4}$
Other backgrounds	±0.4	±0.1	±0.9
Statistical uncertainty	±0.7	±0.4	±0.9
Total systematic uncertainty	$^{+3.4}_{-3.1}$	$^{+1.7}_{-1.5}$	$^{+7.1}_{-7.9}$

A. Detector modeling

The systematic uncertainties related to the detector modeling induce effects on the reconstruction of the physics objects (leptons, jets, and $E_{\mathrm{T}}^{\mathrm{miss}}$) used in the selection and in the reconstruction of the kinematic variables under study.

The jet energy scale (JES) systematic uncertainty on the signal, acting on both the efficiency and bin migrations, is evaluated using 21 separate components [46], which allow proper treatment of correlations across the kinematic bins. The impact of the JES uncertainty on the background is evaluated using the overall JES variation defined as the sum in quadrature of the individual components, and is added to the signal JES systematic uncertainty linearly to account for the correlation between them. The simplified treatment of the JES uncertainty for the background has a negligible effect on the results.

The uncertainty on the jet energy resolution is modeled by varying the jet energies according to the systematic uncertainties of the resolution measurement performed on data [61]. The contribution from this uncertainty is generally small except for the $p_{\mathrm{T}}^{t\bar{t}}$ distribution.

The uncertainty on the jet reconstruction efficiency is accounted for by randomly removing jets, in the simulation, according to the uncertainty on the jet reconstruction efficiency measured in data [45]. The effect of this uncertainty is negligible for all the spectra.

The corrections accounting for differences in b-tagging efficiencies and mistag rates for c-quarks and light quarks, between data and simulation, are derived from data and parametrized as a function of p_{T} and η [62,63]. The uncertainties in these corrections are propagated through the analysis.

Electron and muon trigger, reconstruction, and selection efficiencies are measured in data using W and Z boson decays and are incorporated as appropriate correction factors into the simulation. A similar procedure is used for the lepton energy and momentum scales and resolutions. The impact of the uncertainties in all these corrections is at the subpercent level.

The uncertainties in the energy scale and resolution corrections for jets and high-p_{T} leptons are propagated to the uncertainty on $E_{\mathrm{T}}^{\mathrm{miss}}$. Other minor systematic uncertainty contributions on the modeling of $E_{\mathrm{T}}^{\mathrm{miss}}$ arise from effects due to the pile-up modeling and the uncertainties in the unassociated-cell term [47]. These contributions are generally at the subpercent level except for the $p_{\mathrm{T}}^{t\bar{t}}$ distribution.

The efficiency of the likelihood cut discussed in Sec. V C is observed to be $2 \pm 1\%$ smaller in data than in simulation, but this discrepancy has no kinematic dependence and hence no effect on the unfolded normalized distributions.

B. Signal modeling

The sources of uncertainty for the signal modeling come from the choice of generator used for the simulation of the $t\bar{t}$ process, the parton shower and hadronization model, the model for initial-and final-state QCD radiation (IFSR), and the choice of PDF.

The uncertainties due to the generator choice are evaluated using MC@NLO+HERWIG to unfold the data, instead of the nominal ALPGEN+HERWIG. These uncertainties are larger than those that would result from using POWHEG+HERWIG as an alternative model for unfolding. The differences between the fully corrected data distributions obtained in this way and the nominal ones are symmetrized and taken as systematic uncertainties.

The parton shower and hadronization systematic uncertainties (referred to as fragmentation) are evaluated by comparing the distributions obtained using ALPGEN+HERWIG and ALPGEN+PYTHIA to unfold the data. The ALPGEN+PYTHIA sample is generated using ALPGEN (v2.14) and uses the CTEQ5L PDF [64] for the hard process and parton shower.

The effect of IFSR modeling is determined by using two different ALPGEN+PYTHIA samples with varied radiation settings. The distribution of the number of additional partons is changed by varying the renormalization scale associated with α_{S} consistently in the hard matrix element as well as in the parton shower. The parameters controlling the level of radiation via parton showering [65] were adjusted to encompass the ATLAS measurement of additional jet activity in $t\bar{t}$ events [66]. These samples are generated with dedicated Perugia 2011 tunes and used to fully correct the data through the unfolding. The IFSR uncertainty is assumed to be half the difference between the two unfolded distributions.

The PDF systematic uncertainty is evaluated by studying the effect on the signal efficiency of using different PDF sets to reweight simulated events at the hard-process level. The PDF sets used are CT10 [25], MSTW2008NLO [67], and NNPDF2.3 [68]. Both the uncertainties within a given PDF set and the variations between the different PDF sets are taken into account [69].

The systematic uncertainties due to the finite size of the simulated samples are evaluated by varying the content of the migration matrix within statistical uncertainties and evaluating the standard deviation of the ensemble of results unfolded with the varied matrices. Simultaneously, the efficiency is rederived using the parton spectrum projected from the varied migration matrix and therefore accounts for the same statistical fluctuations.

C. Background modeling

The normalization of the W + jets background is varied within the uncertainty of the data-driven method, which amounts to 15% and 13% for the e + jets and μ + jets

channels, respectively. An additional uncertainty of 18% ($e+$jets) and 21% ($\mu+$jets) comes from determining the flavor composition of the sample. This includes the uncertainty on the extrapolation of the flavor composition to jet multiplicities beyond two (the $f^{\text{tag}}_{2\to\geq 4}$ term described in Sec. VI B).

The multijet background uncertainties are estimated by comparing alternative estimates and their agreement with data in control regions. The resulting normalization uncertainties are 50% and 20% for the $e+$jets and $\mu+$jets channels respectively.

The statistical uncertainty on the background simulation samples is taken into account by fluctuating the background sum with a Gaussian distribution in each bin within the uncertainties and propagating the effect to the unfolded distributions.

The uncertainty on the $Z+$jets background normalization is taken to be 50% in the four-jet bin and the uncertainty on the diboson normalization is taken to be 40% in the same jet multiplicity bin. The effect of these uncertainties in the final results is negligible. Effects of the uncertainties in the normalizations of the single top and dilepton $t\bar{t}$ backgrounds are also negligible.

D. Main sources of systematic uncertainties

For p_{T}^{t} and $m_{t\bar{t}}$ the largest systematic uncertainties come from JES, signal generator choice, and b-quark tagging efficiency. For $p_{\text{T}}^{t\bar{t}}$ the uncertainty from IFSR is the largest, followed by signal generator choice, fragmentation, and jet energy resolution. Finally, for $y_{t\bar{t}}$ the main uncertainties come from the signal generator choice and fragmentation.

X. RESULTS

The unfolded and combined normalized differential cross sections are shown in Table V. The absolute cross sections, calculated by integrating the spectra before normalization (160 pb for the $e+$jets and $\mu+$jets channels combined, with a relative uncertainty of 15%), agree with

TABLE V. Normalized differential cross sections for the different variables considered. The cross section in each bin is given as the integral of the normalized differential cross section over the bin width, divided by the bin width. The calculation of the cross sections in the last bins includes events falling outside of the bin edges, and the normalization is done within the quoted bin width. The reported total uncertainty in the second column is obtained by adding the statistical and systematic uncertainties in quadrature.

p_{T}^{t} [GeV]	$\frac{1}{\sigma}\frac{d\sigma}{dp_{\text{T}}^{t}}$ [10^{-3} GeV^{-1}]	Statistical [%]	Systematic [%]
0–50	3.4 ± 0.2	± 2.4	± 5.1
50–100	6.7 ± 0.2	± 1.2	± 1.9
100–150	5.3 ± 0.2	± 2.5	± 2.6
150–200	2.6 ± 0.1	± 2.0	± 4.8
200–250	1.12 ± 0.06	± 2.4	± 4.8
250–350	0.32 ± 0.02	± 3.5	± 5.5
350–800	0.018 ± 0.002	± 6.1	± 11
$m_{t\bar{t}}$ [GeV]	$\frac{1}{\sigma}\frac{d\sigma}{dm_{t\bar{t}}}$ [10^{-3} GeV^{-1}]	Statistical [%]	Systematic [%]
250–450	2.52 ± 0.09	± 1.2	± 3.1
450–550	2.76 ± 0.09	± 1.5	± 2.8
550–700	1.01 ± 0.05	± 2.7	± 4.2
700–950	0.23 ± 0.02	± 3.2	± 6.3
950–2700	0.0071 ± 0.0007	± 5.5	± 8.5
$p_{\text{T}}^{t\bar{t}}$ [GeV]	$\frac{1}{\sigma}\frac{d\sigma}{dp_{\text{T}}^{t\bar{t}}}$ [10^{-3} GeV^{-1}]	Statistical [%]	Systematic [%]
0–40	14.1 ± 0.09	± 1.5	± 6.2
40–170	3.0 ± 0.2	± 1.8	± 7.4
170–340	0.25 ± 0.04	± 4.5	± 16
340–1000	0.008 ± 0.001	± 7.7	± 16
$\lvert y_{t\bar{t}}\rvert$	$\frac{1}{\sigma}\frac{d\sigma}{d\lvert y_{t\bar{t}}\rvert}$	Statistical [%]	Systematic [%]
0.0–0.5	0.86 ± 0.03	± 0.7	± 3.2
0.5–1.0	0.64 ± 0.01	± 0.4	± 1.6
1.0–2.5	0.17 ± 0.01	± 0.9	± 7.5

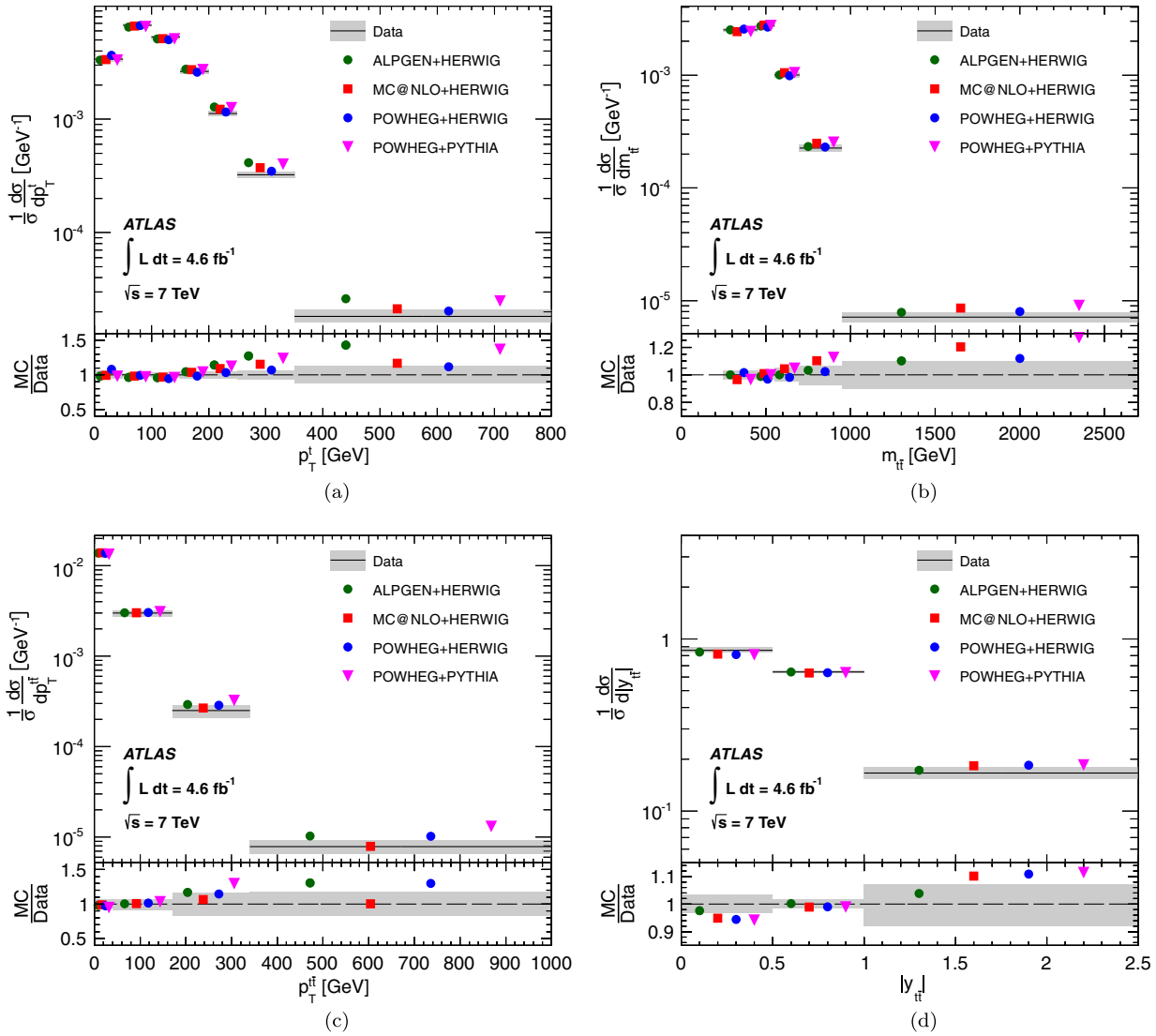

FIG. 8 (color online). Normalized differential cross sections for the (a) transverse momentum of the hadronically decaying top quark (p_{T}^{t}), and the (b) mass ($m_{t\bar{t}}$), (c) transverse momentum ($p_{\mathrm{T}}^{t\bar{t}}$) and the (d) absolute value of the rapidity ($|y_{t\bar{t}}|$) of the $t\bar{t}$ system. Generator predictions are shown as markers for ALPGEN+HERWIG (circles), MC@NLO+HERWIG (squares), POWHEG+HERWIG (triangles), and POWHEG+PYTHIA (inverted triangles). The markers are offset within each bin to allow for better visibility. The gray bands indicate the total uncertainty on the data in each bin. The lower part of each figure shows the ratio of the generator predictions to data. For $p_{\mathrm{T}}^{t\bar{t}}$ the POWHEG+PYTHIA marker cannot be seen in the last bin of the ratio plot because it falls beyond the axis range. The cross section in each bin is given as the integral of the differential cross section over the bin width, divided by the bin width. The calculation of the cross sections in the last bins includes events falling outside of the bin edges, and the normalization is done within the quoted bin width. The bin ranges along the horizontal axis (and not the position of the markers) can be associated with the normalized differential cross-section values along the vertical axis.

the theoretical calculations within uncertainties. The total uncertainty is dominated by systematic sources as discussed in Sec. IX.

The unfolded distributions are also shown compared to different MC generators in Fig. 8. ALPGEN and MC@NLO use HERWIG for parton shower and hadronization, while the PDFs are different as mentioned in Sec. IV, and POWHEG is shown interfaced with both HERWIG and PYTHIA.

The covariance matrices for the normalized unfolded spectra due to the statistical and systematic uncertainties are displayed in Table VI. They are obtained by evaluating the covariance between the kinematic bins using pseudoexperiments simultaneously in both the $e+\mathrm{jets}$ and $\mu+\mathrm{jets}$ channels and combining them as described in Sec. VIII B.

The correlations due to statistical fluctuations are shown in Appendix B. They are evaluated by varying the data event counts independently in every bin before unfolding, propagating the statistical uncertainties through the unfolding separately for the $e+\mathrm{jets}$ and $\mu+\mathrm{jets}$ channels, and then performing the combination of the two channels.

TABLE VI. Bin-wise full covariance matrices for the normalized differential cross sections. From top to bottom: top-quark p_{T}; and mass, transverse momentum, and absolute value of the rapidity of the $t\bar{t}$ system. The elements of the covariance matrices are in units of 10^{-6} GeV^{-2} for all the spectra except for $|y_{t\bar{t}}|$.

p_{T}^{t} [GeV]	0–50	50–100	100–150	150–200	200–250	250–350	350–800
0–50	4.34×10^{-2}	1.04×10^{-2}	-2.13×10^{-2}	-2.23×10^{-2}	-8.16×10^{-3}	-1.49×10^{-3}	1.06×10^{-4}
50–100	1.04×10^{-2}	2.97×10^{-2}	-1.39×10^{-2}	-1.36×10^{-2}	-7.13×10^{-3}	-2.10×10^{-3}	-1.43×10^{-4}
100–150	-2.13×10^{-2}	-1.39×10^{-2}	3.25×10^{-2}	3.70×10^{-3}	-2.39×10^{-5}	-2.73×10^{-4}	-4.08×10^{-5}
150–200	-2.23×10^{-2}	-1.36×10^{-2}	3.70×10^{-3}	2.06×10^{-2}	8.48×10^{-3}	1.68×10^{-3}	-2.64×10^{-5}
200–250	-8.16×10^{-3}	-7.13×10^{-3}	-2.39×10^{-5}	8.48×10^{-3}	4.44×10^{-3}	1.09×10^{-3}	2.44×10^{-5}
250–350	-1.49×10^{-3}	-2.10×10^{-3}	-2.73×10^{-4}	1.68×10^{-3}	1.09×10^{-3}	4.44×10^{-4}	2.33×10^{-5}
350–800	1.06×10^{-4}	-1.43×10^{-4}	-4.08×10^{-5}	-2.64×10^{-5}	2.44×10^{-5}	2.33×10^{-5}	3.78×10^{-6}

$m_{t\bar{t}}$ [GeV]	250–450	450–550	550–700	700–950	950–2700
250–450	7.28×10^{-3}	-6.76×10^{-3}	-3.66×10^{-3}	-7.62×10^{-4}	-2.29×10^{-5}
450–550	-6.76×10^{-3}	8.20×10^{-3}	3.06×10^{-3}	2.77×10^{-4}	1.99×10^{-6}
550–700	-3.66×10^{-3}	3.06×10^{-3}	2.43×10^{-3}	2.21×10^{-4}	3.25×10^{-6}
700–950	-7.62×10^{-4}	2.77×10^{-4}	2.21×10^{-4}	2.85×10^{-4}	1.16×10^{-5}
950–2700	-2.29×10^{-5}	1.99×10^{-6}	3.25×10^{-6}	1.16×10^{-5}	5.60×10^{-7}

$p_{\mathrm{T}}^{t\bar{t}}$ [GeV]	[0,40]	[40,170]	[170,340]	[340,1000]
[0,40]	7.70×10^{-1}	-1.92×10^{-1}	-3.16×10^{-2}	-6.19×10^{-4}
[40,170]	-1.92×10^{-1}	4.89×10^{-2}	7.34×10^{-3}	1.31×10^{-4}
[170,340]	-3.16×10^{-2}	7.34×10^{-3}	1.68×10^{-3}	3.82×10^{-5}
[340,1000]	-6.19×10^{-4}	1.31×10^{-4}	3.82×10^{-5}	1.78×10^{-6}

$\lvert y_{t\bar{t}} \rvert$	0.0–0.5	0.5–1.0	1.0–2.5
0.0–0.5	6.35×10^{-4}	1.72×10^{-4}	-2.69×10^{-4}
0.5–1.0	1.72×10^{-4}	9.56×10^{-5}	-8.90×10^{-5}
1.0–2.5	-2.69×10^{-4}	-8.90×10^{-5}	1.19×10^{-4}

Large off-diagonal correlations come from the normalization constraint for the spectra and the regularization in the unfolding procedure. The statistical correlations between bins of different variables have also been evaluated and are presented in Appendix B.

XI. INTERPRETATION

The level of agreement between the measured distributions, simulations with different MC generators and theoretical predictions was quantified by calculating χ^2 values, employing the full covariance matrices, evaluated as described in Sec. X, and inferring p-values (probabilities that the χ^2 is larger than or equal to the observed value) from the χ^2 and the number of degrees of freedom (NDF). The normalization constraint used to derive the normalized differential cross sections lowers by one unit the NDF and the rank of the $N_{\mathrm{b}} \times N_{\mathrm{b}}$ covariance matrix, where N_{b} is the number of bins of the spectrum under consideration. In order to evaluate the χ^2 the following relation was used:

$$\chi^2 = V_{N_{\mathrm{b}}-1}^{\mathrm{T}} \cdot \mathrm{Cov}_{N_{\mathrm{b}}-1}^{-1} \cdot V_{N_{\mathrm{b}}-1} \tag{9}$$

where $V_{N_{\mathrm{b}}-1}$ is the vector of differences between data and predictions obtained discarding one of the N_{b} elements and $\mathrm{Cov}_{N_{\mathrm{b}}-1}$ is the $(N_{\mathrm{b}}-1) \times (N_{\mathrm{b}}-1)$ submatrix derived from the full covariance matrix discarding the corresponding row and column. The submatrix obtained in this way is invertible and allows the χ^2 to be computed. The χ^2 value does not depend on the choice of the element discarded for the vector $V_{N_{\mathrm{b}}-1}$ and the corresponding submatrix $\mathrm{Cov}_{N_{\mathrm{b}}-1}$.

The predictions from MC generators do not include theoretical uncertainties and were evaluated using a specific set of tuned parameters. The p-values comparing the measured spectra to the predictions of MC generators shown in Fig. 8 are listed in Table VII. No single generator performs best for all the kinematic variables; however, the difference in χ^2 between generators demonstrates that the data have sufficient precision to probe the predictions. For p_{T}^{t} the agreement with ALPGEN+HERWIG and POWHEG +PYTHIA is particularly bad due to a significant discrepancy in the tail of the distribution. MC@NLO+HERWIG and POWHEG+HERWIG predict shapes closer to the measured distribution. As can be seen in Fig. 8, there is a general trend of data being softer in p_{T}^{t} above 200 GeV compared to all generators. The shape of the $m_{t\bar{t}}$ distribution is best described by ALPGEN+HERWIG and POWHEG+HERWIG. The $p_{\mathrm{T}}^{t\bar{t}}$ shape is described best by MC@NLO+HERWIG

TABLE VII. Comparison between the measured normalized differential cross sections and the predictions from several MC generators and theoretical calculations. For each variable and prediction a χ^2 and a p-value are calculated using the covariance matrix of each measured spectrum. The number of degrees of freedom (NDF) is equal to $N_b - 1$ where N_b is the number of bins in the distribution. In the last column p_T^t, $m_{t\bar{t}}$, and $p_T^{t\bar{t}}$ are compared to NLO + NNLL predictions [12] and [13–15].

	ALPGEN+HERWIG		MC@NLO+HERWIG		POWHEG+HERWIG		POWHEG+PYTHIA		NLO QCD		NLO + NNLL	
Variable	χ^2/NDF	p-value	χ^2/NDF	p-value	χ^2/NDF	p-value	χ^2/NDF	p-value	χ^2/NDF	p-value	χ^2/NDF	p-value
p_T^t	24.0/6	0.00	8.0/6	0.24	4.8/6	0.57	18.9/6	0.00	9.5/6	0.15	7.6/6	0.27
$m_{t\bar{t}}$	2.6/4	0.63	6.9/4	0.14	5.5/4	0.24	12.9/4	0.01	5.5/4	0.24	5.9/4	0.20
$p_T^{t\bar{t}}$	4.2/3	0.25	0.5/3	0.93	3.5/3	0.32	17.8/3	0.00	14.4/3	0.00	8.6/3	0.02
$\lvert y_{t\bar{t}}\rvert$	1.6/2	0.45	3.4/2	0.18	4.3/2	0.11	4.8/2	0.09	3.7/2	0.16		

and particularly badly by POWHEG+PYTHIA while the $y_{t\bar{t}}$ shape is described best by ALPGEN+HERWIG.

The distributions are also shown compared to QCD calculations at NLO (based on MCFM [70] version 6.5 with the CT10 PDF) in Fig. 9 and to NLO + NNLL calculations for p_T^t [12], $m_{t\bar{t}}$ [13], and $p_T^{t\bar{t}}$ [14,15], all using the MSTW2008NNLO [67] PDF, in Fig. 10. The p-values for these comparisons are shown in Table VII.

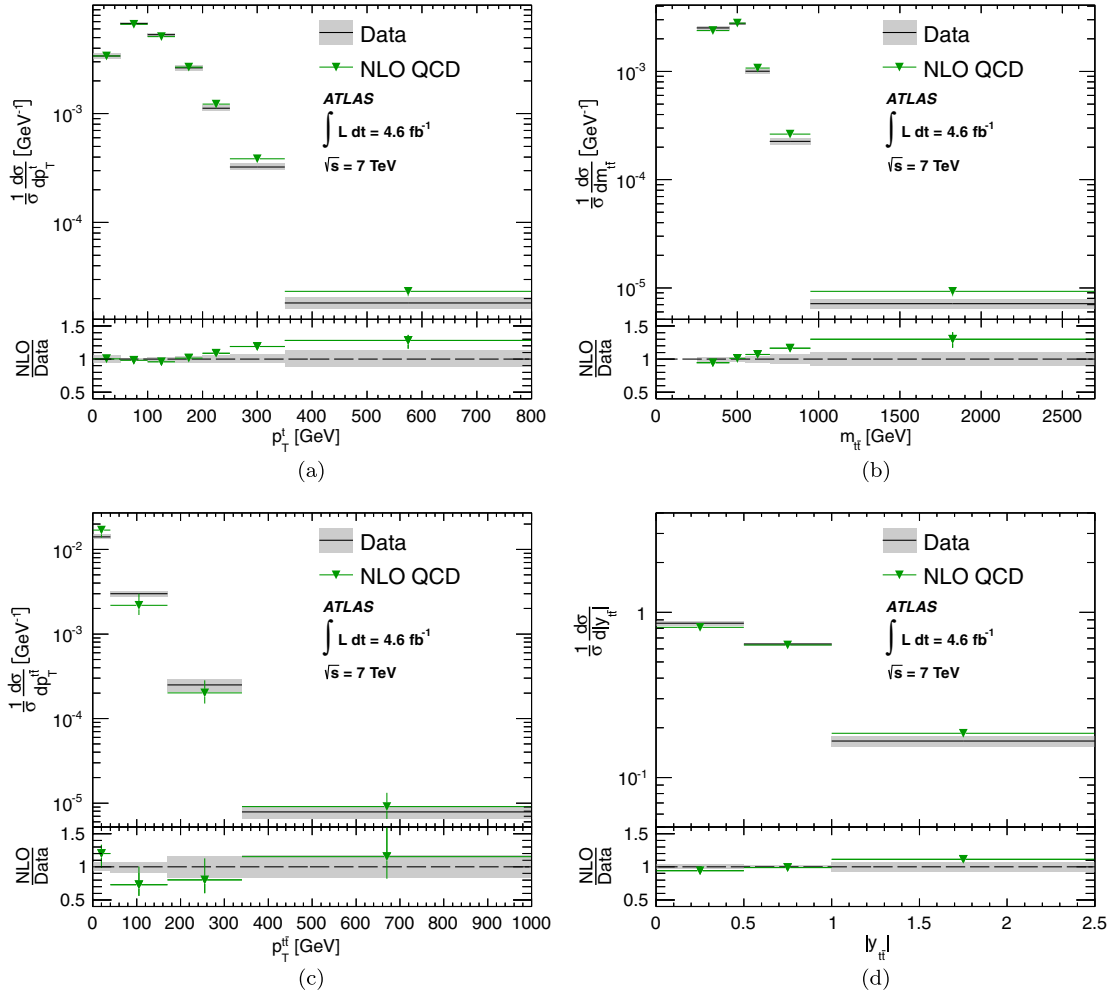

FIG. 9 (color online). Normalized differential cross sections for the (a) transverse momentum of the hadronically decaying top-quark (p_T^t), and the (b) mass ($m_{t\bar{t}}$), (c) transverse momentum ($p_T^{t\bar{t}}$) and the (d) absolute value of the rapidity ($|y_{t\bar{t}}|$) of the $t\bar{t}$ system. The distributions are compared to NLO QCD predictions (based on MCFM [70] with the CT10 PDF). The bin ranges along the horizontal axis (and not the position of the markers) can be associated with the normalized differential cross-section values along the vertical axis. The error bars correspond to the PDF and fixed scale uncertainties in the theoretical prediction. The gray bands indicate the total uncertainty on the data in each bin. The lower part of each figure shows the ratio of the NLO QCD predictions to data. The cross section in each bin is given as the integral of the differential cross section over the bin width, divided by the bin width. The calculation of the cross sections in the last bins includes events falling outside of the bin edges, and the normalization is done within the quoted bin width.

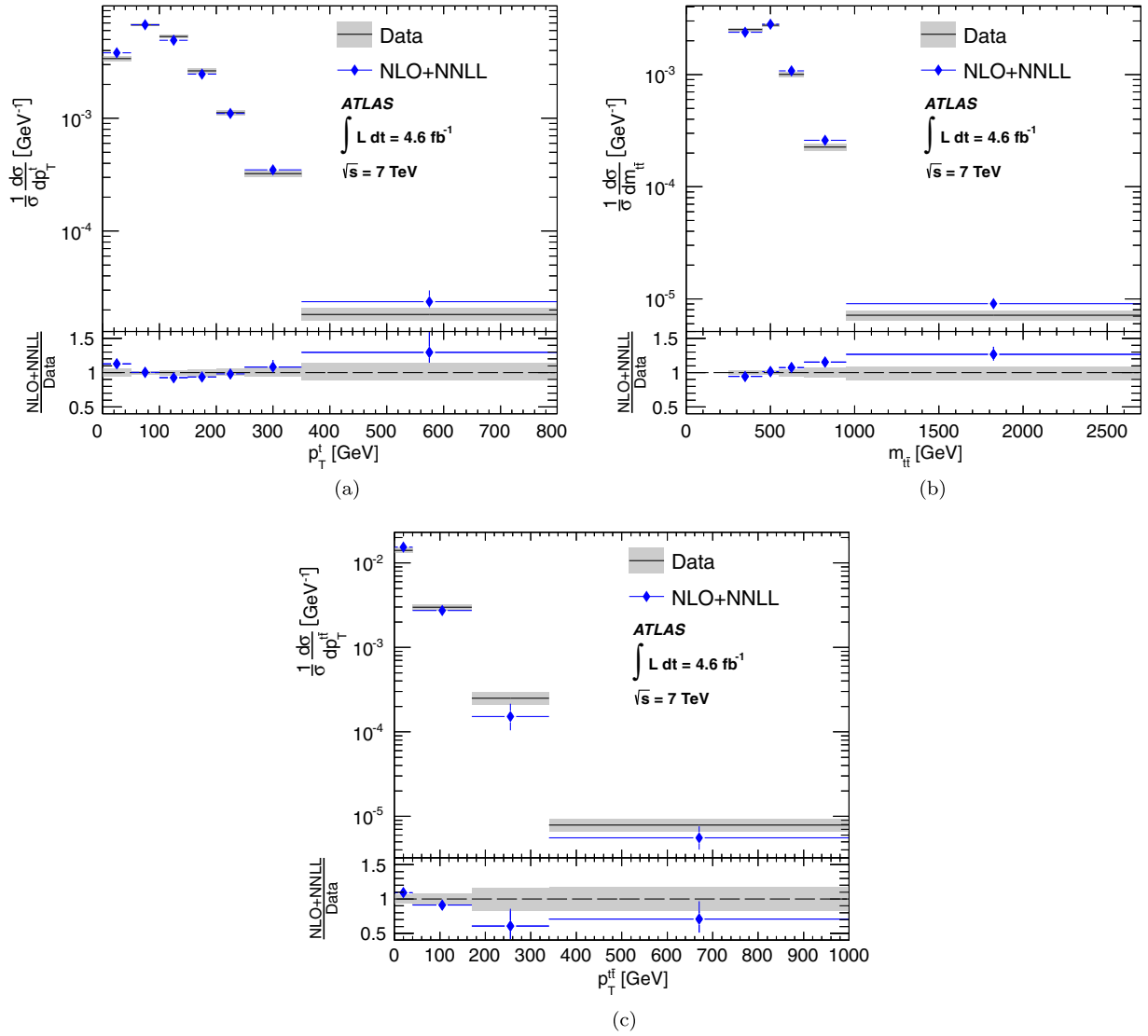

FIG. 10 (color online). Normalized differential cross sections for the (a) transverse momentum of the hadronically decaying top-quark (p_{T}^{t}), the (b) mass of the $t\bar{t}$ system ($m_{t\bar{t}}$), and the (c) transverse momentum of the $t\bar{t}$ system ($p_{\mathrm{T}}^{t\bar{t}}$). The distributions are compared to the predictions from NLO + NNLL calculations for p_{T}^{t} [12], $m_{t\bar{t}}$ [13], and $p_{\mathrm{T}}^{t\bar{t}}$ [14,15], all using the MSTW2008NNLO PDF. The bin ranges along the horizontal axis (and not the position of the markers) can be associated with the normalized differential cross-section values along the vertical axis. The error bars correspond to the fixed (and dynamic in the case of p_{T}^{t}) scale uncertainties in the theoretical prediction. The gray bands indicate the total uncertainty on the data in each bin. The lower part of each figure shows the ratio of the NLO + NNLL calculations to data. The cross section in each bin is given as the integral of the differential cross section over the bin width, divided by the bin width. The calculation of the cross sections in the last bins includes events falling outside of the bin edges, and the normalization is done within the quoted bin width.

The uncertainties in the NLO predictions due to the parton distribution functions were evaluated at the 68% confidence level (C.L.) using the CT10 PDF error sets. Another source of uncertainty considered is the one related to the factorization and renormalization scales. The nominal value was assumed to be $\mu = m_{\mathrm{t}}$ for both scales, and is varied simultaneously up and down from $2m_t$ to $m_t/2$. The full covariance matrix, including the bin-wise correlations induced by the uncertainties in the scale and in the different PDF components, was used for the χ^2 evaluation.

For the NLO + NNLL predictions of $m_{t\bar{t}}$ and $p_{\mathrm{T}}^{t\bar{t}}$ spectra, the calculation is performed using the mass of the $t\bar{t}$ system as the dynamic scale of the process. The uncertainties come from doubling and halving this scale and from the PDF uncertainty evaluated at the 68% C.L. using the MSTW2008NNLO PDF error sets. For the NLO + NNLL prediction of the p_{T}^{t} spectrum, besides the fixed scale uncertainty, the contribution of the alternative dynamic scale $\mu = \sqrt{m_t^2 + p_{\mathrm{T}}^{t\,2}}$ is also included; in this case the PDF uncertainty is not provided. For both the

above theoretical calculations the bin-wise correlations were taken into account in evaluating the χ^2s and p-values, which are shown in Table VII.

The data are softer than both the NLO and NLO + NNLL QCD calculations in the tail of the p_{T}^{t} distribution. The measured $m_{t\bar{t}}$ spectrum also falls more quickly than either the NLO or NLO + NNLL predictions. The $p_{\mathrm{T}}^{t\bar{t}}$ spectrum agrees poorly with both the NLO and NLO + NNLL predictions. No electroweak corrections are included in these predictions, and these were shown in Refs. [71–74] to have non-negligible effects in the p_{T}^{t} and $m_{t\bar{t}}$ distributions.

The predictions of various NLO PDF sets are evaluated using MCFM, interfaced to four different PDF sets: CT10 [25], MSTW2008NLO [67], NNPDF2.3 [68], and HERAPDF1.5 [75]. The uncertainties in the predictions include the PDF uncertainties [76] and the fixed scale uncertainties already described. The comparisons between data and the different predictions are presented in Fig. 11 for the normalized differential cross sections and the p-values for these comparisons are shown in Table VIII. The significant changes in χ^2 between the different PDF sets for the p_{T}^{t}, $m_{t\bar{t}}$, and $y_{t\bar{t}}$ distributions indicate that the data can be used to improve the precision of future PDF fits.

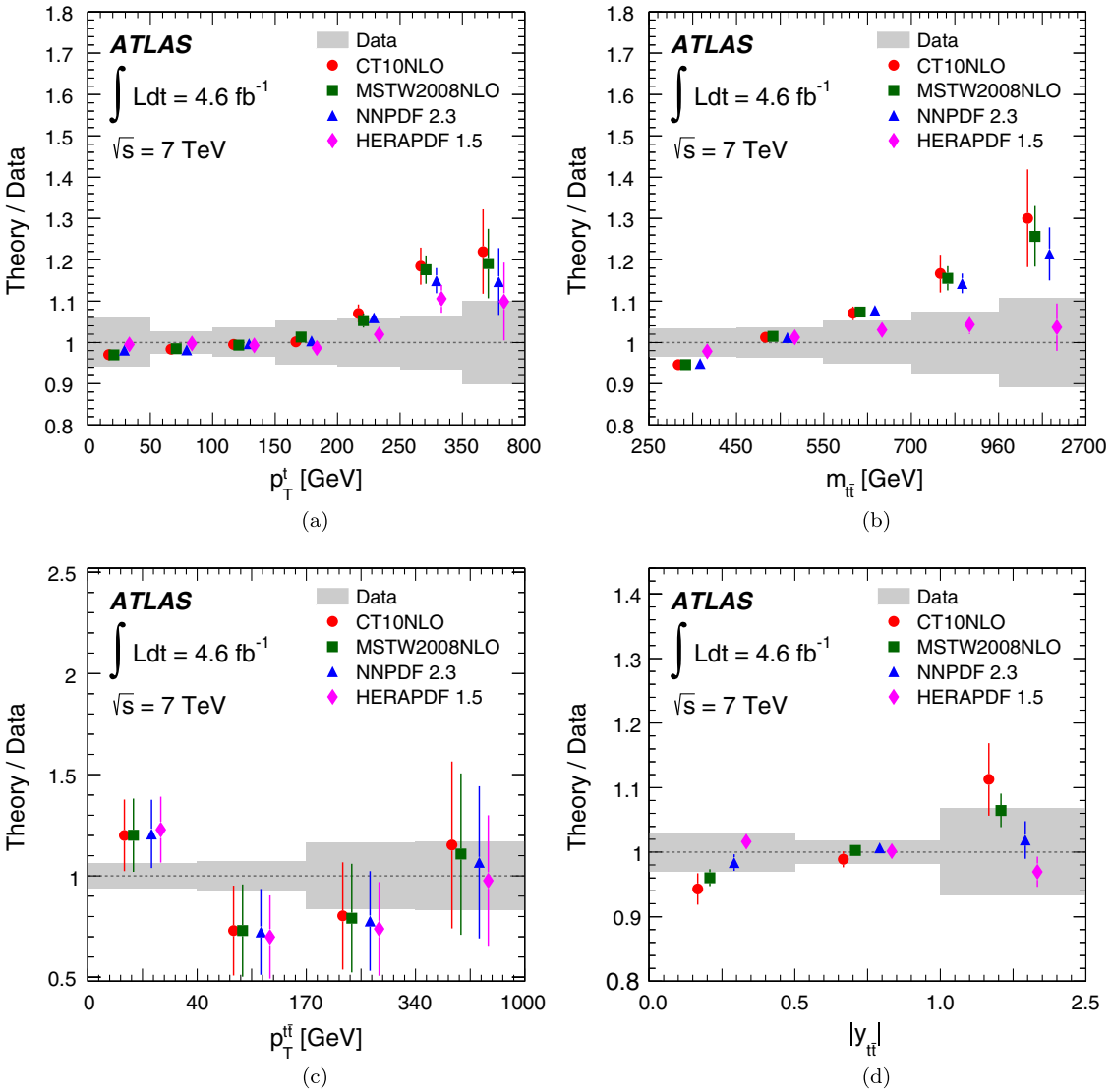

FIG. 11 (color online). Ratios of the NLO QCD predictions [70] to the measured normalized differential cross sections for different PDF sets (CT10 [25], MSTW2008NLO [67], NNPDF2.3 [68], and HERAPDF1.5 [75]) (markers) for the (a) transverse momentum of the hadronically decaying top-quark (p_{T}^{t}), and the (b) mass ($m_{t\bar{t}}$), the (c) transverse momentum ($p_{\mathrm{T}}^{t\bar{t}}$), and the (d) absolute value of the rapidity ($|y_{t\bar{t}}|$) of the $t\bar{t}$ system. The markers are offset in each bin and the bins are of equal size to allow for better visibility. The gray bands indicate the total uncertainty on the data in each bin, while the error bars denote the uncertainties in the predictions, which include the internal PDF set variations and also fixed scale uncertainties.

TABLE VIII. Comparison between the measured normalized differential cross sections and the NLO predictions (MCFM) for different parton distribution functions. For each kinematic variable and each parton distribution function, a χ^2 and a p-value are calculated using the covariance matrix of each measured spectrum as well as the theory PDF and scale covariance matrix. The number of degrees of freedom (NDF) is equal to $N_b - 1$ where N_b is the number of bins in the distribution.

	CT10		MSTW2008NLO		NNPDF 2.3		HERAPDF 1.5	
Variable	χ^2/NDF	p-value	χ^2/NDF	p-value	χ^2/NDF	p-value	χ^2/NDF	p-value
p_T^t	9.5/6	0.15	9.8/6	0.14	8.2/6	0.22	5.5/6	0.49
$m_{t\bar{t}}$	5.5/4	0.24	6.0/4	0.20	5.2/4	0.27	0.63/4	0.96
$p_T^{t\bar{t}}$	14.4/3	0.00	13.0/3	0.01	12.4/3	0.01	9.1/3	0.03
$\lvert y_{t\bar{t}}\rvert$	3.7/2	0.16	4.0/2	0.13	1.3/2	0.52	0.44/2	0.80

As can be seen in Fig. 11, a certain tension between data and all predictions is observed in the case of the top-quark p_T distribution at high p_T values. For the $m_{t\bar{t}}$ distribution, the agreement with HERAPDF1.5 is better than that with the other PDF predictions. For the $p_T^{t\bar{t}}$ distribution, one should note that MCFM is effectively only a leading-order calculation and resummation effects are expected to play an important role at low $p_T^{t\bar{t}}$. Finally, for the $|y_{t\bar{t}}|$ distribution, the NNPDF2.3 and especially HERAPDF1.5 sets are in better agreement with the data.

XII. CONCLUSION

Kinematic distributions of the top quarks in $t\bar{t}$ events, selected in the ℓ + jets channel, were measured using data from 7 TeV proton–proton collisions collected by the ATLAS detector at the CERN Large Hadron Collider. This data set corresponds to an integrated luminosity of 4.6 fb^{-1}. Normalized differential cross sections have been measured as a function of the top-quark transverse momentum and as a function of the mass, transverse momentum, and rapidity of the $t\bar{t}$ system. These results agree with the previous ATLAS measurements and supersede them with a larger data set, smaller uncertainties, and an additional variable.

In general the Monte Carlo predictions and the QCD calculations agree with data in a wide kinematic region. However, data are softer than all predictions in the tail of the p_T^t spectrum, particularly in the case of the ALPGEN +HERWIG and POWHEG+PYTHIA generators. The same trend is observed for the NLO + NNLL predictions of the $m_{t\bar{t}}$ and p_T^t spectra which tend to be above the data in the tail of the distributions. Nevertheless the overall agreement is still found to be reasonable for these two variables while it is worst for $p_T^{t\bar{t}}$. The distributions show some preference for HERAPDF1.5 when used in conjunction with a fixed-order NLO QCD calculation. More precise conclusions about PDFs will be possible from the comparison of these measurements to future calculations at NNLO + NNLL in QCD and after including electroweak effects.

ACKNOWLEDGMENTS

We thank CERN for the very successful operation of the LHC, as well as the support staff from our institutions without whom ATLAS could not be operated efficiently. We acknowledge the support of ANPCyT, Argentina; YerPhI, Armenia; ARC, Australia; BMWF and FWF, Austria; ANAS, Azerbaijan; SSTC, Belarus; CNPq and FAPESP, Brazil; NSERC, NRC and CFI, Canada; CERN; CONICYT, Chile; CAS, MOST and NSFC, China; COLCIENCIAS, Colombia; MSMT CR, MPO CR and VSC CR, Czech Republic; DNRF, DNSRC and Lundbeck Foundation, Denmark; EPLANET, ERC and NSRF, European Union; IN2P3-CNRS, CEA-DSM/IRFU, France; GNSF, Georgia; BMBF, DFG, HGF, MPG and AvH Foundation, Germany; GSRT and NSRF, Greece; ISF, MINERVA, GIF, DIP and Benoziyo Center, Israel; INFN, Italy; MEXT and JSPS, Japan; CNRST, Morocco; FOM and NWO, Netherlands; BRF and RCN, Norway; MNiSW, Poland; GRICES and FCT, Portugal; MERYS (MECTS), Romania; MES of Russia and ROSATOM, Russian Federation; JINR; MSTD, Serbia; MSSR, Slovakia; ARRS and MIZŠ, Slovenia; DST/NRF, South Africa; MICINN, Spain; SRC and Wallenberg Foundation, Sweden; SER, SNSF and Cantons of Bern and Geneva, Switzerland; NSC, Taiwan; TAEK, Turkey; STFC, the Royal Society and Leverhulme Trust, United Kingdom; DOE and NSF, United States of America. The crucial computing support from all WLCG partners is acknowledged gratefully, in particular from CERN and the ATLAS Tier-1 facilities at TRIUMF (Canada), NDGF (Denmark, Norway, Sweden), CC-IN2P3 (France), KIT/GridKA (Germany), INFN-CNAF (Italy), NL-T1 (Netherlands), PIC (Spain), ASGC (Taiwan), RAL (UK) and BNL (USA) and in the Tier-2 facilities worldwide.

APPENDIX A: ADDITIONAL TABLES OF SYSTEMATIC UNCERTAINTIES

Included here are Tables IX, X, XI, and XII with the contribution of each individual source of systematic uncertainty calculated as a percentage of the normalized differential cross section in each bin for each variable. Those that

TABLE IX. The individual systematic uncertainties calculated as a percentage of the normalized differential cross section in each bin.

$\frac{1}{\sigma}\frac{d\sigma}{dp_{\mathrm{T}}^{t}}$ Uncertainties [%]/Bins [GeV]	0–50	50–100	100–150	150–200	200–250	250–350	350–800
b-quark jets (JES)	−1.81 +1.52	−0.41 +0.55	+1.12 −0.97	+0.89 −1.10	+0.46 −0.52	+0.07 −0.23	−0.01 −0.11
Close-by jets (JES)	−1.56 +1.45	−0.45 +0.61	+0.40 −0.77	+1.39 −1.01	+1.13 −1.02	+1.47 −1.39	+1.80 −1.65
Effective detector NP set 1 (JES)	−1.51 +1.06	−0.47 +0.54	+0.54 −0.40	+1.16 −1.20	+1.20 −1.04	+1.17 −0.97	+1.49 −0.51
Effective detector NP set 2 (JES)	−0.21 +0.09	+0.00 +0.05	−0.06 −0.08	+0.24 −0.06	+0.23 +0.05	+0.12 −0.18	+0.28 −0.26
Effective mixed NP set 1 (JES)	−0.03 +0.04	−0.02 +0.11	−0.07 −0.12	+0.11 −0.09	+0.07 −0.10	+0.23 +0.04	+0.79 +0.34
Effective mixed NP set 2 (JES)	−0.03 +0.03	−0.03 +0.12	+0.04 −0.25	−0.01 +0.07	+0.04 +0.00	+0.08 +0.18	+0.24 +0.85
Effective model NP set 1 (JES)	+0.28 +0.05	+0.02 +0.04	−0.28 −0.22	+0.30 −0.24	+0.19 +0.48	−0.64 +0.85	−1.40 +1.51
Effective model NP set 2 (JES)	−0.53 +0.59	−0.10 +0.17	−0.11 −0.22	+0.62 −0.38	+0.63 −0.51	+0.76 −0.48	+1.34 −0.48
Effective model NP set 3 (JES)	+0.66 −0.80	+0.23 −0.14	−0.34 +0.05	−0.44 +0.69	−0.46 +0.84	−0.42 +0.77	−0.28 +0.88
Effective model NP set 4 (JES)	−0.14 +0.16	+0.03 +0.02	−0.06 −0.12	+0.08 +0.03	+0.21 −0.06	+0.10 −0.05	+0.23 +0.10
Effective statistical NP set 1 (JES)	+0.52 −0.65	+0.26 −0.07	−0.39 +0.02	−0.18 +0.39	−0.20 +0.61	−0.82 +0.92	−1.16 +1.53
Effective statistical NP set 2 (JES)	−0.20 +0.21	+0.04 +0.06	−0.05 −0.14	+0.15 −0.07	+0.10 −0.12	+0.19 −0.14	+0.49 +0.04
Effective statistical NP set 3 (JES)	−0.44 +0.43	−0.14 +0.18	+0.16 −0.30	+0.33 −0.20	+0.39 −0.28	+0.32 −0.30	+0.46 −0.02
η-intercalibration (JES)	−0.71 +0.63	−0.14 +0.26	+0.24 −0.35	+0.64 −0.69	+0.39 −0.23	−0.06 +0.00	−0.29 +0.19
η-intercalibration statistics (JES)	−0.15 −0.16	−0.06 −0.01	−0.02 +0.02	+0.24 +0.08	+0.34 +0.03	+0.02 +0.20	+0.13 +0.62
Flavor composition (JES)	+0.02 +0.13	−0.00 +0.23	−0.13 −0.23	+0.04 −0.15	+0.25 −0.19	+0.27 −0.26	+0.43 +0.01
Flavor response (JES)	+0.41 −0.81	+0.17 −0.11	−0.24 +0.39	−0.26 +0.21	−0.15 +0.44	−0.47 +0.46	−0.51 +0.64
Pile-up offset μ (JES)	−0.02 +0.35	−0.11 +0.02	−0.10 −0.22	+0.23 −0.19	+0.50 +0.19	+0.28 +0.07	+0.05 +0.60
Pile-up offset N_{PV} (JES)	+0.13 −0.28	+0.13 +0.08	−0.20 −0.06	−0.06 +0.05	−0.09 +0.24	−0.05 +0.31	+0.25 +0.62
Relative nonclosure MC (JES)	−0.08 +0.10	−0.02 +0.13	−0.13 −0.24	+0.23 +0.01	+0.30 +0.01	+0.18 −0.05	+0.25 +0.26
Single particle high-p_{T} (JES)	+0.02 +0.02	−0.01 −0.01	+0.01 −0.00	+0.01 +0.01	+0.01 +0.01	−0.02 −0.02	−0.02 −0.01
JES uncertainty in background	−0.05 +0.14	+0.39 −0.04	+0.03 −0.13	−0.58 −0.07	−0.98 +0.29	−0.21 +0.27	+0.74 +1.23
Jet energy resolution	+0.44 −0.44	+0.12 −0.12	−0.51 +0.51	+0.01 −0.01	+0.30 −0.31	−0.07 +0.07	+0.53 −0.54
Jet reconstruction efficiency	+0.10 −0.10	+0.01 −0.01	−0.05 +0.05	−0.03 +0.03	−0.03 +0.03	−0.07 +0.07	−0.14 +0.15
b-quark tagging efficiency	−1.36 +1.09	−0.77 +0.59	+0.35 −0.35	+1.33 −1.08	+2.06 −1.50	+2.59 −1.61	+3.00 −1.62
c-quark tagging efficiency	−0.03 +0.01	+0.01 −0.01	+0.07 −0.07	−0.06 +0.06	−0.10 +0.10	−0.12 +0.12	−0.23 +0.23
Light-jet tagging efficiency	+0.30 −0.29	+0.03 −0.03	−0.22 +0.22	−0.03 +0.02	−0.01 +0.00	+0.07 −0.07	+0.21 −0.18
e energy resolution	−0.06 +0.07	+0.04 −0.03	+0.01 +0.02	−0.05 −0.03	−0.12 −0.03	+0.13 +0.02	+0.42 −0.11
e energy scale	+0.22 −0.16	+0.04 +0.01	−0.15 +0.18	+0.01 −0.07	−0.03 −0.18	−0.19 −0.12	−0.34 +0.02
μ ID momentum resolution	+0.38 +0.38	+0.04 +0.10	−0.32 −0.40	−0.02 +0.00	+0.08 +0.08	+0.07 +0.09	+0.20 +0.23
μ MS momentum resolution	+0.39 +0.27	+0.18 +0.02	−0.43 −0.12	−0.13 −0.12	−0.03 −0.09	+0.08 −0.04	+0.32 +0.27
μ momentum scale	+0.27 −0.26	−0.00 +0.00	−0.29 +0.29	+0.04 −0.04	+0.27 −0.27	+0.28 −0.27	+0.36 −0.36
ℓ ID efficiency	+0.58 −0.56	+0.08 −0.08	−0.95 +0.92	+0.45 −0.43	+0.66 −0.63	+0.84 −0.80	+0.49 −0.47
ℓ reconstruction efficiency	+0.21 −0.21	+0.03 −0.03	−0.36 +0.35	+0.17 −0.17	+0.26 −0.25	+0.33 −0.33	+0.21 −0.21
ℓ trigger efficiency	−0.20 +0.19	−0.01 +0.01	+0.44 −0.43	−0.28 +0.28	−0.42 +0.41	−0.52 +0.52	−0.35 +0.35
$E_{\mathrm{T}}^{\mathrm{miss}}$ unassociated cells	−0.14 +0.42	−0.07 +0.05	+0.24 −0.37	+0.08 −0.14	−0.25 +0.30	−0.44 +0.29	+0.07 +0.31
$E_{\mathrm{T}}^{\mathrm{miss}}$ pile-up	−0.10 +0.56	−0.13 +0.09	+0.10 −0.59	−0.02 −0.11	+0.19 +0.39	+0.56 +0.55	+0.76 +0.71
MC generator	−1.52 +1.89	+0.54 −0.67	+0.16 −0.20	+1.52 −1.89	−0.11 +0.13	−2.79 +3.47	−8.57 +10.66
Fragmentation	−0.61 +0.58	+0.71 −0.68	−0.72 +0.70	+0.88 −0.84	−0.96 +0.92	−0.70 +0.68	+1.94 −1.87
IFSR	+2.23 −2.15	+0.90 −0.87	−0.08 +0.08	−3.22 +3.11	−3.22 +3.11	−1.56 +1.51	−0.09 +0.09
PDF	+0.14 −0.14	+0.14 −0.14	+0.04 −0.04	−0.16 +0.16	−0.45 +0.47	−0.81 +0.84	−0.79 +0.82
MC statistics	+1.01 −1.01	+0.40 −0.40	+0.67 −0.67	+0.90 −0.90	+1.08 −1.08	+1.44 −1.44	+2.60 −2.60
W + jets bb4	+0.32 −0.35	+0.05 −0.06	−0.14 +0.15	−0.12 +0.14	−0.12 +0.19	−0.32 +0.29	−0.29 +0.38
W + jets bb5	+0.32 +0.03	+0.05 +0.01	−0.14 −0.01	−0.12 −0.02	−0.12 −0.06	−0.32 +0.04	−0.29 −0.07
W + jets bbcc	−0.10 +0.09	−0.06 +0.06	−0.06 +0.06	+0.24 −0.23	+0.27 −0.26	+0.12 −0.12	+0.22 −0.23
W + jets bbccc	+1.08 −1.12	+0.20 −0.22	−0.48 +0.42	−0.45 +0.56	−0.50 +0.64	−0.84 +0.99	−1.00 +1.12
W + jets c4	+0.48 −0.38	+0.11 −0.11	−0.09 +0.12	−0.38 +0.29	−0.44 +0.33	−0.53 +0.36	−0.54 +0.34

(Table continued)

TABLE IX. (*Continued*)

$\frac{1}{\sigma}\frac{d\sigma}{dp_{\mathrm{T}}^{t}}$ Uncertainties [%]/Bins [GeV]	0–50	50–100	100–150	150–200	200–250	250–350	350–800
$W+$ jets c5	$^{+0.48}_{-0.16}$	$^{+0.11}_{-0.00}$	$^{-0.09}_{-0.03}$	$^{-0.38}_{+0.13}$	$^{-0.44}_{+0.16}$	$^{-0.53}_{+0.24}$	$^{-0.54}_{+0.24}$
$W+$ jets charge asymmetry	$^{+0.96}_{-1.11}$	$^{+0.17}_{-0.19}$	$^{-0.41}_{+0.51}$	$^{-0.44}_{+0.48}$	$^{-0.47}_{+0.49}$	$^{-0.64}_{+0.69}$	$^{-0.51}_{+0.57}$
Multijet normalization	$^{+1.35}_{-1.36}$	$^{+0.01}_{-0.01}$	$^{-0.75}_{+0.76}$	$^{-0.39}_{+0.40}$	$^{-0.11}_{+0.11}$	$^{+0.66}_{-0.67}$	$^{+0.76}_{-0.77}$
Multijet shape	$^{+0.11}_{-0.59}$	$^{+0.04}_{+0.07}$	$^{-0.46}_{+0.25}$	$^{+0.45}_{+0.12}$	$^{+0.46}_{+0.03}$	$^{+0.15}_{-0.14}$	$^{+0.11}_{-0.32}$
$Z+$ jets background normalization	$^{+0.59}_{-0.60}$	$^{+0.15}_{-0.15}$	$^{-0.42}_{+0.42}$	$^{-0.21}_{+0.21}$	$^{-0.16}_{+0.16}$	$^{-0.06}_{+0.06}$	$^{-0.13}_{+0.12}$
Dilepton background normalization	$^{+0.22}_{-0.21}$	$^{+0.10}_{-0.09}$	$^{-0.05}_{+0.04}$	$^{-0.16}_{+0.15}$	$^{-0.32}_{+0.30}$	$^{-0.43}_{+0.41}$	$^{-0.50}_{+0.47}$

TABLE X. The individual systematic uncertainties calculated as a percentage of the normalized differential cross section in each bin.

$\frac{1}{\sigma}\frac{d\sigma}{dm_{t\bar{t}}}$ Uncertainties [%]/Bins [GeV]	250–450	450–550	550–700	700–950	950–2700
b-quark jets (JES)	$^{-0.32}_{+0.53}$	$^{+0.25}_{-0.33}$	$^{+0.44}_{-0.78}$	$^{+0.40}_{-0.80}$	$^{+0.35}_{-0.93}$
Close-by jets (JES)	$^{-0.44}_{+0.45}$	$^{+0.12}_{-0.17}$	$^{+0.68}_{-0.55}$	$^{+1.19}_{-1.29}$	$^{+1.46}_{-2.03}$
Effective detector NP set 1 (JES)	$^{-0.75}_{+0.47}$	$^{+0.44}_{-0.31}$	$^{+1.00}_{-0.40}$	$^{+1.49}_{-1.27}$	$^{+1.87}_{-1.61}$
Effective detector NP set 2 (JES)	$^{-0.11}_{-0.05}$	$^{+0.08}_{+0.02}$	$^{+0.11}_{+0.05}$	$^{+0.24}_{+0.18}$	$^{+0.34}_{+0.19}$
Effective mixed NP set 1 (JES)	$^{-0.03}_{-0.04}$	$^{-0.05}_{-0.04}$	$^{+0.06}_{+0.29}$	$^{+0.30}_{-0.13}$	$^{+0.23}_{-0.25}$
Effective mixed NP set 2 (JES)	$^{-0.03}_{-0.10}$	$^{+0.03}_{+0.04}$	$^{+0.01}_{+0.21}$	$^{+0.07}_{+0.08}$	$^{+0.14}_{+0.13}$
Effective model NP set 1 (JES)	$^{-0.22}_{+0.04}$	$^{+0.28}_{-0.19}$	$^{+0.48}_{+0.18}$	$^{-0.43}_{+0.11}$	$^{-1.00}_{+0.13}$
Effective model NP set 2 (JES)	$^{-0.37}_{+0.13}$	$^{+0.24}_{-0.07}$	$^{+0.54}_{-0.13}$	$^{+0.53}_{-0.37}$	$^{+0.59}_{-0.49}$
Effective model NP set 3 (JES)	$^{+0.15}_{-0.30}$	$^{-0.03}_{+0.15}$	$^{-0.18}_{+0.44}$	$^{-0.57}_{+0.67}$	$^{-0.48}_{+0.66}$
Effective model NP set 4 (JES)	$^{-0.10}_{+0.04}$	$^{+0.04}_{-0.12}$	$^{+0.21}_{+0.13}$	$^{+0.15}_{-0.09}$	$^{+0.02}_{-0.22}$
Effective statistical NP set 1 (JES)	$^{+0.24}_{-0.27}$	$^{-0.20}_{+0.05}$	$^{-0.27}_{+0.62}$	$^{-0.31}_{+0.44}$	$^{-0.42}_{+0.63}$
Effective statistical NP set 2 (JES)	$^{-0.09}_{-0.02}$	$^{+0.03}_{+0.03}$	$^{+0.27}_{-0.00}$	$^{-0.04}_{-0.02}$	$^{-0.12}_{+0.20}$
Effective statistical NP set 3 (JES)	$^{-0.11}_{+0.10}$	$^{-0.01}_{-0.09}$	$^{+0.21}_{-0.01}$	$^{+0.35}_{-0.37}$	$^{+0.32}_{-0.52}$
η-intercalibration (JES)	$^{-0.84}_{+0.79}$	$^{+0.37}_{-0.42}$	$^{+1.27}_{-0.95}$	$^{+1.85}_{-1.87}$	$^{+2.11}_{-2.67}$
η-intercalibration statistics (JES)	$^{-0.17}_{-0.01}$	$^{+0.15}_{-0.02}$	$^{+0.28}_{+0.10}$	$^{+0.07}_{-0.02}$	$^{+0.10}_{-0.15}$
Flavor composition (JES)	$^{-0.03}_{+0.07}$	$^{-0.11}_{-0.08}$	$^{+0.13}_{+0.14}$	$^{+0.37}_{-0.46}$	$^{+0.40}_{-0.78}$
Flavor response (JES)	$^{+0.05}_{-0.09}$	$^{-0.13}_{-0.08}$	$^{-0.01}_{+0.33}$	$^{+0.15}_{+0.26}$	$^{+0.27}_{+0.28}$
Pile-up offset μ (JES)	$^{-0.08}_{+0.03}$	$^{+0.00}_{+0.07}$	$^{+0.33}_{-0.01}$	$^{-0.08}_{-0.42}$	$^{-0.35}_{-0.95}$
Pile-up offset N_{PV} (JES)	$^{+0.08}_{-0.03}$	$^{-0.07}_{-0.08}$	$^{-0.02}_{+0.00}$	$^{-0.23}_{+0.48}$	$^{-0.44}_{+0.55}$
Relative nonclosure MC (JES)	$^{-0.18}_{+0.03}$	$^{+0.04}_{+0.04}$	$^{+0.41}_{-0.02}$	$^{+0.28}_{-0.29}$	$^{+0.15}_{-0.46}$
Single particle high-p_{T} (JES)	$^{-0.01}_{-0.01}$	$^{+0.01}_{+0.01}$	$^{+0.02}_{+0.02}$	$^{-0.05}_{-0.04}$	$^{-0.09}_{-0.06}$
JES uncertainty in background	$^{+0.16}_{-0.08}$	$^{-0.28}_{+0.13}$	$^{-0.12}_{+0.28}$	$^{+0.19}_{-0.46}$	$^{+0.44}_{-0.94}$
Jet energy resolution	$^{-0.57}_{+0.58}$	$^{+0.90}_{-0.91}$	$^{+0.16}_{-0.17}$	$^{+0.24}_{-0.24}$	$^{-0.03}_{+0.03}$
Jet reconstruction efficiency	$^{-0.03}_{+0.03}$	$^{+0.09}_{-0.09}$	$^{-0.10}_{+0.10}$	$^{+0.05}_{-0.05}$	$^{+0.23}_{-0.24}$
b-quark tagging efficiency	$^{-0.99}_{+0.77}$	$^{+0.42}_{-0.39}$	$^{+1.62}_{-1.27}$	$^{+1.99}_{-1.33}$	$^{+2.21}_{-1.23}$
c-quark tagging efficiency	$^{+0.07}_{-0.07}$	$^{-0.04}_{+0.04}$	$^{-0.18}_{+0.17}$	$^{+0.06}_{-0.05}$	$^{+0.12}_{-0.10}$
Light-jet tagging efficiency	$^{+0.06}_{-0.06}$	$^{-0.12}_{+0.12}$	$^{+0.03}_{-0.04}$	$^{-0.03}_{+0.03}$	$^{-0.14}_{+0.13}$
e energy resolution	$^{-0.01}_{+0.01}$	$^{+0.02}_{-0.02}$	$^{+0.13}_{+0.04}$	$^{-0.23}_{-0.07}$	$^{-0.39}_{-0.11}$
e energy scale	$^{+0.07}_{-0.10}$	$^{-0.11}_{+0.15}$	$^{-0.03}_{+0.24}$	$^{+0.01}_{-0.37}$	$^{-0.08}_{-0.30}$
μ ID momentum resolution	$^{+0.01}_{+0.11}$	$^{-0.05}_{-0.11}$	$^{+0.07}_{-0.20}$	$^{-0.01}_{+0.06}$	$^{-0.01}_{+0.10}$
μ MS momentum resolution	$^{+0.11}_{+0.07}$	$^{+0.01}_{+0.03}$	$^{-0.32}_{-0.25}$	$^{-0.15}_{-0.09}$	$^{-0.10}_{-0.06}$
μ momentum scale	$^{-0.03}_{+0.03}$	$^{-0.05}_{+0.05}$	$^{+0.12}_{-0.12}$	$^{+0.18}_{-0.18}$	$^{+0.20}_{-0.20}$
ℓ ID efficiency	$^{+0.40}_{-0.38}$	$^{-0.69}_{+0.66}$	$^{-0.73}_{+0.70}$	$^{+1.42}_{-1.36}$	$^{+1.61}_{-1.54}$
ℓ reconstruction efficiency	$^{+0.15}_{-0.15}$	$^{-0.26}_{+0.26}$	$^{-0.24}_{+0.23}$	$^{+0.45}_{-0.44}$	$^{+0.46}_{-0.46}$
ℓ trigger efficiency	$^{-0.15}_{+0.15}$	$^{+0.32}_{-0.32}$	$^{+0.27}_{-0.27}$	$^{-0.74}_{+0.73}$	$^{-0.81}_{+0.80}$
$E_{\mathrm{T}}^{\mathrm{miss}}$ unassociated cells	$^{-0.03}_{-0.04}$	$^{+0.02}_{+0.14}$	$^{+0.02}_{-0.02}$	$^{+0.02}_{-0.21}$	$^{+0.50}_{-0.37}$

(Table continued)

TABLE X. (*Continued*)

$\frac{1}{\sigma}\frac{d\sigma}{dm_{t\bar{t}}}$ Uncertainties [%]/Bins [GeV]	250–450	450–550	550–700	700–950	950–2700
$E_{\mathrm{T}}^{\mathrm{miss}}$ pile-up	−0.10 −0.05	+0.04 −0.02	+0.15 +0.19	+0.19 +0.11	+0.64 −0.29
MC generator	−2.19 +2.73	+1.88 −2.34	+2.57 −3.20	+2.97 −3.71	+2.51 −3.13
Fragmentation	+0.20 −0.20	−0.21 +0.20	+0.54 −0.52	−1.75 +1.69	−2.21 +2.14
IFSR	+0.55 −0.54	−0.18 +0.18	−0.92 +0.89	−1.50 +1.45	−0.40 +0.38
PDF	−0.07 +0.07	−0.07 +0.08	−0.02 +0.02	+0.54 −0.56	+2.20 −2.26
MC statistics	+0.41 −0.41	+0.41 −0.41	+0.63 −0.63	+1.04 −1.04	+1.60 −1.60
$W+$ jets bb4	−0.08 +0.01	−0.06 +0.02	+0.14 −0.04	+0.48 −0.04	+0.80 −0.15
$W+$ jets bb5	−0.08 +0.07	−0.06 +0.03	+0.14 −0.10	+0.48 −0.41	+0.80 −0.61
$W+$ jets bbcc	−0.17 +0.16	−0.09 +0.09	+0.45 −0.41	+0.60 −0.58	+0.96 −0.91
$W+$ jets bbccc	+0.03 +0.01	−0.13 +0.06	−0.16 +0.07	+0.57 −0.39	+1.03 −0.82
$W+$ jets c4	−0.05 −0.03	+0.13 −0.03	+0.01 +0.07	−0.21 +0.17	−0.17 +0.17
$W+$ jets c5	−0.05 +0.09	+0.13 −0.12	+0.01 −0.09	−0.21 +0.07	−0.17 +0.03
$W+$ jets charge asymmetry	−0.05 +0.06	−0.02 +0.05	+0.04 −0.00	+0.34 −0.52	+0.63 −0.90
Multijet normalization	+0.26 −0.27	−0.67 +0.67	−0.76 +0.75	+2.11 −2.02	+4.17 −3.96
Multijet shape	+0.04 +0.07	−0.18 +0.18	−0.25 +0.31	+0.82 −1.52	+1.45 −3.65
$Z+$ jets background normalization	+0.14 −0.14	−0.25 +0.25	−0.17 +0.17	+0.32 −0.32	+0.49 −0.48
Dilepton background normalization	+0.14 −0.13	−0.06 +0.06	−0.22 +0.21	−0.30 +0.29	−0.34 +0.33

TABLE XI. The individual systematic uncertainties calculated as a percentage of the normalized differential cross section in each bin.

$\frac{1}{\sigma}\frac{d\sigma}{dp_{\mathrm{T}}^{t\bar{t}}}$ Uncertainties [%]/Bins [GeV]	0–40	40–170	170–340	340–1000
b-quark jets (JES)	−0.02 +0.03	−0.01 +0.03	+0.38 −0.53	+0.30 −0.76
Close-by jets (JES)	−0.73 +0.82	+0.88 −1.04	+1.40 −1.19	+1.40 −1.28
Effective detector NP set 1 (JES)	−0.53 +0.53	+0.51 −0.49	+2.00 −2.12	+2.76 −3.18
Effective detector NP set 2 (JES)	+0.03 −0.05	−0.01 +0.07	−0.31 +0.00	−0.70 −0.09
Effective mixed NP set 1 (JES)	−0.10 +0.03	+0.13 +0.02	+0.09 −0.47	+0.18 −1.07
Effective mixed NP set 2 (JES)	−0.01 +0.04	+0.06 −0.04	−0.33 −0.05	−0.76 −0.25
Effective model NP set 1 (JES)	−0.59 +0.48	+0.75 −0.61	+0.89 −0.72	+0.39 −0.56
Effective model NP set 2 (JES)	+0.01 +0.21	−0.03 −0.18	+0.12 −0.97	+0.16 −1.55
Effective model NP set 3 (JES)	+0.13 −0.09	−0.11 +0.13	−0.56 +0.05	−0.70 +0.01
Effective model NP set 4 (JES)	−0.06 +0.09	+0.09 −0.08	+0.06 −0.40	−0.06 −0.64
Effective statistical NP set 1 (JES)	−0.16 +0.25	+0.22 −0.33	+0.18 −0.24	−0.09 −0.05
Effective statistical NP set 2 (JES)	+0.09 −0.01	−0.11 +0.03	−0.18 −0.09	−0.28 −0.21
Effective statistical NP set 3 (JES)	−0.12 +0.05	+0.15 −0.01	+0.16 −0.49	+0.20 −0.90
η-intercalibration (JES)	−0.90 +1.03	+0.96 −1.14	+2.71 −2.80	+3.31 −3.64
η-intercalibration statistics (JES)	−0.16 +0.17	+0.21 −0.15	+0.23 −0.71	−0.11 −1.17
Flavor composition (JES)	−0.04 +0.09	+0.02 −0.09	+0.26 −0.35	+0.33 −0.49
Flavor response (JES)	−0.36 +0.42	+0.45 −0.48	+0.58 −0.97	+0.54 −1.24
Pile-up offset μ (JES)	−0.19 +0.10	+0.20 −0.10	+0.68 −0.36	+0.61 −0.34
Pile-up offset N_{PV} (JES)	−0.07 +0.14	+0.09 −0.15	+0.07 −0.41	−0.25 −0.82
Relative nonclosure MC (JES)	−0.04 +0.14	+0.09 −0.15	−0.23 −0.46	−0.52 −0.74
Single particle high-p_{T} (JES)	+0.03 +0.03	−0.04 −0.03	−0.08 −0.08	−0.10 −0.12
JES uncertainty in background	−1.20 +1.13	+1.37 −1.35	+2.78 −2.35	+3.89 −2.60
Jet energy resolution	+3.42 −3.49	−4.07 +4.16	−7.06 +7.22	−8.01 +8.19
Jet reconstruction efficiency	−0.04 +0.04	+0.07 −0.07	−0.12 +0.12	−0.29 +0.29
b-quark tagging efficiency	−0.01 −0.10	−0.04 +0.13	+0.36 +0.17	+0.98 −0.13

(Table continued)

TABLE XI. (*Continued*)

$\frac{1}{\sigma}\frac{d\sigma}{dp_{\mathrm{T}}^{t\bar{t}}}$ Uncertainties [%]/Bins [GeV]	0–40	40–170	170–340	340–1000
c-quark tagging efficiency	−0.07 +0.06	+0.07 −0.07	+0.23 −0.19	+0.31 −0.24
Light-jet tagging efficiency	−0.01 +0.03	+0.01 −0.03	+0.06 −0.08	+0.12 −0.15
e energy resolution	+0.00 −0.05	−0.01 +0.09	−0.02 −0.14	+0.16 −0.28
e energy scale	−0.15 +0.19	+0.28 −0.22	−0.40 −0.37	−0.74 −0.70
μ ID momentum resolution	−0.14 −0.01	+0.20 +0.01	+0.04 −0.03	−0.15 −0.10
μ MS momentum resolution	−0.01 −0.08	+0.00 +0.10	+0.07 +0.15	+0.17 +0.06
μ momentum scale	−0.26 +0.26	+0.33 −0.33	+0.35 −0.35	+0.37 −0.37
ℓ ID efficiency	−0.75 +0.73	+1.03 −1.00	+0.49 −0.47	+0.48 −0.46
ℓ reconstruction efficiency	−0.29 +0.28	+0.39 −0.39	+0.20 −0.20	+0.21 −0.21
ℓ trigger efficiency	+0.35 −0.34	−0.48 +0.48	−0.17 +0.17	−0.12 +0.12
$E_{\mathrm{T}}^{\mathrm{miss}}$ unassociated cells	−1.56 +1.65	+2.01 −2.14	+2.10 −2.07	+1.79 −1.81
$E_{\mathrm{T}}^{\mathrm{miss}}$ pile-up	−1.16 +1.05	+1.48 −1.34	+1.60 −1.43	+1.46 −1.59
MC generator	−3.46 +4.24	+4.15 −5.09	+7.96 −9.76	−1.21 +1.49
Fragmentation	+0.63 −0.62	−0.12 +0.12	−6.90 +6.77	−2.65 +2.60
IFSR	−1.29 +1.19	+1.04 −0.96	+6.22 −5.76	+10.25 −9.49
PDF	−0.07 +0.08	+0.06 −0.06	+0.24 −0.25	+1.30 −1.35
MC statistics	+0.57 −0.57	+0.75 −0.75	+1.66 −1.66	+2.77 −2.77
$W+$ jets bb4	−0.21 −0.21	+0.18 +0.23	+0.99 +0.52	+1.60 +0.66
$W+$ jets bb5	−0.21 +0.40	+0.18 −0.40	+0.99 −1.46	+1.60 −2.19
$W+$ jets bbcc	−0.37 +0.35	+0.42 −0.39	+0.93 −0.87	+1.28 −1.20
$W+$ jets bbccc	+0.15 −0.27	−0.24 +0.40	+0.14 −0.06	+0.61 −0.56
$W+$ jets c4	+0.18 −0.41	−0.29 +0.50	+0.19 +0.77	+0.54 +0.89
$W+$ jets c5	+0.18 +0.23	−0.29 −0.19	+0.19 −1.06	+0.54 −1.60
$W+$ jets charge asymmetry	+0.02 +0.01	−0.12 +0.10	+0.70 −0.92	+1.40 −1.81
Multijet normalization	−0.76 +0.76	+1.03 −1.05	+0.51 −0.51	+0.36 −0.35
Multijet shape	−0.03 +0.08	+0.02 −0.08	+0.24 −0.27	+0.51 −0.43
$Z+$ jets background normalization	−0.22 +0.23	+0.26 −0.27	+0.47 −0.47	+0.67 −0.68
Dilepton background normalization	−0.22 +0.21	+0.26 −0.25	+0.49 −0.46	+0.64 −0.60

TABLE XII. The individual systematic uncertainties calculated as a percentage of the normalized differential cross section in each bin.

$\frac{1}{\sigma}\frac{d\sigma}{d\lvert y_{t\bar{t}}\rvert}$ Uncertainties [%]	0.0–0.5	0.5–1.0	1.0–2.5
b-quark jets (JES)	+0.01 −0.04	−0.02 +0.02	+0.02 +0.04
Close-by jets (JES)	−0.24 +0.13	−0.02 +0.01	+0.44 −0.24
Effective detector NP set 1 (JES)	−0.13 +0.09	+0.01 +0.01	+0.20 −0.17
Effective detector NP set 2 (JES)	+0.00 +0.00	−0.01 +0.01	+0.00 −0.01
Effective mixed NP set 1 (JES)	−0.01 +0.01	−0.03 −0.01	+0.06 −0.02
Effective mixed NP set 2 (JES)	−0.03 +0.02	−0.02 +0.01	+0.08 −0.05
Effective model NP set 1 (JES)	−0.07 +0.04	−0.01 +0.00	+0.13 −0.07
Effective model NP set 2 (JES)	+0.01 −0.01	+0.00 −0.00	−0.02 +0.01
Effective model NP set 3 (JES)	−0.02 −0.01	+0.02 +0.01	+0.01 −0.00
Effective model NP set 4 (JES)	+0.01 +0.02	−0.03 −0.02	+0.01 −0.02
Effective statistical NP set 1 (JES)	−0.05 +0.01	−0.01 +0.02	+0.09 −0.05
Effective statistical NP set 2 (JES)	−0.02 +0.02	−0.01 −0.01	+0.04 −0.01
Effective statistical NP set 3 (JES)	−0.05 +0.01	−0.01 −0.03	+0.10 +0.02
η-intercalibration (JES)	−0.52 +0.41	+0.02 −0.03	+0.87 −0.67

(Table continued)

TABLE XII. (*Continued*)

$\frac{1}{\sigma}\frac{d\sigma}{d\lvert y_{t\bar{t}}\rvert}$ Uncertainties [%]	0.0–0.5	0.5–1.0	1.0–2.5
η-intercalibration statistics (JES)	−0.07	−0.01	+0.13
	−0.02	+0.01	+0.02
Flavor composition (JES)	−0.04	+0.00	+0.06
	+0.02	−0.02	−0.01
Flavor response (JES)	−0.07	+0.01	+0.11
	+0.07	−0.03	−0.09
Pile-up offset μ (JES)	−0.08	+0.00	+0.14
	+0.05	−0.04	−0.04
Pile-up offset N_{PV} (JES)	−0.06	+0.01	+0.09
	−0.03	+0.03	+0.01
Relative nonclosure MC (JES)	−0.04	−0.03	+0.11
	+0.06	+0.02	−0.13
Single particle high-p_{T} (JES)	−0.00	+0.00	+0.00
	−0.00	+0.00	+0.00
JES uncertainty in background	−0.16	+0.04	+0.23
	+0.21	+0.07	−0.45
Jet energy resolution	+0.12	+0.14	−0.38
	−0.12	−0.14	+0.38
Jet reconstruction efficiency	+0.01	+0.00	−0.02
	−0.01	−0.00	+0.02
b-quark tagging efficiency	+0.01	−0.00	−0.01
	−0.00	+0.00	−0.00
c-quark tagging efficiency	−0.03	+0.01	+0.03
	+0.03	−0.01	−0.03
Light-jet tagging efficiency	−0.01	−0.01	+0.03
	+0.00	+0.01	−0.02
e energy resolution	+0.03	+0.02	−0.07
	−0.00	−0.00	+0.01
e energy scale	−0.06	−0.02	+0.14
	+0.08	+0.01	−0.15
μ ID momentum resolution	+0.01	−0.01	+0.01
	+0.03	−0.02	−0.01
μ MS momentum resolution	−0.04	+0.02	+0.05
	−0.06	+0.03	+0.07
μ momentum scale	+0.03	−0.04	+0.00
	−0.03	+0.04	−0.00
ℓ ID efficiency	−0.35	−0.10	+0.73
	+0.34	+0.09	−0.70
ℓ reconstruction efficiency	−0.12	−0.02	+0.23
	+0.12	+0.02	−0.23
ℓ trigger efficiency	+0.21	+0.02	−0.38
	−0.20	−0.02	+0.38
$E_{\mathrm{T}}^{\mathrm{miss}}$ unassociated cells	+0.13	−0.06	−0.15
	−0.08	+0.04	+0.09
$E_{\mathrm{T}}^{\mathrm{miss}}$ pile-up	+0.07	−0.01	−0.11
	+0.01	−0.01	−0.01
MC generator	−2.00	−1.19	+4.97
	+2.48	+1.48	−6.19
Fragmentation	−1.89	−0.83	+4.31
	+1.81	+0.80	−4.15
IFSR	−0.11	+0.08	+0.09
	+0.11	−0.07	−0.09
PDF	−1.06	−0.07	+1.92
	+1.08	+0.08	−1.97
MC statistics	+0.19	+0.03	+0.29
	−0.19	−0.03	−0.29
$W+$jets bb4	−0.08	+0.01	+0.11
	+0.04	−0.00	−0.07
$W+$jets bb5	−0.08	+0.01	+0.11
	+0.03	−0.01	−0.04
$W+$jets bbcc	−0.25	+0.04	+0.39
	+0.24	−0.03	−0.37
$W+$jets bbccc	−0.05	−0.02	+0.11
	+0.01	+0.01	−0.03
$W+$jets c4	+0.11	+0.00	−0.19
	−0.06	+0.00	+0.10
$W+$jets c5	+0.11	+0.00	−0.19
	−0.06	−0.00	+0.11
$W+$jets charge asymmetry	−0.05	+0.01	+0.08
	+0.07	−0.01	−0.11
Multijet normalization	−0.35	−0.13	+0.77
	+0.35	+0.13	−0.77
Multijet shape	−0.09	−0.05	+0.22
	+0.09	+0.05	−0.22
$Z+$jets background normalization	−0.14	−0.05	+0.30
	+0.14	+0.05	−0.30
Dilepton background normalization	−0.01	−0.00	+0.02
	+0.01	+0.00	−0.02

contribute to the uncertainty on the jet energy scale are denoted (JES) and are described in detail in Ref. [46].

The muon momentum resolution uncertainties are split into parts specific to the inner-detector (ID) and muon spectrometer (MS). The $W+$jets uncertainties represent the uncertainties in the normalization of the $W+$heavy-flavor production except for $W+$jets charge asymmetry and refer to the overall data-driven normalization of the $W+$jets background, with the numbers 4 (5) referring to $=4$ (≥ 5) jet multiplicity bins.

APPENDIX B: STATISTICAL CORRELATIONS AMONG VARIABLES

Statistical correlations among the variables are evaluated by unfolding statistically coupled (co-varied)

TABLE XIII. Statistical correlation matrix between the normalized differential cross sections. All variables are included to show the correlations between different bins of different variables. From left to right and bottom to top the rows and columns are labeled by bin number for each variable and the variables are ordered: p_{T}^{t}, $m_{t\bar{t}}$, $p_{\mathrm{T}}^{t\bar{t}}$, and $|y_{t\bar{t}}|$.

3	0.14	0.02	−0.22	0.14	0.16	0.13	0.03	0.23	−0.25	−0.19	0.18	0.12	−0.24	0.28	0.02	−0.01	−0.90	0.11	1.00
2	−0.01	0.02	0.04	−0.05	−0.07	−0.05	−0.02	0.02	0.07	−0.06	−0.06	−0.04	0.10	−0.11	−0.02	−0.01	−0.53	1.00	0.11
1	−0.12	−0.03	0.17	−0.10	−0.11	−0.09	−0.02	−0.21	0.19	0.19	−0.12	−0.09	0.16	−0.19	−0.01	0.01	1.00	−0.53	−0.90
4	−0.03	−0.06	−0.02	0.04	0.10	0.14	0.15	−0.03	−0.01	0.04	0.03	0.02	−0.45	0.23	0.92	1.00	0.01	−0.01	−0.01
3	−0.03	−0.08	−0.02	0.08	0.12	0.14	0.14	−0.03	−0.02	0.04	0.04	0.02	−0.65	0.44	1.00	0.92	−0.01	−0.02	0.02
2	0.05	−0.06	−0.14	0.17	0.18	0.14	0.08	0.09	−0.18	−0.05	0.19	0.13	−0.97	1.00	0.44	0.23	−0.19	−0.11	0.28
1	−0.04	0.07	0.12	−0.17	−0.19	−0.16	−0.11	−0.07	0.16	0.03	−0.17	−0.12	1.00	−0.97	−0.65	−0.45	0.16	0.10	−0.24
5	−0.01	−0.06	−0.10	0.03	0.21	0.42	0.27	−0.09	−0.19	−0.24	0.92	1.00	−0.12	0.13	0.02	0.02	−0.09	−0.04	0.12
4	−0.02	−0.07	−0.15	0.10	0.33	0.49	0.29	−0.06	−0.28	−0.23	1.00	0.92	−0.17	0.19	0.04	0.03	−0.12	−0.06	0.18
3	−0.14	−0.24	0.12	0.18	0.16	0.03	0.09	−0.73	0.23	1.00	−0.23	−0.24	0.03	−0.05	0.04	0.04	0.19	−0.06	−0.19
2	−0.25	−0.26	0.32	0.09	−0.05	−0.14	−0.14	−0.72	1.00	0.23	−0.28	−0.19	0.16	−0.18	−0.02	−0.01	0.19	0.07	−0.25
1	0.27	0.36	−0.24	−0.22	−0.19	−0.12	−0.08	1.00	−0.72	−0.73	−0.06	−0.09	−0.07	0.09	−0.03	−0.03	−0.21	0.02	0.23
7	0.05	0.02	−0.20	−0.17	0.11	0.74	1.00	−0.08	−0.14	0.09	0.29	0.27	−0.11	0.08	0.14	0.15	−0.02	−0.02	0.03
6	0.04	−0.09	−0.28	−0.03	0.50	1.00	0.74	−0.12	−0.14	0.03	0.49	0.42	−0.16	0.14	0.14	0.14	−0.09	−0.05	0.13
5	−0.01	−0.25	−0.36	0.57	1.00	0.50	0.11	−0.19	−0.05	0.16	0.33	0.21	−0.19	0.18	0.12	0.10	−0.11	−0.07	0.16
4	−0.26	−0.41	−0.07	1.00	0.57	−0.03	−0.17	−0.22	0.09	0.18	0.10	0.03	−0.17	0.17	0.08	0.04	−0.10	−0.05	0.14
3	−0.73	−0.60	1.00	−0.07	−0.36	−0.28	−0.20	−0.24	0.32	0.12	−0.15	−0.10	0.12	−0.14	−0.02	−0.02	0.17	0.04	−0.22
2	0.32	1.00	−0.60	−0.41	−0.25	−0.09	0.02	0.36	−0.26	−0.24	−0.07	−0.06	0.07	−0.06	−0.08	−0.06	−0.03	0.02	0.02
1	1.00	0.32	−0.73	−0.26	−0.01	0.04	0.05	0.27	−0.25	−0.14	−0.02	−0.01	−0.04	0.05	−0.03	−0.03	−0.12	−0.01	0.14
	1	2	3	4	5	6	7	1	2	3	4	5	1	2	3	4	1	2	3

replicas of individual spectra in data using the "bootstrap" method [77]. The result is obtained by unfolding the separate $e+\text{jets}$ and $\mu+\text{jets}$ spectra, combining with the same procedure used for the nominal result, and normalizing each replica to obtain the normalized differential cross section. The results are tabulated in Table XIII and presented graphically in Fig. 12.

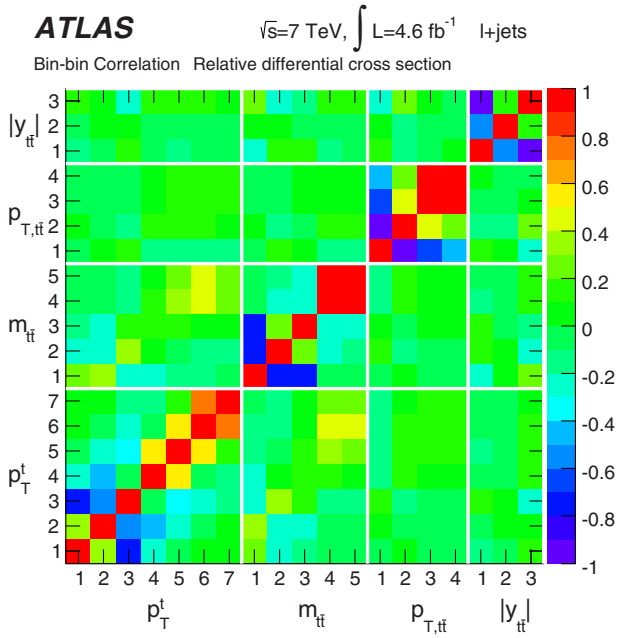

FIG. 12 (color online). Graphical representation of the statistical correlation matrix between the normalized differential cross sections. All variables are included to show the correlations between different bins of different variables. From left to right and bottom to top the rows and columns are labeled by bin number for each variable and the variables are ordered: p_{T}^{t}, $m_{t\bar{t}}$, $p_{\mathrm{T}}^{t\bar{t}}$, and $|y_{t\bar{t}}|$.

[1] S. Moch and P. Uwer, Phys. Rev. D **78**, 034003 (2008).
[2] R. Frederix and F. Maltoni, J. High Energy Phys. 01 (2009) 047.
[3] ATLAS Collaboration, Phys. Lett. B **717**, 89 (2012).
[4] ATLAS Collaboration, J. High Energy Phys. 05 (2012) 059.
[5] ATLAS Collaboration, Phys. Lett. B **711**, 244 (2012).
[6] CMS Collaboration, J. High Energy Phys. 11 (2012) 067.
[7] CMS Collaboration, Phys. Rev. D **85**, 112007 (2012).
[8] CMS Collaboration, Phys. Lett. B **720**, 83 (2013).
[9] CMS Collaboration, J. High Energy Phys. 05 (2013) 065.
[10] CMS Collaboration, Eur. Phys. J. C **73**, 2339 (2013).
[11] ATLAS Collaboration, Eur. Phys. J. C **73**, 2261 (2013).
[12] N. Kidonakis, Phys. Rev. D **82**, 114030 (2010).
[13] V. Ahrens, A. Ferroglia, M. Neubert, B. D. Pecjak, and L. L. Yang, J. High Energy Phys. 09 (2010) 097.
[14] H. X. Zhu, C. S. Li, H. T. Li, D. Y. Shao, and L. L. Yang, Phys. Rev. Lett. **110**, 082001 (2013).
[15] H. T. Li, C. S. Li, D. Y. Shao, L. L. Yang, and H. X. Zhu, Phys. Rev. D **88**, 074004 (2013).
[16] ATLAS Collaboration, JINST **3**, S08003 (2008).
[17] ATLAS uses a right-handed coordinate system with its origin at the nominal interaction point (IP) in the center of the detector and the z axis along the beam pipe. The x axis points from the IP to the center of the LHC ring, and the y axis points upward. Cylindrical coordinates (r, ϕ) are used in the transverse plane, ϕ being the azimuthal angle around the beam pipe. The pseudorapidity is defined in terms of the polar angle θ as $\eta = -\ln\tan(\theta/2)$. The distance in η–ϕ coordinates is $\Delta R = \sqrt{(\Delta\eta)^2 + (\Delta\phi)^2}$, also used to define cone radii.
[18] ATLAS Collaboration, Eur. Phys. J. C **73**, 2518 (2013).
[19] M. L. Mangano, M. Moretti, F. Piccinini, R. Pittau, and A. D. Polosa, J. High Energy Phys. 07 (2003) 001.
[20] J. Pumplin, D. R. Stump, J. Huston, H.-L. Lai, P. Nadolsky, and W.-K. Tung, J. High Energy Phys. 07 (2002) 012.
[21] G. Corcella, I. G Knowles, G. Marchesini, S. Moretti, K. Odagiri, P. Richardson, M. H. Seymour, and B. R Webber, J. High Energy Phys. 01 (2001) 010.
[22] J. Butterworth, J. R. Forshaw, and M. Seymour, Z. Phys. C **72**, 637 (1996).
[23] ATLAS Collaboration, Report No. ATL-PHYS-PUB-2011-008 [http://cdsweb.cern.ch/record/1345343].
[24] M. L. Mangano, M. Moretti, and R. Pittau, Nucl. Phys. **B632**, 343 (2002).
[25] H.-L. Lai, M. Guzzi, J. Huston, Z. Li, P. M. Nadolsky , J. Pumplin, and C.-P. Yuan, Phys. Rev. D **82**, 074024 (2010).
[26] S. Frixione, P. Nason, and B. R. Webber, J. High Energy Phys. 08 (2003) 007.
[27] S. Frixione, P. Nason, and G. Ridolfi, J. High Energy Phys. 09 (2007) 126.
[28] T. Sjöstrand, S. Mrenna, and P. Z. Skands, J. High Energy Phys. 05 (2006) 026.
[29] P. Z. Skands, Phys. Rev. D **82**, 074018 (2010).
[30] M. Aliev, H. Lacker, U. Langenfeld, S. Moch, P. Uwer, and M. Wiedermann, Comput. Phys. Commun. **182**, 1034 (2011).
[31] M. Czakon, P. Fiedler, and A. Mitov, Phys. Rev. Lett. **110**, 252004 (2013).
[32] B. P. Kersevan and E. Richter-Was, Comput. Phys. Commun. **184**, 919 (2013).
[33] A. Sherstnev and R. Thorne, Eur. Phys. J. C **55**, 553 (2008).
[34] ATLAS Collaboration, Report No. ATLAS-PHYS-PUB-2011-009 [http://cdsweb.cern.ch/record/1363300].
[35] S. Agostinelli *et al.* (GEANT4 Collaboration), Nucl. Instrum. Methods Phys. Res., Sect. A **506**, 250 (2003); CERN Report No. CERN-IT-2002-003 [https://cds.cern.ch/search?sysno=002361110CER].
[36] ATLAS Collaboration, Eur. Phys. J. C **70**, 823 (2010).
[37] ATLAS Collaboration, Eur. Phys. J. C **71**, 1577 (2011).
[38] ATLAS Collaboration, Eur. Phys. J. C **74**, 2941 (2014).
[39] ATLAS Collaboration, Eur. Phys. J. C **72**, 1909 (2012).
[40] ATLAS Collaboration, Report No. ATLAS-CONF-2013-088 [http://cdsweb.cern.ch/record/1580207].
[41] ATLAS Collaboration, arXiv:1404.4562.
[42] ATLAS Collaboration, Report No. ATL-PHYS-PUB-2011-006 [http://cdsweb.cern.ch/record/1345327].
[43] W. Lampl *et al.*, Report No. ATL-LARG-PUB-2008-002 [http://cdsweb.cern.ch/record/1099735].
[44] M. Cacciari, G. P. Salam, and G. Soyez, J. High Energy Phys. 04 (2008) 063.
[45] ATLAS Collaboration, Eur. Phys. J. C **73**, 2304 (2013).
[46] ATLAS Collaboration, arXiv:1406.0076.
[47] ATLAS Collaboration, Eur. Phys. J. C **72**, 1844 (2012).
[48] ATLAS Collaboration, Report No. ATLAS-CONF-2012-043 [http://cdsweb.cern.ch/record/1435197].
[49] J. Erdmannn, S. Guindon, K. Kröninger, B. Lemmer, O. Nackenhorst, A. Quadt, and P. Stolte, Nucl. Instrum. Methods Phys. Res., Sect. A **748**, 18 (2014).
[50] N. Kidonakis, Phys. Rev. D **83**, 091503 (2011).
[51] N. Kidonakis, Phys. Rev. D **81**, 054028 (2010).
[52] N. Kidonakis, Phys. Rev. D **82**, 054018 (2010).
[53] C. Anastasiou, L. J. Dixon, K. Melnikov, and F. Petriello, Phys. Rev. D **69**, 094008 (2004).
[54] J. M. Campbell, R. K. Ellis, and C. Williams, J. High Energy Phys. 07 (2011) 018.
[55] C.-H. Kom and W. J. Stirling, Eur. Phys. J. C **69**, 67 (2010).
[56] Technically, the parton level, used both for the unfolding and for the predictions of the MC generators, is defined as status-code 155 for HERWIG and 3 for PYTHIA.
[57] J. Beringer *et al.* (Particle Data Group), Phys. Rev. D **86**, 010001 (2012); http://pdg.lbl.gov/.
[58] A. Hoecker and V. Kartvelishvili, Nucl. Instrum. Methods Phys. Res., Sect. A **372**, 469 (1996).
[59] R. Group, C. Ciobanu, K. Lannon, and C. Plager, in Proceedings of the 34th International Conference on High Energy Physics (ICHEP2008) (Philadelphia, PA, 2008), arXiv:0809.4670.
[60] L. Lyons, D. Gibaut, and P. Clifford, Nucl. Instrum. Methods Phys. Res., Sect. A **270**, 110 (1988).
[61] ATLAS Collaboration, Eur. Phys. J. C **73**, 2306 (2013).
[62] ATLAS Collaboration, Report No. ATLAS-CONF-2011-102 [http://cdsweb.cern.ch/record/1369219].
[63] ATLAS Collaboration, Report No. ATLAS-CONF-2011-089 [http://cdsweb.cern.ch/record/1356198].
[64] H. Lai, J. Huston, S. Kuhlmann, J. Morfin, F. Olness, J. F. Owens, J. Pumplin, and W. K. Tung (CTEQ Collaboration), Eur. Phys. J. C **12**, 375 (2000).
[65] ATLAS Collaboration, Report No. ATL-PHYS-PUB-2013-005 [http://cdsweb.cern.ch/record/1532067].

[66] ATLAS Collaboration, Eur. Phys. J. C **72**, 2043 (2012).
[67] A. Martin, W. Stirling, R. Thorne, and G. Watt, Eur. Phys. J. C **63**, 189 (2009).
[68] R. D. Ball *et al.*, Nucl. Phys. **B867**, 244 (2013).
[69] M. Botje *et al.*, arXiv:1101.0538.
[70] J. Campbell, K. Ellis, and C. Williams, MCFM—Monte Carlo for FeMtobarn Processes, http://mcfm.fnal.gov/.
[71] A. V. Manohar and M. Trott, Phys. Lett. B **711**, 313 (2012).
[72] W. Bernreuther, M. Fücker, and Z.-G. Si, Nuovo Cimento Soc. Ital. Fis. **123**, 1036 (2008).
[73] J. H. Kühn, A. Scharf, and P. Uwer, Eur. Phys. J. C **51**, 37 (2007).
[74] J. H. Kühn, A. Scharf, and P. Uwer, arXiv:1305.5773.
[75] F. D. Aaron *et al.* (H1 and ZEUS Collaboration), J. High Energy Phys. 01 (2010) 109.
[76] For HERAPDF1.5, only the 21 member PDFs accounting for experimental uncertainties are taken into account.
[77] G. Bohm and G. Zech, *Introduction to statistics and data analysis for physicists* (Verl. Dt. Elektronen-Synchrotron, Hamburg, 2010) [http://www-library.desy.de/preparch/books/vstatmp_engl.pdf].

G. Aad,[84] T. Abajyan,[21] B. Abbott,[112] J. Abdallah,[152] S. Abdel Khalek,[116] O. Abdinov,[11] R. Aben,[106] B. Abi,[113] M. Abolins,[89] O. S. AbouZeid,[159] H. Abramowicz,[154] H. Abreu,[137] Y. Abulaiti,[147a,147b] B. S. Acharya,[165a,165b,b] L. Adamczyk,[38a] D. L. Adams,[25] J. Adelman,[177] S. Adomeit,[99] T. Adye,[130] T. Agatonovic-Jovin,[13b] J. A. Aguilar-Saavedra,[125a,125f] M. Agustoni,[17] S. P. Ahlen,[22] F. Ahmadov,[64,c] G. Aielli,[134a,134b] T. P. A. Åkesson,[80] G. Akimoto,[156] A. V. Akimov,[95] J. Albert,[170] S. Albrand,[55] M. J. Alconada Verzini,[70] M. Aleksa,[30] I. N. Aleksandrov,[64] C. Alexa,[26a] G. Alexander,[154] G. Alexandre,[49] T. Alexopoulos,[10] M. Alhroob,[165a,165c] G. Alimonti,[90a] L. Alio,[84] J. Alison,[31] B. M. M. Allbrooke,[18] L. J. Allison,[71] P. P. Allport,[73] S. E. Allwood-Spiers,[53] J. Almond,[83] A. Aloisio,[103a,103b] R. Alon,[173] A. Alonso,[36] F. Alonso,[70] C. Alpigiani,[75] A. Altheimer,[35] B. Alvarez Gonzalez,[89] M. G. Alviggi,[103a,103b] K. Amako,[65] Y. Amaral Coutinho,[24a] C. Amelung,[23] D. Amidei,[88] V. V. Ammosov,[129,a] S. P. Amor Dos Santos,[125a,125c] A. Amorim,[125a,125b] S. Amoroso,[48] N. Amram,[154] G. Amundsen,[23] C. Anastopoulos,[140] L. S. Ancu,[17] N. Andari,[30] T. Andeen,[35] C. F. Anders,[58b] G. Anders,[30] K. J. Anderson,[31] A. Andreazza,[90a,90b] V. Andrei,[58a] X. S. Anduaga,[70] S. Angelidakis,[9] P. Anger,[44] A. Angerami,[35] F. Anghinolfi,[30] A. V. Anisenkov,[108] N. Anjos,[125a] A. Annovi,[47] A. Antonaki,[9] M. Antonelli,[47] A. Antonov,[97] J. Antos,[145b] F. Anulli,[133a] M. Aoki,[65] L. Aperio Bella,[18] R. Apolle,[119,d] G. Arabidze,[89] I. Aracena,[144] Y. Arai,[65] J. P. Araque,[125a] A. T. H. Arce,[45] J-F. Arguin,[94] S. Argyropoulos,[42] M. Arik,[19a] A. J. Armbruster,[30] O. Arnaez,[82] V. Arnal,[81] O. Arslan,[21] A. Artamonov,[96] G. Artoni,[23] S. Asai,[156] N. Asbah,[94] A. Ashkenazi,[154] S. Ask,[28] B. Åsman,[147a,147b] L. Asquith,[6] K. Assamagan,[25] R. Astalos,[145a] M. Atkinson,[166] N. B. Atlay,[142] B. Auerbach,[6] E. Auge,[116] K. Augsten,[127] M. Aurousseau,[146b] G. Avolio,[30] G. Azuelos,[94,e] Y. Azuma,[156] M. A. Baak,[30] C. Bacci,[135a,135b] H. Bachacou,[137] K. Bachas,[155] M. Backes,[30] M. Backhaus,[30] J. Backus Mayes,[144] E. Badescu,[26a] P. Bagiacchi,[133a,133b] P. Bagnaia,[133a,133b] Y. Bai,[33a] D. C. Bailey,[159] T. Bain,[35] J. T. Baines,[130] O. K. Baker,[177] S. Baker,[77] P. Balek,[128] F. Balli,[137] E. Banas,[39] Sw. Banerjee,[174] A. Bangert,[151] A. A. E. Bannoura,[176] V. Bansal,[170] H. S. Bansil,[18] L. Barak,[173] S. P. Baranov,[95] T. Barber,[48] E. L. Barberio,[87] D. Barberis,[50a,50b] M. Barbero,[84] T. Barillari,[100] M. Barisonzi,[176] T. Barklow,[144] N. Barlow,[28] B. M. Barnett,[130] R. M. Barnett,[15] Z. Barnovska,[5] A. Baroncelli,[135a] G. Barone,[49] A. J. Barr,[119] F. Barreiro,[81] J. Barreiro Guimarães da Costa,[57] R. Bartoldus,[144] A. E. Barton,[71] P. Bartos,[145a] V. Bartsch,[150] A. Bassalat,[116] A. Basye,[166] R. L. Bates,[53] L. Batkova,[145a] J. R. Batley,[28] M. Battistin,[30] F. Bauer,[137] H. S. Bawa,[144,f] T. Beau,[79] P. H. Beauchemin,[162] R. Beccherle,[123a,123b] P. Bechtle,[21] H. P. Beck,[17] K. Becker,[176] S. Becker,[99] M. Beckingham,[139] C. Becot,[116] A. J. Beddall,[19c] A. Beddall,[19c] S. Bedikian,[177] V. A. Bednyakov,[64] C. P. Bee,[149] L. J. Beemster,[106] T. A. Beermann,[176] M. Begel,[25] K. Behr,[119] C. Belanger-Champagne,[86] P. J. Bell,[49] W. H. Bell,[49] G. Bella,[154] L. Bellagamba,[20a] A. Bellerive,[29] M. Bellomo,[85] A. Belloni,[57] K. Belotskiy,[97] O. Beltramello,[30] O. Benary,[154] D. Benchekroun,[136a] K. Bendtz,[147a,147b] N. Benekos,[166] Y. Benhammou,[154] E. Benhar Noccioli,[49] J. A. Benitez Garcia,[160b] D. P. Benjamin,[45] J. R. Bensinger,[23] K. Benslama,[131] S. Bentvelsen,[106] D. Berge,[106] E. Bergeaas Kuutmann,[16] N. Berger,[5] F. Berghaus,[170] E. Berglund,[106] J. Beringer,[15] C. Bernard,[22] P. Bernat,[77] C. Bernius,[78] F. U. Bernlochner,[170] T. Berry,[76] P. Berta,[128] C. Bertella,[84] F. Bertolucci,[123a,123b] M. I. Besana,[90a] G. J. Besjes,[105] O. Bessidskaia,[147a,147b] N. Besson,[137] C. Betancourt,[48] S. Bethke,[100] W. Bhimji,[46] R. M. Bianchi,[124] L. Bianchini,[23] M. Bianco,[30] O. Biebel,[99] S. P. Bieniek,[77] K. Bierwagen,[54] J. Biesiada,[15] M. Biglietti,[135a] J. Bilbao De Mendizabal,[49] H. Bilokon,[47] M. Bindi,[54] S. Binet,[116] A. Bingul,[19c] C. Bini,[133a,133b] C. W. Black,[151] J. E. Black,[144] K. M. Black,[22] D. Blackburn,[139] R. E. Blair,[6] J.-B. Blanchard,[137] T. Blazek,[145a] I. Bloch,[42] C. Blocker,[23] W. Blum,[82,a] U. Blumenschein,[54] G. J. Bobbink,[106] V. S. Bobrovnikov,[108] S. S. Bocchetta,[80] A. Bocci,[45] C. R. Boddy,[119] M. Boehler,[48] J. Boek,[176] T. T. Boek,[176] J. A. Bogaerts,[30] A. G. Bogdanchikov,[108] A. Bogouch,[91,a] C. Bohm,[147a] J. Bohm,[126]

V. Boisvert,[76] T. Bold,[38a] V. Boldea,[26a] A. S. Boldyrev,[98] N. M. Bolnet,[137] M. Bomben,[79] M. Bona,[75] M. Boonekamp,[137] A. Borisov,[129] G. Borissov,[71] M. Borri,[83] S. Borroni,[42] J. Bortfeldt,[99] V. Bortolotto,[135a,135b] K. Bos,[106] D. Boscherini,[20a] M. Bosman,[12] H. Boterenbrood,[106] J. Boudreau,[124] J. Bouffard,[2] E. V. Bouhova-Thacker,[71] D. Boumediene,[34] C. Bourdarios,[116] N. Bousson,[113] S. Boutouil,[136d] A. Boveia,[31] J. Boyd,[30] I. R. Boyko,[64] I. Bozovic-Jelisavcic,[13b] J. Bracinik,[18] P. Branchini,[135a] A. Brandt,[8] G. Brandt,[15] O. Brandt,[58a] U. Bratzler,[157] B. Brau,[85] J. E. Brau,[115] H. M. Braun,[176,a] S. F. Brazzale,[165a,165c] B. Brelier,[159] K. Brendlinger,[121] A. J. Brennan,[87] R. Brenner,[167] S. Bressler,[173] K. Bristow,[146c] T. M. Bristow,[46] D. Britton,[53] F. M. Brochu,[28] I. Brock,[21] R. Brock,[89] C. Bromberg,[89] J. Bronner,[100] G. Brooijmans,[35] T. Brooks,[76] W. K. Brooks,[32b] J. Brosamer,[15] E. Brost,[115] G. Brown,[83] J. Brown,[55] P. A. Bruckman de Renstrom,[39] D. Bruncko,[145b] R. Bruneliere,[48] S. Brunet,[60] A. Bruni,[20a] G. Bruni,[20a] M. Bruschi,[20a] L. Bryngemark,[80] T. Buanes,[14] Q. Buat,[143] F. Bucci,[49] P. Buchholz,[142] R. M. Buckingham,[119] A. G. Buckley,[53] S. I. Buda,[26a] I. A. Budagov,[64] F. Buehrer,[48] L. Bugge,[118] M. K. Bugge,[118] O. Bulekov,[97] A. C. Bundock,[73] H. Burckhart,[30] S. Burdin,[73] B. Burghgrave,[107] S. Burke,[130] I. Burmeister,[43] E. Busato,[34] V. Büscher,[82] P. Bussey,[53] C. P. Buszello,[167] B. Butler,[57] J. M. Butler,[22] A. I. Butt,[3] C. M. Buttar,[53] J. M. Butterworth,[77] P. Butti,[106] W. Buttinger,[28] A. Buzatu,[53] M. Byszewski,[10] S. Cabrera Urbán,[168] D. Caforio,[20a,20b] O. Cakir,[4a] P. Calafiura,[15] G. Calderini,[79] P. Calfayan,[99] R. Calkins,[107] L. P. Caloba,[24a] D. Calvet,[34] S. Calvet,[34] R. Camacho Toro,[49] S. Camarda,[42] D. Cameron,[118] L. M. Caminada,[15] R. Caminal Armadans,[12] S. Campana,[30] M. Campanelli,[77] A. Campoverde,[149] V. Canale,[103a,103b] A. Canepa,[160a] J. Cantero,[81] R. Cantrill,[76] T. Cao,[40] M. D. M. Capeans Garrido,[30] I. Caprini,[26a] M. Caprini,[26a] M. Capua,[37a,37b] R. Caputo,[82] R. Cardarelli,[134a] T. Carli,[30] G. Carlino,[103a] L. Carminati,[90a,90b] S. Caron,[105] E. Carquin,[32a] G. D. Carrillo-Montoya,[146c] J. R. Carter,[28] J. Carvalho,[125a,125c] D. Casadei,[77] M. P. Casado,[12] E. Castaneda-Miranda,[146b] A. Castelli,[106] V. Castillo Gimenez,[168] N. F. Castro,[125a] P. Catastini,[57] A. Catinaccio,[30] J. R. Catmore,[71] A. Cattai,[30] G. Cattani,[134a,134b] S. Caughron,[89] V. Cavaliere,[166] D. Cavalli,[90a] M. Cavalli-Sforza,[12] V. Cavasinni,[123a,123b] F. Ceradini,[135a,135b] B. Cerio,[45] K. Cerny,[128] A. S. Cerqueira,[24b] A. Cerri,[150] L. Cerrito,[75] F. Cerutti,[15] M. Cerv,[30] A. Cervelli,[17] S. A. Cetin,[19b] A. Chafaq,[136a] D. Chakraborty,[107] I. Chalupkova,[128] K. Chan,[3] P. Chang,[166] B. Chapleau,[86] J. D. Chapman,[28] D. Charfeddine,[116] D. G. Charlton,[18] C. C. Chau,[159] C. A. Chavez Barajas,[150] S. Cheatham,[86] A. Chegwidden,[89] S. Chekanov,[6] S. V. Chekulaev,[160a] G. A. Chelkov,[64,g] M. A. Chelstowska,[88] C. Chen,[63] H. Chen,[25] K. Chen,[149] L. Chen,[33d,h] S. Chen,[33c] X. Chen,[146c] Y. Chen,[35] H. C. Cheng,[88] Y. Cheng,[31] A. Cheplakov,[64] R. Cherkaoui El Moursli,[136e] V. Chernyatin,[25,a] E. Cheu,[7] L. Chevalier,[137] V. Chiarella,[47] G. Chiefari,[103a,103b] J. T. Childers,[6] A. Chilingarov,[71] G. Chiodini,[72a] A. S. Chisholm,[18] R. T. Chislett,[77] A. Chitan,[26a] M. V. Chizhov,[64] S. Chouridou,[9] B. K. B. Chow,[99] I. A. Christidi,[77] D. Chromek-Burckhart,[30] M. L. Chu,[152] J. Chudoba,[126] L. Chytka,[114] G. Ciapetti,[133a,133b] A. K. Ciftci,[4a] R. Ciftci,[4a] D. Cinca,[62] V. Cindro,[74] A. Ciocio,[15] P. Cirkovic,[13b] Z. H. Citron,[173] M. Citterio,[90a] M. Ciubancan,[26a] A. Clark,[49] P. J. Clark,[46] R. N. Clarke,[15] W. Cleland,[124] J. C. Clemens,[84] B. Clement,[55] C. Clement,[147a,147b] Y. Coadou,[84] M. Cobal,[165a,165c] A. Coccaro,[139] J. Cochran,[63] L. Coffey,[23] J. G. Cogan,[144] J. Coggeshall,[166] B. Cole,[35] S. Cole,[107] A. P. Colijn,[106] C. Collins-Tooth,[53] J. Collot,[55] T. Colombo,[58c] G. Colon,[85] G. Compostella,[100] P. Conde Muiño,[125a,125b] E. Coniavitis,[167] M. C. Conidi,[12] S. H. Connell,[146b] I. A. Connelly,[76] S. M. Consonni,[90a,90b] V. Consorti,[48] S. Constantinescu,[26a] C. Conta,[120a,120b] G. Conti,[57] F. Conventi,[103a,i] M. Cooke,[15] B. D. Cooper,[77] A. M. Cooper-Sarkar,[119] N. J. Cooper-Smith,[76] K. Copic,[15] T. Cornelissen,[176] M. Corradi,[20a] F. Corriveau,[86,j] A. Corso-Radu,[164] A. Cortes-Gonzalez,[12] G. Cortiana,[100] G. Costa,[90a] M. J. Costa,[168] D. Costanzo,[140] D. Côté,[8] G. Cottin,[28] G. Cowan,[76] B. E. Cox,[83] K. Cranmer,[109] G. Cree,[29] S. Crépé-Renaudin,[55] F. Crescioli,[79] M. Crispin Ortuzar,[119] M. Cristinziani,[21] G. Crosetti,[37a,37b] C.-M. Cuciuc,[26a] T. Cuhadar Donszelmann,[140] J. Cummings,[177] M. Curatolo,[47] C. Cuthbert,[151] H. Czirr,[142] P. Czodrowski,[3] Z. Czyczula,[177] S. D'Auria,[53] M. D'Onofrio,[73] M. J. Da Cunha Sargedas De Sousa,[125a,125b] C. Da Via,[83] W. Dabrowski,[38a] A. Dafinca,[119] T. Dai,[88] O. Dale,[14] F. Dallaire,[94] C. Dallapiccola,[85] M. Dam,[36] A. C. Daniells,[18] M. Dano Hoffmann,[137] V. Dao,[105] G. Darbo,[50a] G. L. Darlea,[26c] S. Darmora,[8] J. A. Dassoulas,[42] W. Davey,[21] C. David,[170] T. Davidek,[128] E. Davies,[119,d] M. Davies,[94] O. Davignon,[79] A. R. Davison,[77] P. Davison,[77] Y. Davygora,[58a] E. Dawe,[143] I. Dawson,[140] R. K. Daya-Ishmukhametova,[23] K. De,[8] R. de Asmundis,[103a] S. De Castro,[20a,20b] S. De Cecco,[79] J. de Graat,[99] N. De Groot,[105] P. de Jong,[106] C. De La Taille,[116] H. De la Torre,[81] F. De Lorenzi,[63] L. De Nooij,[106] D. De Pedis,[133a] A. De Salvo,[133a] U. De Sanctis,[165a,165c] A. De Santo,[150] J. B. De Vivie De Regie,[116] G. De Zorzi,[133a,133b] W. J. Dearnaley,[71] R. Debbe,[25] C. Debenedetti,[46] B. Dechenaux,[55] D. V. Dedovich,[64] J. Degenhardt,[121] I. Deigaard,[106] J. Del Peso,[81] T. Del Prete,[123a,123b] F. Deliot,[137] C. M. Delitzsch,[49] M. Deliyergiyev,[74] A. Dell'Acqua,[30] L. Dell'Asta,[22] M. Dell'Orso,[123a,123b] M. Della Pietra,[103a,i] D. della Volpe,[49] M. Delmastro,[5] P. A. Delsart,[55] C. Deluca,[106] S. Demers,[177] M. Demichev,[64] A. Demilly,[79] S. P. Denisov,[129] D. Derendarz,[39]

J. E. Derkaoui,[136d] F. Derue,[79] P. Dervan,[73] K. Desch,[21] C. Deterre,[42] P. O. Deviveiros,[106] A. Dewhurst,[130] S. Dhaliwal,[106] A. Di Ciaccio,[134a,134b] L. Di Ciaccio,[5] A. Di Domenico,[133a,133b] C. Di Donato,[103a,103b] A. Di Girolamo,[30] B. Di Girolamo,[30] A. Di Mattia,[153] B. Di Micco,[135a,135b] R. Di Nardo,[47] A. Di Simone,[48] R. Di Sipio,[20a,20b] D. Di Valentino,[29] M. A. Diaz,[32a] E. B. Diehl,[88] J. Dietrich,[42] T. A. Dietzsch,[58a] S. Diglio,[87] A. Dimitrievska,[13a] J. Dingfelder,[21] C. Dionisi,[133a,133b] P. Dita,[26a] S. Dita,[26a] F. Dittus,[30] F. Djama,[84] T. Djobava,[51b] M. A. B. do Vale,[24c] A. Do Valle Wemans,[125a,125g] T. K. O. Doan,[5] D. Dobos,[30] E. Dobson,[77] C. Doglioni,[49] T. Doherty,[53] T. Dohmae,[156] J. Dolejsi,[128] Z. Dolezal,[128] B. A. Dolgoshein,[97,a] M. Donadelli,[24d] S. Donati,[123a,123b] P. Dondero,[120a,120b] J. Donini,[34] J. Dopke,[30] A. Doria,[103a] M. T. Dova,[70] A. T. Doyle,[53] M. Dris,[10] J. Dubbert,[88] S. Dube,[15] E. Dubreuil,[34] E. Duchovni,[173] G. Duckeck,[99] O. A. Ducu,[26a] D. Duda,[176] A. Dudarev,[30] F. Dudziak,[63] L. Duflot,[116] L. Duguid,[76] M. Dührssen,[30] M. Dunford,[58a] H. Duran Yildiz,[4a] M. Düren,[52] A. Durglishvili,[51b] M. Dwuznik,[38a] M. Dyndal,[38a] J. Ebke,[99] W. Edson,[2] N. C. Edwards,[46] W. Ehrenfeld,[21] T. Eifert,[144] G. Eigen,[14] K. Einsweiler,[15] T. Ekelof,[167] M. El Kacimi,[136c] M. Ellert,[167] S. Elles,[5] F. Ellinghaus,[82] N. Ellis,[30] J. Elmsheuser,[99] M. Elsing,[30] D. Emeliyanov,[130] Y. Enari,[156] O. C. Endner,[82] M. Endo,[117] R. Engelmann,[149] J. Erdmann,[177] A. Ereditato,[17] D. Eriksson,[147a] G. Ernis,[176] J. Ernst,[2] M. Ernst,[25] J. Ernwein,[137] D. Errede,[166] S. Errede,[166] E. Ertel,[82] M. Escalier,[116] H. Esch,[43] C. Escobar,[124] B. Esposito,[47] A. I. Etienvre,[137] E. Etzion,[154] H. Evans,[60] L. Fabbri,[20a,20b] G. Facini,[30] R. M. Fakhrutdinov,[129] S. Falciano,[133a] J. Faltova,[128] Y. Fang,[33a] M. Fanti,[90a,90b] A. Farbin,[8] A. Farilla,[135a] T. Farooque,[12] S. Farrell,[164] S. M. Farrington,[171] P. Farthouat,[30] F. Fassi,[168] P. Fassnacht,[30] D. Fassouliotis,[9] A. Favareto,[50a,50b] L. Fayard,[116] P. Federic,[145a] O. L. Fedin,[122,k] W. Fedorko,[169] M. Fehling-Kaschek,[48] S. Feigl,[30] L. Feligioni,[84] C. Feng,[33d] E. J. Feng,[6] H. Feng,[88] A. B. Fenyuk,[129] S. Fernandez Perez,[30] S. Ferrag,[53] J. Ferrando,[53] V. Ferrara,[42] A. Ferrari,[167] P. Ferrari,[106] R. Ferrari,[120a] D. E. Ferreira de Lima,[53] A. Ferrer,[168] D. Ferrere,[49] C. Ferretti,[88] A. Ferretto Parodi,[50a,50b] M. Fiascaris,[31] F. Fiedler,[82] A. Filipčič,[74] M. Filipuzzi,[42] F. Filthaut,[105] M. Fincke-Keeler,[170] K. D. Finelli,[151] M. C. N. Fiolhais,[125a,125c] L. Fiorini,[168] A. Firan,[40] J. Fischer,[176] M. J. Fisher,[110] W. C. Fisher,[89] E. A. Fitzgerald,[23] M. Flechl,[48] I. Fleck,[142] P. Fleischmann,[175] S. Fleischmann,[176] G. T. Fletcher,[140] G. Fletcher,[75] T. Flick,[176] A. Floderus,[80] L. R. Flores Castillo,[174,l] A. C. Florez Bustos,[160b] M. J. Flowerdew,[100] A. Formica,[137] A. Forti,[83] D. Fortin,[160a] D. Fournier,[116] H. Fox,[71] S. Fracchia,[12] P. Francavilla,[79] M. Franchini,[20a,20b] S. Franchino,[30] D. Francis,[30] M. Franklin,[57] S. Franz,[61] M. Fraternali,[120a,120b] S. T. French,[28] C. Friedrich,[42] F. Friedrich,[44] D. Froidevaux,[30] J. A. Frost,[28] C. Fukunaga,[157] E. Fullana Torregrosa,[82] B. G. Fulsom,[144] J. Fuster,[168] C. Gabaldon,[55] O. Gabizon,[173] A. Gabrielli,[20a,20b] A. Gabrielli,[133a,133b] S. Gadatsch,[106] S. Gadomski,[49] G. Gagliardi,[50a,50b] P. Gagnon,[60] C. Galea,[105] B. Galhardo,[125a,125c] E. J. Gallas,[119] V. Gallo,[17] B. J. Gallop,[130] P. Gallus,[127] G. Galster,[36] K. K. Gan,[110] R. P. Gandrajula,[62] J. Gao,[33b,h] Y. S. Gao,[144,f] F. M. Garay Walls,[46] F. Garberson,[177] C. García,[168] J. E. García Navarro,[168] M. Garcia-Sciveres,[15] R. W. Gardner,[31] N. Garelli,[144] V. Garonne,[30] C. Gatti,[47] G. Gaudio,[120a] B. Gaur,[142] L. Gauthier,[94] P. Gauzzi,[133a,133b] I. L. Gavrilenko,[95] C. Gay,[169] G. Gaycken,[21] E. N. Gazis,[10] P. Ge,[33d] Z. Gecse,[169] C. N. P. Gee,[130] D. A. A. Geerts,[106] Ch. Geich-Gimbel,[21] K. Gellerstedt,[147a,147b] C. Gemme,[50a] A. Gemmell,[53] M. H. Genest,[55] S. Gentile,[133a,133b] M. George,[54] S. George,[76] D. Gerbaudo,[164] A. Gershon,[154] H. Ghazlane,[136b] N. Ghodbane,[34] B. Giacobbe,[20a] S. Giagu,[133a,133b] V. Giangiobbe,[12] P. Giannetti,[123a,123b] F. Gianotti,[30] B. Gibbard,[25] S. M. Gibson,[76] M. Gilchriese,[15] T. P. S. Gillam,[28] D. Gillberg,[30] G. Gilles,[34] D. M. Gingrich,[3,e] N. Giokaris,[9] M. P. Giordani,[165a,165c] R. Giordano,[103a,103b] F. M. Giorgi,[16] P. F. Giraud,[137] D. Giugni,[90a] C. Giuliani,[48] M. Giulini,[58b] B. K. Gjelsten,[118] I. Gkialas,[155,m] L. K. Gladilin,[98] C. Glasman,[81] J. Glatzer,[30] P. C. F. Glaysher,[46] A. Glazov,[42] G. L. Glonti,[64] M. Goblirsch-Kolb,[100] J. R. Goddard,[75] J. Godfrey,[143] J. Godlewski,[30] C. Goeringer,[82] S. Goldfarb,[88] T. Golling,[177] D. Golubkov,[129] A. Gomes,[125a,125b,125d] L. S. Gomez Fajardo,[42] R. Gonçalo,[125a] J. Goncalves Pinto Firmino Da Costa,[42] L. Gonella,[21] S. González de la Hoz,[168] G. Gonzalez Parra,[12] M. L. Gonzalez Silva,[27] S. Gonzalez-Sevilla,[49] L. Goossens,[30] P. A. Gorbounov,[96] H. A. Gordon,[25] I. Gorelov,[104] B. Gorini,[30] E. Gorini,[72a,72b] A. Gorišek,[74] E. Gornicki,[39] A. T. Goshaw,[6] C. Gössling,[43] M. I. Gostkin,[64] M. Gouighri,[136a] D. Goujdami,[136c] M. P. Goulette,[49] A. G. Goussiou,[139] C. Goy,[5] S. Gozpinar,[23] H. M. X. Grabas,[137] L. Graber,[54] I. Grabowska-Bold,[38a] P. Grafström,[20a,20b] K-J. Grahn,[42] J. Gramling,[49] E. Gramstad,[118] F. Grancagnolo,[72a] S. Grancagnolo,[16] V. Grassi,[149] V. Gratchev,[122] H. M. Gray,[30] E. Graziani,[135a] O. G. Grebenyuk,[122] Z. D. Greenwood,[78,n] K. Gregersen,[36] I. M. Gregor,[42] P. Grenier,[144] J. Griffiths,[8] A. A. Grillo,[138] K. Grimm,[71] S. Grinstein,[12,o] Ph. Gris,[34] Y. V. Grishkevich,[98] J.-F. Grivaz,[116] J. P. Grohs,[44] A. Grohsjean,[42] E. Gross,[173] J. Grosse-Knetter,[54] G. C. Grossi,[134a,134b] J. Groth-Jensen,[173] Z. J. Grout,[150] K. Grybel,[142] L. Guan,[33b] F. Guescini,[49] D. Guest,[177] O. Gueta,[154] C. Guicheney,[34] E. Guido,[50a,50b] T. Guillemin,[116] S. Guindon,[2] U. Gul,[53] C. Gumpert,[44] J. Gunther,[127] J. Guo,[35] S. Gupta,[119] P. Gutierrez,[112] N. G. Gutierrez Ortiz,[53] C. Gutschow,[77] N. Guttman,[154] C. Guyot,[137] C. Gwenlan,[119] C. B. Gwilliam,[73] A. Haas,[109]

C. Haber,[15] H. K. Hadavand,[8] N. Haddad,[136e] P. Haefner,[21] S. Hageböck,[21] Z. Hajduk,[39] H. Hakobyan,[178] M. Haleem,[42] D. Hall,[119] G. Halladjian,[89] K. Hamacher,[176] P. Hamal,[114] K. Hamano,[87] M. Hamer,[54] A. Hamilton,[146a] S. Hamilton,[162] P. G. Hamnett,[42] L. Han,[33b] K. Hanagaki,[117] K. Hanawa,[156] M. Hance,[15] P. Hanke,[58a] J. B. Hansen,[36] J. D. Hansen,[36] P. H. Hansen,[36] K. Hara,[161] A. S. Hard,[174] T. Harenberg,[176] S. Harkusha,[91] D. Harper,[88] R. D. Harrington,[46] O. M. Harris,[139] P. F. Harrison,[171] F. Hartjes,[106] S. Hasegawa,[102] Y. Hasegawa,[141] A. Hasib,[112] S. Hassani,[137] S. Haug,[17] M. Hauschild,[30] R. Hauser,[89] M. Havranek,[126] C. M. Hawkes,[18] R. J. Hawkings,[30] A. D. Hawkins,[80] T. Hayashi,[161] D. Hayden,[89] C. P. Hays,[119] H. S. Hayward,[73] S. J. Haywood,[130] S. J. Head,[18] T. Heck,[82] V. Hedberg,[80] L. Heelan,[8] S. Heim,[121] T. Heim,[176] B. Heinemann,[15] L. Heinrich,[109] S. Heisterkamp,[36] J. Hejbal,[126] L. Helary,[22] C. Heller,[99] M. Heller,[30] S. Hellman,[147a,147b] D. Hellmich,[21] C. Helsens,[30] J. Henderson,[119] R. C. W. Henderson,[71] C. Hengler,[42] A. Henrichs,[177] A. M. Henriques Correia,[30] S. Henrot-Versille,[116] C. Hensel,[54] G. H. Herbert,[16] Y. Hernández Jiménez,[168] R. Herrberg-Schubert,[16] G. Herten,[48] R. Hertenberger,[99] L. Hervas,[30] G. G. Hesketh,[77] N. P. Hessey,[106] R. Hickling,[75] E. Higón-Rodriguez,[168] J. C. Hill,[28] K. H. Hiller,[42] S. Hillert,[21] S. J. Hillier,[18] I. Hinchliffe,[15] E. Hines,[121] M. Hirose,[117] D. Hirschbuehl,[176] J. Hobbs,[149] N. Hod,[106] M. C. Hodgkinson,[140] P. Hodgson,[140] A. Hoecker,[30] M. R. Hoeferkamp,[104] J. Hoffman,[40] D. Hoffmann,[84] J. I. Hofmann,[58a] M. Hohlfeld,[82] T. R. Holmes,[15] T. M. Hong,[121] L. Hooft van Huysduynen,[109] J-Y. Hostachy,[55] S. Hou,[152] A. Hoummada,[136a] J. Howard,[119] J. Howarth,[42] M. Hrabovsky,[114] I. Hristova,[16] J. Hrivnac,[116] T. Hryn'ova,[5] P. J. Hsu,[82] S.-C. Hsu,[139] D. Hu,[35] X. Hu,[25] Y. Huang,[42] Z. Hubacek,[30] F. Hubaut,[84] F. Huegging,[21] T. B. Huffman,[119] E. W. Hughes,[35] G. Hughes,[71] M. Huhtinen,[30] T. A. Hülsing,[82] M. Hurwitz,[15] N. Huseynov,[64,c] J. Huston,[89] J. Huth,[57] G. Iacobucci,[49] G. Iakovidis,[10] I. Ibragimov,[142] L. Iconomidou-Fayard,[116] E. Ideal,[177] P. Iengo,[103a] O. Igonkina,[106] T. Iizawa,[172] Y. Ikegami,[65] K. Ikematsu,[142] M. Ikeno,[65] D. Iliadis,[155] N. Ilic,[159] Y. Inamaru,[66] T. Ince,[100] P. Ioannou,[9] M. Iodice,[135a] K. Iordanidou,[9] V. Ippolito,[57] A. Irles Quiles,[168] C. Isaksson,[167] M. Ishino,[67] M. Ishitsuka,[158] R. Ishmukhametov,[110] C. Issever,[119] S. Istin,[19a] J. M. Iturbe Ponce,[83] A. V. Ivashin,[129] W. Iwanski,[39] H. Iwasaki,[65] J. M. Izen,[41] V. Izzo,[103a] B. Jackson,[121] J. N. Jackson,[73] M. Jackson,[73] P. Jackson,[1] M. R. Jaekel,[30] V. Jain,[2] K. Jakobs,[48] S. Jakobsen,[36] T. Jakoubek,[126] J. Jakubek,[127] D. O. Jamin,[152] D. K. Jana,[78] E. Jansen,[77] H. Jansen,[30] J. Janssen,[21] M. Janus,[171] G. Jarlskog,[80] T. Javůrek,[48] L. Jeanty,[15] G.-Y. Jeng,[151] D. Jennens,[87] P. Jenni,[48,p] J. Jentzsch,[43] C. Jeske,[171] S. Jézéquel,[5] H. Ji,[174] W. Ji,[82] J. Jia,[149] Y. Jiang,[33b] M. Jimenez Belenguer,[42] S. Jin,[33a] A. Jinaru,[26a] O. Jinnouchi,[158] M. D. Joergensen,[36] K. E. Johansson,[147a] P. Johansson,[140] K. A. Johns,[7] K. Jon-And,[147a,147b] G. Jones,[171] R. W. L. Jones,[71] T. J. Jones,[73] J. Jongmanns,[58a] P. M. Jorge,[125a,125b] K. D. Joshi,[83] J. Jovicevic,[148] X. Ju,[174] C. A. Jung,[43] R. M. Jungst,[30] P. Jussel,[61] A. Juste Rozas,[12,o] M. Kaci,[168] A. Kaczmarska,[39] M. Kado,[116] H. Kagan,[110] M. Kagan,[144] E. Kajomovitz,[45] S. Kama,[40] N. Kanaya,[156] M. Kaneda,[30] S. Kaneti,[28] T. Kanno,[158] V. A. Kantserov,[97] J. Kanzaki,[65] B. Kaplan,[109] A. Kapliy,[31] D. Kar,[53] K. Karakostas,[10] N. Karastathis,[10] M. Karnevskiy,[82] S. N. Karpov,[64] K. Karthik,[109] V. Kartvelishvili,[71] A. N. Karyukhin,[129] L. Kashif,[174] G. Kasieczka,[58b] R. D. Kass,[110] A. Kastanas,[14] Y. Kataoka,[156] A. Katre,[49] J. Katzy,[42] V. Kaushik,[7] K. Kawagoe,[69] T. Kawamoto,[156] G. Kawamura,[54] S. Kazama,[156] V. F. Kazanin,[108] M. Y. Kazarinov,[64] R. Keeler,[170] R. Kehoe,[40] M. Keil,[54] J. S. Keller,[42] H. Keoshkerian,[5] O. Kepka,[126] B. P. Kerševan,[74] S. Kersten,[176] K. Kessoku,[156] J. Keung,[159] F. Khalil-zada,[11] H. Khandanyan,[147a,147b] A. Khanov,[113] A. Khodinov,[97] A. Khomich,[58a] T. J. Khoo,[28] G. Khoriauli,[21] A. Khoroshilov,[176] V. Khovanskiy,[96] E. Khramov,[64] J. Khubua,[51b] H. Y. Kim,[8] H. Kim,[147a,147b] S. H. Kim,[161] N. Kimura,[172] O. Kind,[16] B. T. King,[73] M. King,[168] R. S. B. King,[119] S. B. King,[169] J. Kirk,[130] A. E. Kiryunin,[100] T. Kishimoto,[66] D. Kisielewska,[38a] F. Kiss,[48] T. Kitamura,[66] T. Kittelmann,[124] K. Kiuchi,[161] E. Kladiva,[145b] M. Klein,[73] U. Klein,[73] K. Kleinknecht,[82] P. Klimek,[147a,147b] A. Klimentov,[25] R. Klingenberg,[43] J. A. Klinger,[83] E. B. Klinkby,[36] T. Klioutchnikova,[30] P. F. Klok,[105] E.-E. Kluge,[58a] P. Kluit,[106] S. Kluth,[100] E. Kneringer,[61] E. B. F. G. Knoops,[84] A. Knue,[53] T. Kobayashi,[156] M. Kobel,[44] M. Kocian,[144] P. Kodys,[128] P. Koevesarki,[21] T. Koffas,[29] E. Koffeman,[106] L. A. Kogan,[119] S. Kohlmann,[176] Z. Kohout,[127] T. Kohriki,[65] T. Koi,[144] H. Kolanoski,[16] I. Koletsou,[5] J. Koll,[89] A. A. Komar,[95,a] Y. Komori,[156] T. Kondo,[65] N. Kondrashova,[42] K. Köneke,[48] A. C. König,[105] S. König,[82] T. Kono,[65,q] R. Konoplich,[109,r] N. Konstantinidis,[77] R. Kopeliansky,[153] S. Koperny,[38a] L. Köpke,[82] A. K. Kopp,[48] K. Korcyl,[39] K. Kordas,[155] A. Korn,[77] A. A. Korol,[108,s] I. Korolkov,[12] E. V. Korolkova,[140] V. A. Korotkov,[129] O. Kortner,[100] S. Kortner,[100] V. V. Kostyukhin,[21] V. M. Kotov,[64] A. Kotwal,[45] C. Kourkoumelis,[9] V. Kouskoura,[155] A. Koutsman,[160a] R. Kowalewski,[170] T. Z. Kowalski,[38a] W. Kozanecki,[137] A. S. Kozhin,[129] V. Kral,[127] V. A. Kramarenko,[98] G. Kramberger,[74] D. Krasnopevtsev,[97] M. W. Krasny,[79] A. Krasznahorkay,[30] J. K. Kraus,[21] A. Kravchenko,[25] S. Kreiss,[109] M. Kretz,[58c] J. Kretzschmar,[73] K. Kreutzfeldt,[52] P. Krieger,[159] K. Kroeninger,[54] H. Kroha,[100] J. Kroll,[121] J. Kroseberg,[21] J. Krstic,[13a] U. Kruchonak,[64] H. Krüger,[21] T. Kruker,[17] N. Krumnack,[63] Z. V. Krumshteyn,[64] A. Kruse,[174] M. C. Kruse,[45] M. Kruskal,[22]

T. Kubota,[87] S. Kuday,[4a] S. Kuehn,[48] A. Kugel,[58c] A. Kuhl,[138] T. Kuhl,[42] V. Kukhtin,[64] Y. Kulchitsky,[91] S. Kuleshov,[32b] M. Kuna,[133a,133b] J. Kunkle,[121] A. Kupco,[126] H. Kurashige,[66] Y. A. Kurochkin,[91] R. Kurumida,[66] V. Kus,[126] E. S. Kuwertz,[148] M. Kuze,[158] J. Kvita,[143] A. La Rosa,[49] L. La Rotonda,[37a,37b] L. Labarga,[81] C. Lacasta,[168] F. Lacava,[133a,133b] J. Lacey,[29] H. Lacker,[16] D. Lacour,[79] V. R. Lacuesta,[168] E. Ladygin,[64] R. Lafaye,[5] B. Laforge,[79] T. Lagouri,[177] S. Lai,[48] H. Laier,[58a] L. Lambourne,[77] S. Lammers,[60] C. L. Lampen,[7] W. Lampl,[7] E. Lançon,[137] U. Landgraf,[48] M. P. J. Landon,[75] V. S. Lang,[58a] C. Lange,[42] A. J. Lankford,[164] F. Lanni,[25] K. Lantzsch,[30] S. Laplace,[79] C. Lapoire,[21] J. F. Laporte,[137] T. Lari,[90a] M. Lassnig,[30] P. Laurelli,[47] V. Lavorini,[37a,37b] W. Lavrijsen,[15] A. T. Law,[138] P. Laycock,[73] B. T. Le,[55] O. Le Dortz,[79] E. Le Guirriec,[84] E. Le Menedeu,[12] T. LeCompte,[6] F. Ledroit-Guillon,[55] C. A. Lee,[152] H. Lee,[106] J. S. H. Lee,[117] S. C. Lee,[152] L. Lee,[177] G. Lefebvre,[79] M. Lefebvre,[170] F. Legger,[99] C. Leggett,[15] A. Lehan,[73] M. Lehmacher,[21] G. Lehmann Miotto,[30] X. Lei,[7] A. G. Leister,[177] M. A. L. Leite,[24d] R. Leitner,[128] D. Lellouch,[173] B. Lemmer,[54] K. J. C. Leney,[77] T. Lenz,[106] G. Lenzen,[176] B. Lenzi,[30] R. Leone,[7] K. Leonhardt,[44] S. Leontsinis,[10] C. Leroy,[94] C. G. Lester,[28] C. M. Lester,[121] J. Levêque,[5] D. Levin,[88] L. J. Levinson,[173] M. Levy,[18] A. Lewis,[119] G. H. Lewis,[109] A. M. Leyko,[21] M. Leyton,[41] B. Li,[33b,t] B. Li,[84] H. Li,[149] H. L. Li,[31] S. Li,[45] X. Li,[88] Y. Li,[33c,u] Z. Liang,[119,v] H. Liao,[34] B. Liberti,[134a] P. Lichard,[30] K. Lie,[166] J. Liebal,[21] W. Liebig,[14] C. Limbach,[21] A. Limosani,[87] M. Limper,[62] S. C. Lin,[152,w] F. Linde,[106] B. E. Lindquist,[149] J. T. Linnemann,[89] E. Lipeles,[121] A. Lipniacka,[14] M. Lisovyi,[42] T. M. Liss,[166] D. Lissauer,[25] A. Lister,[169] A. M. Litke,[138] B. Liu,[152] D. Liu,[152] J. B. Liu,[33b] K. Liu,[33b,x] L. Liu,[88] M. Liu,[45] M. Liu,[33b] Y. Liu,[33b] M. Livan,[120a,120b] S. S. A. Livermore,[119] A. Lleres,[55] J. Llorente Merino,[81] S. L. Lloyd,[75] F. Lo Sterzo,[152] E. Lobodzinska,[42] P. Loch,[7] W. S. Lockman,[138] T. Loddenkoetter,[21] F. K. Loebinger,[83] A. E. Loevschall-Jensen,[36] A. Loginov,[177] C. W. Loh,[169] T. Lohse,[16] K. Lohwasser,[48] M. Lokajicek,[126] V. P. Lombardo,[5] J. D. Long,[88] R. E. Long,[71] L. Lopes,[125a] D. Lopez Mateos,[57] B. Lopez Paredes,[140] J. Lorenz,[99] N. Lorenzo Martinez,[60] M. Losada,[163] P. Loscutoff,[15] X. Lou,[41] A. Lounis,[116] J. Love,[6] P. A. Love,[71] A. J. Lowe,[144,f] F. Lu,[33a] H. J. Lubatti,[139] C. Luci,[133a,133b] A. Lucotte,[55] F. Luehring,[60] W. Lukas,[61] L. Luminari,[133a] O. Lundberg,[147a,147b] B. Lund-Jensen,[148] M. Lungwitz,[82] D. Lynn,[25] R. Lysak,[126] E. Lytken,[80] H. Ma,[25] L. L. Ma,[33d] G. Maccarrone,[47] A. Macchiolo,[100] B. Maček,[74] J. Machado Miguens,[125a,125b] D. Macina,[30] D. Madaffari,[84] R. Madar,[48] H. J. Maddocks,[71] W. F. Mader,[44] A. Madsen,[167] M. Maeno,[8] T. Maeno,[25] E. Magradze,[54] K. Mahboubi,[48] J. Mahlstedt,[106] S. Mahmoud,[73] C. Maiani,[137] C. Maidantchik,[24a] A. Maio,[125a,125b,125d] S. Majewski,[115] Y. Makida,[65] N. Makovec,[116] P. Mal,[137,y] B. Malaescu,[79] Pa. Malecki,[39] V. P. Maleev,[122] F. Malek,[55] U. Mallik,[62] D. Malon,[6] C. Malone,[144] S. Maltezos,[10] V. M. Malyshev,[108] S. Malyukov,[30] J. Mamuzic,[13b] B. Mandelli,[30] L. Mandelli,[90a] I. Mandić,[74] R. Mandrysch,[62] J. Maneira,[125a,125b] A. Manfredini,[100] L. Manhaes de Andrade Filho,[24b] J. A. Manjarres Ramos,[160b] A. Mann,[99] P. M. Manning,[138] A. Manousakis-Katsikakis,[9] B. Mansoulie,[137] R. Mantifel,[86] L. Mapelli,[30] L. March,[168] J. F. Marchand,[29] G. Marchiori,[79] M. Marcisovsky,[126] C. P. Marino,[170] C. N. Marques,[125a] F. Marroquim,[24a] S. P. Marsden,[83] Z. Marshall,[15] L. F. Marti,[17] S. Marti-Garcia,[168] B. Martin,[30] B. Martin,[89] T. A. Martin,[171] V. J. Martin,[46] B. Martin dit Latour,[14] H. Martinez,[137] M. Martinez,[12,o] S. Martin-Haugh,[130] A. C. Martyniuk,[77] M. Marx,[139] F. Marzano,[133a] A. Marzin,[30] L. Masetti,[82] T. Mashimo,[156] R. Mashinistov,[95] J. Masik,[83] A. L. Maslennikov,[108] I. Massa,[20a,20b] N. Massol,[5] P. Mastrandrea,[149] A. Mastroberardino,[37a,37b] T. Masubuchi,[156] H. Matsunaga,[156] T. Matsushita,[66] P. Mättig,[176] S. Mättig,[42] J. Mattmann,[82] J. Maurer,[26a] S. J. Maxfield,[73] D. A. Maximov,[108,s] R. Mazini,[152] L. Mazzaferro,[134a,134b] G. Mc Goldrick,[159] S. P. Mc Kee,[88] A. McCarn,[88] R. L. McCarthy,[149] T. G. McCarthy,[29] N. A. McCubbin,[130] K. W. McFarlane,[56,a] J. A. Mcfayden,[77] G. Mchedlidze,[54] T. Mclaughlan,[18] S. J. McMahon,[130] R. A. McPherson,[170,j] A. Meade,[85] J. Mechnich,[106] M. Medinnis,[42] S. Meehan,[31] R. Meera-Lebbai,[112] S. Mehlhase,[36] A. Mehta,[73] K. Meier,[58a] C. Meineck,[99] B. Meirose,[80] C. Melachrinos,[31] B. R. Mellado Garcia,[146c] F. Meloni,[90a,90b] A. Mengarelli,[20a,20b] S. Menke,[100] E. Meoni,[162] K. M. Mercurio,[57] S. Mergelmeyer,[21] N. Meric,[137] P. Mermod,[49] L. Merola,[103a,103b] C. Meroni,[90a] F. S. Merritt,[31] H. Merritt,[110] A. Messina,[30,z] J. Metcalfe,[25] A. S. Mete,[164] C. Meyer,[82] C. Meyer,[31] J-P. Meyer,[137] J. Meyer,[30] R. P. Middleton,[130] S. Migas,[73] L. Mijović,[137] G. Mikenberg,[173] M. Mikestikova,[126] M. Mikuž,[74] D. W. Miller,[31] C. Mills,[46] A. Milov,[173] D. A. Milstead,[147a,147b] D. Milstein,[173] A. A. Minaenko,[129] M. Miñano Moya,[168] I. A. Minashvili,[64] A. I. Mincer,[109] B. Mindur,[38a] M. Mineev,[64] Y. Ming,[174] L. M. Mir,[12] G. Mirabelli,[133a] T. Mitani,[172] J. Mitrevski,[99] V. A. Mitsou,[168] S. Mitsui,[65] A. Miucci,[49] P. S. Miyagawa,[140] J. U. Mjörnmark,[80] T. Moa,[147a,147b] K. Mochizuki,[84] V. Moeller,[28] S. Mohapatra,[35] W. Mohr,[48] S. Molander,[147a,147b] R. Moles-Valls,[168] K. Mönig,[42] C. Monini,[55] J. Monk,[36] E. Monnier,[84] J. Montejo Berlingen,[12] F. Monticelli,[70] S. Monzani,[133a,133b] R. W. Moore,[3] C. Mora Herrera,[49] A. Moraes,[53] N. Morange,[62] J. Morel,[54] D. Moreno,[82] M. Moreno Llácer,[54] P. Morettini,[50a] M. Morgenstern,[44] M. Morii,[57] S. Moritz,[82] A. K. Morley,[148] G. Mornacchi,[30] J. D. Morris,[75] L. Morvaj,[102] H. G. Moser,[100] M. Mosidze,[51b] J. Moss,[110] R. Mount,[144]

E. Mountricha,[25] S. V. Mouraviev,[95,a] E. J. W. Moyse,[85] S. Muanza,[84] R. D. Mudd,[18] F. Mueller,[58a] J. Mueller,[124] K. Mueller,[21] T. Mueller,[28] T. Mueller,[82] D. Muenstermann,[49] Y. Munwes,[154] J. A. Murillo Quijada,[18] W. J. Murray,[171,130] H. Musheghyan,[54] E. Musto,[153] A. G. Myagkov,[129,aa] M. Myska,[126] O. Nackenhorst,[54] J. Nadal,[54] K. Nagai,[61] R. Nagai,[158] Y. Nagai,[84] K. Nagano,[65] A. Nagarkar,[110] Y. Nagasaka,[59] M. Nagel,[100] A. M. Nairz,[30] Y. Nakahama,[30] K. Nakamura,[65] T. Nakamura,[156] I. Nakano,[111] H. Namasivayam,[41] G. Nanava,[21] R. Narayan,[58b] T. Nattermann,[21] T. Naumann,[42] G. Navarro,[163] R. Nayyar,[7] H. A. Neal,[88] P. Yu. Nechaeva,[95] T. J. Neep,[83] A. Negri,[120a,120b] G. Negri,[30] M. Negrini,[20a] S. Nektarijevic,[49] A. Nelson,[164] T. K. Nelson,[144] S. Nemecek,[126] P. Nemethy,[109] A. A. Nepomuceno,[24a] M. Nessi,[30,bb] M. S. Neubauer,[166] M. Neumann,[176] R. M. Neves,[109] P. Nevski,[25] P. R. Newman,[18] D. H. Nguyen,[6] R. B. Nickerson,[119] R. Nicolaidou,[137] B. Nicquevert,[30] J. Nielsen,[138] N. Nikiforou,[35] A. Nikiforov,[16] V. Nikolaenko,[129,aa] I. Nikolic-Audit,[79] K. Nikolics,[49] K. Nikolopoulos,[18] P. Nilsson,[8] Y. Ninomiya,[156] A. Nisati,[133a] R. Nisius,[100] T. Nobe,[158] L. Nodulman,[6] M. Nomachi,[117] I. Nomidis,[155] S. Norberg,[112] M. Nordberg,[30] S. Nowak,[100] M. Nozaki,[65] L. Nozka,[114] K. Ntekas,[10] G. Nunes Hanninger,[87] T. Nunnemann,[99] E. Nurse,[77] F. Nuti,[87] B. J. O'Brien,[46] F. O'grady,[7] D. C. O'Neil,[143] V. O'Shea,[53] F. G. Oakham,[29,e] H. Oberlack,[100] T. Obermann,[21] J. Ocariz,[79] A. Ochi,[66] M. I. Ochoa,[77] S. Oda,[69] S. Odaka,[65] H. Ogren,[60] A. Oh,[83] S. H. Oh,[45] C. C. Ohm,[30] H. Ohman,[167] T. Ohshima,[102] W. Okamura,[117] H. Okawa,[25] Y. Okumura,[31] T. Okuyama,[156] A. Olariu,[26a] A. G. Olchevski,[64] S. A. Olivares Pino,[46] D. Oliveira Damazio,[25] E. Oliver Garcia,[168] D. Olivito,[121] A. Olszewski,[39] J. Olszowska,[39] A. Onofre,[125a,125e] P. U. E. Onyisi,[31,cc] C. J. Oram,[160a] M. J. Oreglia,[31] Y. Oren,[154] D. Orestano,[135a,135b] N. Orlando,[72a,72b] C. Oropeza Barrera,[53] R. S. Orr,[159] B. Osculati,[50a,50b] R. Ospanov,[121] G. Otero y Garzon,[27] H. Otono,[69] M. Ouchrif,[136d] E. A. Ouellette,[170] F. Ould-Saada,[118] A. Ouraou,[137] K. P. Oussoren,[106] Q. Ouyang,[33a] A. Ovcharova,[15] M. Owen,[83] V. E. Ozcan,[19a] N. Ozturk,[8] K. Pachal,[119] A. Pacheco Pages,[12] C. Padilla Aranda,[12] M. Pagáčová,[48] S. Pagan Griso,[15] E. Paganis,[140] C. Pahl,[100] F. Paige,[25] P. Pais,[85] K. Pajchel,[118] G. Palacino,[160b] S. Palestini,[30] D. Pallin,[34] A. Palma,[125a,125b] J. D. Palmer,[18] Y. B. Pan,[174] E. Panagiotopoulou,[10] J. G. Panduro Vazquez,[76] P. Pani,[106] N. Panikashvili,[88] S. Panitkin,[25] D. Pantea,[26a] L. Paolozzi,[134a,134b] Th. D. Papadopoulou,[10] K. Papageorgiou,[155,m] A. Paramonov,[6] D. Paredes Hernandez,[34] M. A. Parker,[28] F. Parodi,[50a,50b] J. A. Parsons,[35] U. Parzefall,[48] E. Pasqualucci,[133a] S. Passaggio,[50a] A. Passeri,[135a] F. Pastore,[135a,135b,a] Fr. Pastore,[76] G. Pásztor,[49,dd] S. Pataraia,[176] N. D. Patel,[151] J. R. Pater,[83] S. Patricelli,[103a,103b] T. Pauly,[30] J. Pearce,[170] M. Pedersen,[118] S. Pedraza Lopez,[168] R. Pedro,[125a,125b] S. V. Peleganchuk,[108] D. Pelikan,[167] H. Peng,[33b] B. Penning,[31] J. Penwell,[60] D. V. Perepelitsa,[25] E. Perez Codina,[160a] M. T. Pérez García-Estañ,[168] V. Perez Reale,[35] L. Perini,[90a,90b] H. Pernegger,[30] R. Perrino,[72a] R. Peschke,[42] V. D. Peshekhonov,[64] K. Peters,[30] R. F. Y. Peters,[83] B. A. Petersen,[87] J. Petersen,[30] T. C. Petersen,[36] E. Petit,[42] A. Petridis,[147a,147b] C. Petridou,[155] E. Petrolo,[133a] F. Petrucci,[135a,135b] M. Petteni,[143] N. E. Pettersson,[158] R. Pezoa,[32b] P. W. Phillips,[130] G. Piacquadio,[144] E. Pianori,[171] A. Picazio,[49] E. Piccaro,[75] M. Piccinini,[20a,20b] S. M. Piec,[42] R. Piegaia,[27] D. T. Pignotti,[110] J. E. Pilcher,[31] A. D. Pilkington,[77] J. Pina,[125a,125b,125d] M. Pinamonti,[165a,165c,ee] A. Pinder,[119] J. L. Pinfold,[3] A. Pingel,[36] B. Pinto,[125a] S. Pires,[79] C. Pizio,[90a,90b] M.-A. Pleier,[25] V. Pleskot,[128] E. Plotnikova,[64] P. Plucinski,[147a,147b] S. Poddar,[58a] F. Podlyski,[34] R. Poettgen,[82] L. Poggioli,[116] D. Pohl,[21] M. Pohl,[49] G. Polesello,[120a] A. Policicchio,[37a,37b] R. Polifka,[159] A. Polini,[20a] C. S. Pollard,[45] V. Polychronakos,[25] K. Pommès,[30] L. Pontecorvo,[133a] B. G. Pope,[89] G. A. Popeneciu,[26b] D. S. Popovic,[13a] A. Poppleton,[30] X. Portell Bueso,[12] G. E. Pospelov,[100] S. Pospisil,[127] K. Potamianos,[15] I. N. Potrap,[64] C. J. Potter,[150] C. T. Potter,[115] G. Poulard,[30] J. Poveda,[60] V. Pozdnyakov,[64] R. Prabhu,[77] P. Pralavorio,[84] A. Pranko,[15] S. Prasad,[30] R. Pravahan,[8] S. Prell,[63] D. Price,[83] J. Price,[73] L. E. Price,[6] D. Prieur,[124] M. Primavera,[72a] M. Proissl,[46] K. Prokofiev,[47] F. Prokoshin,[32b] E. Protopapadaki,[137] S. Protopopescu,[25] J. Proudfoot,[6] M. Przybycien,[38a] H. Przysiezniak,[5] E. Ptacek,[115] E. Pueschel,[85] D. Puldon,[149] M. Purohit,[25,ff] P. Puzo,[116] Y. Pylypchenko,[62] J. Qian,[88] G. Qin,[53] A. Quadt,[54] D. R. Quarrie,[15] W. B. Quayle,[165a,165b] D. Quilty,[53] A. Qureshi,[160b] V. Radeka,[25] V. Radescu,[42] S. K. Radhakrishnan,[149] P. Radloff,[115] P. Rados,[87] F. Ragusa,[90a,90b] G. Rahal,[179] S. Rajagopalan,[25] M. Rammensee,[30] M. Rammes,[142] A. S. Randle-Conde,[40] C. Rangel-Smith,[79] K. Rao,[164] F. Rauscher,[99] T. C. Rave,[48] T. Ravenscroft,[53] M. Raymond,[30] A. L. Read,[118] D. M. Rebuzzi,[120a,120b] A. Redelbach,[175] G. Redlinger,[25] R. Reece,[138] K. Reeves,[41] L. Rehnisch,[16] A. Reinsch,[115] H. Reisin,[27] M. Relich,[164] C. Rembser,[30] Z. L. Ren,[152] A. Renaud,[116] M. Rescigno,[133a] S. Resconi,[90a] O. L. Rezanova,[108,s] P. Reznicek,[128] R. Rezvani,[94] R. Richter,[100] M. Ridel,[79] P. Rieck,[16] M. Rijssenbeek,[149] A. Rimoldi,[120a,120b] L. Rinaldi,[20a] E. Ritsch,[61] I. Riu,[12] F. Rizatdinova,[113] E. Rizvi,[75] S. H. Robertson,[86,j] A. Robichaud-Veronneau,[119] D. Robinson,[28] J. E. M. Robinson,[83] A. Robson,[53] C. Roda,[123a,123b] L. Rodrigues,[30] S. Roe,[30] O. Røhne,[118] S. Rolli,[162] A. Romaniouk,[97] M. Romano,[20a,20b] G. Romeo,[27] E. Romero Adam,[168] N. Rompotis,[139] L. Roos,[79] E. Ros,[168] S. Rosati,[133a] K. Rosbach,[49] M. Rose,[76] P. L. Rosendahl,[14]

O. Rosenthal,[142] V. Rossetti,[147a,147b] E. Rossi,[103a,103b] L. P. Rossi,[50a] R. Rosten,[139] M. Rotaru,[26a] I. Roth,[173] J. Rothberg,[139] D. Rousseau,[116] C. R. Royon,[137] A. Rozanov,[84] Y. Rozen,[153] X. Ruan,[146c] F. Rubbo,[12] I. Rubinskiy,[42] V. I. Rud,[98] C. Rudolph,[44] M. S. Rudolph,[159] F. Rühr,[48] A. Ruiz-Martinez,[63] Z. Rurikova,[48] N. A. Rusakovich,[64] A. Ruschke,[99] J. P. Rutherfoord,[7] N. Ruthmann,[48] Y. F. Ryabov,[122] M. Rybar,[128] G. Rybkin,[116] N. C. Ryder,[119] A. F. Saavedra,[151] S. Sacerdoti,[27] A. Saddique,[3] I. Sadeh,[154] H. F-W. Sadrozinski,[138] R. Sadykov,[64] F. Safai Tehrani,[133a] H. Sakamoto,[156] Y. Sakurai,[172] G. Salamanna,[75] A. Salamon,[134a] M. Saleem,[112] D. Salek,[106] P. H. Sales De Bruin,[139] D. Salihagic,[100] A. Salnikov,[144] J. Salt,[168] B. M. Salvachua Ferrando,[6] D. Salvatore,[37a,37b] F. Salvatore,[150] A. Salvucci,[105] A. Salzburger,[30] D. Sampsonidis,[155] A. Sanchez,[103a,103b] J. Sánchez,[168] V. Sanchez Martinez,[168] H. Sandaker,[14] H. G. Sander,[82] M. P. Sanders,[99] M. Sandhoff,[176] T. Sandoval,[28] C. Sandoval,[163] R. Sandstroem,[100] D. P. C. Sankey,[130] A. Sansoni,[47] C. Santoni,[34] R. Santonico,[134a,134b] H. Santos,[125a] I. Santoyo Castillo,[150] K. Sapp,[124] A. Sapronov,[64] J. G. Saraiva,[125a,125d] B. Sarrazin,[21] G. Sartisohn,[176] O. Sasaki,[65] Y. Sasaki,[156] G. Sauvage,[5,a] E. Sauvan,[5] P. Savard,[159,e] D. O. Savu,[30] C. Sawyer,[119] L. Sawyer,[78,n] D. H. Saxon,[53] J. Saxon,[121] C. Sbarra,[20a] A. Sbrizzi,[3] T. Scanlon,[30] D. A. Scannicchio,[164] M. Scarcella,[151] J. Schaarschmidt,[173] P. Schacht,[100] D. Schaefer,[121] R. Schaefer,[42] A. Schaelicke,[46] S. Schaepe,[21] S. Schaetzel,[58b] U. Schäfer,[82] A. C. Schaffer,[116] D. Schaile,[99] R. D. Schamberger,[149] V. Scharf,[58a] V. A. Schegelsky,[122] D. Scheirich,[128] M. Schernau,[164] M. I. Scherzer,[35] C. Schiavi,[50a,50b] J. Schieck,[99] C. Schillo,[48] M. Schioppa,[37a,37b] S. Schlenker,[30] E. Schmidt,[48] K. Schmieden,[30] C. Schmitt,[82] C. Schmitt,[99] S. Schmitt,[58b] B. Schneider,[17] Y. J. Schnellbach,[73] U. Schnoor,[44] L. Schoeffel,[137] A. Schoening,[58b] B. D. Schoenrock,[89] A. L. S. Schorlemmer,[54] M. Schott,[82] D. Schouten,[160a] J. Schovancova,[25] S. Schramm,[159] M. Schreyer,[175] C. Schroeder,[82] N. Schuh,[82] M. J. Schultens,[21] H.-C. Schultz-Coulon,[58a] H. Schulz,[16] M. Schumacher,[48] B. A. Schumm,[138] Ph. Schune,[137] A. Schwartzman,[144] Ph. Schwegler,[100] Ph. Schwemling,[137] R. Schwienhorst,[89] J. Schwindling,[137] T. Schwindt,[21] M. Schwoerer,[5] F. G. Sciacca,[17] E. Scifo,[116] G. Sciolla,[23] W. G. Scott,[130] F. Scuri,[123a,123b] F. Scutti,[21] J. Searcy,[88] G. Sedov,[42] E. Sedykh,[122] S. C. Seidel,[104] A. Seiden,[138] F. Seifert,[127] J. M. Seixas,[24a] G. Sekhniaidze,[103a] S. J. Sekula,[40] K. E. Selbach,[46] D. M. Seliverstov,[122,a] G. Sellers,[73] N. Semprini-Cesari,[20a,20b] C. Serfon,[30] L. Serin,[116] L. Serkin,[54] T. Serre,[84] R. Seuster,[160a] H. Severini,[112] F. Sforza,[100] A. Sfyrla,[30] E. Shabalina,[54] M. Shamim,[115] L. Y. Shan,[33a] J. T. Shank,[22] Q. T. Shao,[87] M. Shapiro,[15] P. B. Shatalov,[96] K. Shaw,[165a,165b] P. Sherwood,[77] S. Shimizu,[66] C. O. Shimmin,[164] M. Shimojima,[101] M. Shiyakova,[64] A. Shmeleva,[95] M. J. Shochet,[31] D. Short,[119] S. Shrestha,[63] E. Shulga,[97] M. A. Shupe,[7] S. Shushkevich,[42] P. Sicho,[126] D. Sidorov,[113] A. Sidoti,[133a] F. Siegert,[44] Dj. Sijacki,[13a] O. Silbert,[173] J. Silva,[125a,125d] Y. Silver,[154] D. Silverstein,[144] S. B. Silverstein,[147a] V. Simak,[127] O. Simard,[5] Lj. Simic,[13a] S. Simion,[116] E. Simioni,[82] B. Simmons,[77] R. Simoniello,[90a,90b] M. Simonyan,[36] P. Sinervo,[159] N. B. Sinev,[115] V. Sipica,[142] G. Siragusa,[175] A. Sircar,[78] A. N. Sisakyan,[64,a] S. Yu. Sivoklokov,[98] J. Sjölin,[147a,147b] T. B. Sjursen,[14] L. A. Skinnari,[15] H. P. Skottowe,[57] K. Yu. Skovpen,[108] P. Skubic,[112] M. Slater,[18] T. Slavicek,[127] K. Sliwa,[162] V. Smakhtin,[173] B. H. Smart,[46] L. Smestad,[118] S. Yu. Smirnov,[97] Y. Smirnov,[97] L. N. Smirnova,[98,gg] O. Smirnova,[80] K. M. Smith,[53] M. Smizanska,[71] K. Smolek,[127] A. A. Snesarev,[95] G. Snidero,[75] S. Snyder,[25] R. Sobie,[170,j] F. Socher,[44] A. Soffer,[154] D. A. Soh,[152,v] C. A. Solans,[30] M. Solar,[127] J. Solc,[127] E. Yu. Soldatov,[97] U. Soldevila,[168] E. Solfaroli Camillocci,[133a,133b] A. A. Solodkov,[129] O. V. Solovyanov,[129] V. Solovyev,[122] P. Sommer,[48] H. Y. Song,[33b] N. Soni,[1] A. Sood,[15] B. Sopko,[127] V. Sopko,[127] V. Sorin,[12] M. Sosebee,[8] R. Soualah,[165a,165c] P. Soueid,[94] A. M. Soukharev,[108] D. South,[42] S. Spagnolo,[72a,72b] F. Spanò,[76] W. R. Spearman,[57] R. Spighi,[20a] G. Spigo,[30] M. Spousta,[128] T. Spreitzer,[159] B. Spurlock,[8] R. D. St. Denis,[53] S. Staerz,[44] J. Stahlman,[121] R. Stamen,[58a] E. Stanecka,[39] R. W. Stanek,[6] C. Stanescu,[135a] M. Stanescu-Bellu,[42] M. M. Stanitzki,[42] S. Stapnes,[118] E. A. Starchenko,[129] J. Stark,[55] P. Staroba,[126] P. Starovoitov,[42] R. Staszewski,[39] P. Stavina,[145a,a] G. Steele,[53] P. Steinberg,[25] B. Stelzer,[143] H. J. Stelzer,[30] O. Stelzer-Chilton,[160a] H. Stenzel,[52] S. Stern,[100] G. A. Stewart,[53] J. A. Stillings,[21] M. C. Stockton,[86] M. Stoebe,[86] K. Stoerig,[48] G. Stoicea,[26a] P. Stolte,[54] S. Stonjek,[100] A. R. Stradling,[8] A. Straessner,[44] J. Strandberg,[148] S. Strandberg,[147a,147b] A. Strandlie,[118] E. Strauss,[144] M. Strauss,[112] P. Strizenec,[145b] R. Ströhmer,[175] D. M. Strom,[115] R. Stroynowski,[40] S. A. Stucci,[17] B. Stugu,[14] N. A. Styles,[42] D. Su,[144] J. Su,[124] HS. Subramania,[3] R. Subramaniam,[78] A. Succurro,[12] Y. Sugaya,[117] C. Suhr,[107] M. Suk,[127] V. V. Sulin,[95] S. Sultansoy,[4c] T. Sumida,[67] X. Sun,[33a] J. E. Sundermann,[48] K. Suruliz,[140] G. Susinno,[37a,37b] M. R. Sutton,[150] Y. Suzuki,[65] M. Svatos,[126] S. Swedish,[169] M. Swiatlowski,[144] I. Sykora,[145a] T. Sykora,[128] D. Ta,[89] K. Tackmann,[42] J. Taenzer,[159] A. Taffard,[164] R. Tafirout,[160a] N. Taiblum,[154] Y. Takahashi,[102] H. Takai,[25] R. Takashima,[68] H. Takeda,[66] T. Takeshita,[141] Y. Takubo,[65] M. Talby,[84] A. A. Talyshev,[108,s] J. Y. C. Tam,[175] M. C. Tamsett,[78,hh] K. G. Tan,[87] J. Tanaka,[156] R. Tanaka,[116] S. Tanaka,[132] S. Tanaka,[65] A. J. Tanasijczuk,[143] K. Tani,[66] N. Tannoury,[84] S. Tapprogge,[82] S. Tarem,[153] F. Tarrade,[29] G. F. Tartarelli,[90a] P. Tas,[128] M. Tasevsky,[126] T. Tashiro,[67]

E. Tassi,[37a,37b] A. Tavares Delgado,[125a,125b] Y. Tayalati,[136d] C. Taylor,[77] F. E. Taylor,[93] G. N. Taylor,[87] W. Taylor,[160b] F. A. Teischinger,[30] M. Teixeira Dias Castanheira,[75] P. Teixeira-Dias,[76] K. K. Temming,[48] H. Ten Kate,[30] P. K. Teng,[152] S. Terada,[65] K. Terashi,[156] J. Terron,[81] S. Terzo,[100] M. Testa,[47] R. J. Teuscher,[159,j] J. Therhaag,[21] T. Theveneaux-Pelzer,[34] S. Thoma,[48] J. P. Thomas,[18] J. Thomas-Wilsker,[76] E. N. Thompson,[35] P. D. Thompson,[18] P. D. Thompson,[159] A. S. Thompson,[53] L. A. Thomsen,[36] E. Thomson,[121] M. Thomson,[28] W. M. Thong,[87] R. P. Thun,[88,a] F. Tian,[35] M. J. Tibbetts,[15] V. O. Tikhomirov,[95,ii] Yu. A. Tikhonov,[108,s] S. Timoshenko,[97] E. Tiouchichine,[84] P. Tipton,[177] S. Tisserant,[84] T. Todorov,[5] S. Todorova-Nova,[128] B. Toggerson,[164] J. Tojo,[69] S. Tokár,[145a] K. Tokushuku,[65] K. Tollefson,[89] L. Tomlinson,[83] M. Tomoto,[102] L. Tompkins,[31] K. Toms,[104] N. D. Topilin,[64] E. Torrence,[115] H. Torres,[143] E. Torró Pastor,[168] J. Toth,[84,dd] F. Touchard,[84] D. R. Tovey,[140] H. L. Tran,[116] T. Trefzger,[175] L. Tremblet,[30] A. Tricoli,[30] I. M. Trigger,[160a] S. Trincaz-Duvoid,[79] M. F. Tripiana,[70] N. Triplett,[25] W. Trischuk,[159] B. Trocmé,[55] C. Troncon,[90a] M. Trottier-McDonald,[143] M. Trovatelli,[135a,135b] P. True,[89] M. Trzebinski,[39] A. Trzupek,[39] C. Tsarouchas,[30] J. C-L. Tseng,[119] P. V. Tsiareshka,[91] D. Tsionou,[137] G. Tsipolitis,[10] N. Tsirintanis,[9] S. Tsiskaridze,[12] V. Tsiskaridze,[48] E. G. Tskhadadze,[51a] I. I. Tsukerman,[96] V. Tsulaia,[15] S. Tsuno,[65] D. Tsybychev,[149] A. Tua,[140] A. Tudorache,[26a] V. Tudorache,[26a] A. N. Tuna,[121] S. A. Tupputi,[20a,20b] S. Turchikhin,[98,gg] D. Turecek,[127] I. Turk Cakir,[4d] R. Turra,[90a,90b] P. M. Tuts,[35] A. Tykhonov,[74] M. Tylmad,[147a,147b] M. Tyndel,[130] K. Uchida,[21] I. Ueda,[156] R. Ueno,[29] M. Ughetto,[84] M. Ugland,[14] M. Uhlenbrock,[21] F. Ukegawa,[161] G. Unal,[30] A. Undrus,[25] G. Unel,[164] F. C. Ungaro,[48] Y. Unno,[65] D. Urbaniec,[35] P. Urquijo,[21] G. Usai,[8] A. Usanova,[61] L. Vacavant,[84] V. Vacek,[127] B. Vachon,[86] N. Valencic,[106] S. Valentinetti,[20a,20b] A. Valero,[168] L. Valery,[34] S. Valkar,[128] E. Valladolid Gallego,[168] S. Vallecorsa,[49] J. A. Valls Ferrer,[168] P. C. Van Der Deijl,[106] R. van der Geer,[106] H. van der Graaf,[106] R. Van Der Leeuw,[106] D. van der Ster,[30] N. van Eldik,[30] P. van Gemmeren,[6] J. Van Nieuwkoop,[143] I. van Vulpen,[106] M. C. van Woerden,[30] M. Vanadia,[133a,133b] W. Vandelli,[30] R. Vanguri,[121] A. Vaniachine,[6] P. Vankov,[42] F. Vannucci,[79] G. Vardanyan,[178] R. Vari,[133a] E. W. Varnes,[7] T. Varol,[85] D. Varouchas,[79] A. Vartapetian,[8] K. E. Varvell,[151] F. Vazeille,[34] T. Vazquez Schroeder,[54] J. Veatch,[7] F. Veloso,[125a,125c] S. Veneziano,[133a] A. Ventura,[72a,72b] D. Ventura,[85] M. Venturi,[48] N. Venturi,[159] A. Venturini,[23] V. Vercesi,[120a] M. Verducci,[139] W. Verkerke,[106] J. C. Vermeulen,[106] A. Vest,[44] M. C. Vetterli,[143,e] O. Viazlo,[80] I. Vichou,[166] T. Vickey,[146c,jj] O. E. Vickey Boeriu,[146c] G. H. A. Viehhauser,[119] S. Viel,[169] R. Vigne,[30] M. Villa,[20a,20b] M. Villaplana Perez,[168] E. Vilucchi,[47] M. G. Vincter,[29] V. B. Vinogradov,[64] J. Virzi,[15] O. Vitells,[173] I. Vivarelli,[150] F. Vives Vaque,[3] S. Vlachos,[10] D. Vladoiu,[99] M. Vlasak,[127] A. Vogel,[21] P. Vokac,[127] G. Volpi,[123a,123b] M. Volpi,[87] H. von der Schmitt,[100] H. von Radziewski,[48] E. von Toerne,[21] V. Vorobel,[128] K. Vorobev,[97] M. Vos,[168] R. Voss,[30] J. H. Vossebeld,[73] N. Vranjes,[137] M. Vranjes Milosavljevic,[106] V. Vrba,[126] M. Vreeswijk,[106] T. Vu Anh,[48] R. Vuillermet,[30] I. Vukotic,[31] Z. Vykydal,[127] P. Wagner,[21] W. Wagner,[176] S. Wahrmund,[44] J. Wakabayashi,[102] J. Walder,[71] R. Walker,[99] W. Walkowiak,[142] R. Wall,[177] P. Waller,[73] B. Walsh,[177] C. Wang,[152,kk] C. Wang,[45] F. Wang,[174] H. Wang,[15] H. Wang,[40] J. Wang,[42] J. Wang,[33a] K. Wang,[86] R. Wang,[104] S. M. Wang,[152] T. Wang,[21] X. Wang,[177] A. Warburton,[86] C. P. Ward,[28] D. R. Wardrope,[77] M. Warsinsky,[48] A. Washbrook,[46] C. Wasicki,[42] I. Watanabe,[66] P. M. Watkins,[18] A. T. Watson,[18] I. J. Watson,[151] M. F. Watson,[18] G. Watts,[139] S. Watts,[83] B. M. Waugh,[77] S. Webb,[83] M. S. Weber,[17] S. W. Weber,[175] J. S. Webster,[31] A. R. Weidberg,[119] P. Weigell,[100] B. Weinert,[60] J. Weingarten,[54] C. Weiser,[48] H. Weits,[106] P. S. Wells,[30] T. Wenaus,[25] D. Wendland,[16] Z. Weng,[152,v] T. Wengler,[30] S. Wenig,[30] N. Wermes,[21] M. Werner,[48] P. Werner,[30] M. Wessels,[58a] J. Wetter,[162] K. Whalen,[29] A. White,[8] M. J. White,[1] R. White,[32b] S. White,[123a,123b] D. Whiteson,[164] D. Wicke,[176] F. J. Wickens,[130] W. Wiedenmann,[174] M. Wielers,[130] P. Wienemann,[21] C. Wiglesworth,[36] L. A. M. Wiik-Fuchs,[21] P. A. Wijeratne,[77] A. Wildauer,[100] M. A. Wildt,[42,ll] H. G. Wilkens,[30] J. Z. Will,[99] H. H. Williams,[121] S. Williams,[28] C. Willis,[89] S. Willocq,[85] A. Wilson,[88] J. A. Wilson,[18] I. Wingerter-Seez,[5] S. Winkelmann,[48] F. Winklmeier,[115] M. Wittgen,[144] T. Wittig,[43] J. Wittkowski,[99] S. J. Wollstadt,[82] M. W. Wolter,[39] H. Wolters,[125a,125c] B. K. Wosiek,[39] J. Wotschack,[30] M. J. Woudstra,[83] K. W. Wozniak,[39] M. Wright,[53] M. Wu,[55] S. L. Wu,[174] X. Wu,[49] Y. Wu,[88] E. Wulf,[35] T. R. Wyatt,[83] B. M. Wynne,[46] S. Xella,[36] M. Xiao,[137] D. Xu,[33a] L. Xu,[33b,mm] B. Yabsley,[151] S. Yacoob,[146b,nn] M. Yamada,[65] H. Yamaguchi,[156] Y. Yamaguchi,[156] A. Yamamoto,[65] K. Yamamoto,[63] S. Yamamoto,[156] T. Yamamura,[156] T. Yamanaka,[156] K. Yamauchi,[102] Y. Yamazaki,[66] Z. Yan,[22] H. Yang,[33e] H. Yang,[174] U. K. Yang,[83] Y. Yang,[110] S. Yanush,[92] L. Yao,[33a] W-M. Yao,[15] Y. Yasu,[65] E. Yatsenko,[42] K. H. Yau Wong,[21] J. Ye,[40] S. Ye,[25] A. L. Yen,[57] E. Yildirim,[42] M. Yilmaz,[4b] R. Yoosoofmiya,[124] K. Yorita,[172] R. Yoshida,[6] K. Yoshihara,[156] C. Young,[144] C. J. S. Young,[30] S. Youssef,[22] D. R. Yu,[15] J. Yu,[8] J. M. Yu,[88] J. Yu,[113] L. Yuan,[66] A. Yurkewicz,[107] B. Zabinski,[39] R. Zaidan,[62] A. M. Zaitsev,[129,aa] A. Zaman,[149] S. Zambito,[23] L. Zanello,[133a,133b] D. Zanzi,[100] A. Zaytsev,[25] C. Zeitnitz,[176] M. Zeman,[127] A. Zemla,[38a] K. Zengel,[23] O. Zenin,[129] T. Ženiš,[145a] D. Zerwas,[116] G. Zevi della Porta,[57] D. Zhang,[88] F. Zhang,[174] H. Zhang,[89] J. Zhang,[6]

L. Zhang,[152] X. Zhang,[33d] Z. Zhang,[116] Z. Zhao,[33b] A. Zhemchugov,[64] J. Zhong,[119] B. Zhou,[88] L. Zhou,[35] N. Zhou,[164] C. G. Zhu,[33d] H. Zhu,[33a] J. Zhu,[88] Y. Zhu,[33b] X. Zhuang,[33a] A. Zibell,[99] D. Zieminska,[60] N. I. Zimine,[64] C. Zimmermann,[82] R. Zimmermann,[21] S. Zimmermann,[21] S. Zimmermann,[48] Z. Zinonos,[54] M. Ziolkowski,[142] R. Zitoun,[5] G. Zobernig,[174] A. Zoccoli,[20a,20b] M. zur Nedden,[16] G. Zurzolo,[103a,103b] V. Zutshi[107] and L. Zwalinski[30]

(ATLAS Collaboration)

[1]*Department of Physics, University of Adelaide, Adelaide, Australia*
[2]*Physics Department, SUNY Albany, Albany, New York, USA*
[3]*Department of Physics, University of Alberta, Edmonton, Alberta, Canada*
[4a]*Department of Physics, Ankara University, Ankara, Turkey*
[4b]*Department of Physics, Gazi University, Ankara, Turkey*
[4c]*Division of Physics, TOBB University of Economics and Technology, Ankara, Turkey*
[4d]*Turkish Atomic Energy Authority, Ankara, Turkey*
[5]*LAPP, CNRS/IN2P3 and Université de Savoie, Annecy-le-Vieux, France*
[6]*High Energy Physics Division, Argonne National Laboratory, Argonne, Illinois, USA*
[7]*Department of Physics, University of Arizona, Tucson, Arizona, USA*
[8]*Department of Physics, The University of Texas at Arlington, Arlington, Texas, USA*
[9]*Physics Department, University of Athens, Athens, Greece*
[10]*Physics Department, National Technical University of Athens, Zografou, Greece*
[11]*Institute of Physics, Azerbaijan Academy of Sciences, Baku, Azerbaijan*
[12]*Institut de Física d'Altes Energies and Departament de Física de la Universitat Autònoma de Barcelona, Barcelona, Spain*
[13a]*Institute of Physics, University of Belgrade, Belgrade, Serbia*
[13b]*Vinca Institute of Nuclear Sciences, University of Belgrade, Belgrade, Serbia*
[14]*Department for Physics and Technology, University of Bergen, Bergen, Norway*
[15]*Physics Division, Lawrence Berkeley National Laboratory and University of California, Berkeley, California, USA*
[16]*Department of Physics, Humboldt University, Berlin, Germany*
[17]*Albert Einstein Center for Fundamental Physics and Laboratory for High Energy Physics, University of Bern, Bern, Switzerland*
[18]*School of Physics and Astronomy, University of Birmingham, Birmingham, United Kingdom*
[19a]*Department of Physics, Bogazici University, Istanbul, Turkey*
[19b]*Department of Physics, Dogus University, Istanbul, Turkey*
[19c]*Department of Physics Engineering, Gaziantep University, Gaziantep, Turkey*
[20a]*INFN Sezione di Bologna, Italy*
[20b]*Dipartimento di Fisica e Astronomia, Università di Bologna, Bologna, Italy*
[21]*Physikalisches Institut, University of Bonn, Bonn, Germany*
[22]*Department of Physics, Boston University, Boston MA, USA*
[23]*Department of Physics, Brandeis University, Waltham MA, USA*
[24a]*Universidade Federal do Rio De Janeiro COPPE/EE/IF, Rio de Janeiro, Brazil*
[24b]*Federal University of Juiz de Fora (UFJF), Juiz de Fora, Brazil*
[24c]*Federal University of Sao Joao del Rei (UFSJ), Sao Joao del Rei, Brazil*
[24d]*Instituto de Fisica, Universidade de Sao Paulo, Sao Paulo, Brazil*
[25]*Physics Department, Brookhaven National Laboratory, Upton, New York, USA*
[26a]*National Institute of Physics and Nuclear Engineering, Bucharest, Romania*
[26b]*National Institute for Research and Development of Isotopic and Molecular Technologies, Physics Department, Cluj Napoca, Romania*
[26c]*University Politehnica Bucharest, Bucharest, Romania*
[26d]*West University in Timisoara, Timisoara, Romania*
[27]*Departamento de Física, Universidad de Buenos Aires, Buenos Aires, Argentina*
[28]*Cavendish Laboratory, University of Cambridge, Cambridge, United Kingdom*
[29]*Department of Physics, Carleton University, Ottawa, Ontario, Canada*
[30]*CERN, Geneva, Switzerland*
[31]*Enrico Fermi Institute, University of Chicago, Chicago, Illinois, USA*
[32a]*Departamento de Física, Pontificia Universidad Católica de Chile, Santiago, Chile*
[32b]*Departamento de Física, Universidad Técnica Federico Santa María, Valparaíso, Chile*
[33a]*Institute of High Energy Physics, Chinese Academy of Sciences, Beijing, China*
[33b]*Department of Modern Physics, University of Science and Technology of China, Anhui, China*

[33c]Department of Physics, Nanjing University, Jiangsu, China
[33d]School of Physics, Shandong University, Shandong, China
[33e]Physics Department, Shanghai Jiao Tong University, Shanghai, China
[34]Laboratoire de Physique Corpusculaire, Clermont Université and Université Blaise Pascal and CNRS/IN2P3, Clermont-Ferrand, France
[35]Nevis Laboratory, Columbia University, Irvington, New York, USA
[36]Niels Bohr Institute, University of Copenhagen, Kobenhavn, Denmark
[37a]INFN Gruppo Collegato di Cosenza, Laboratori Nazionali di Frascati, Italy
[37b]Dipartimento di Fisica, Università della Calabria, Rende, Italy
[38a]AGH University of Science and Technology, Faculty of Physics and Applied Computer Science, Krakow, Poland
[38b]Marian Smoluchowski Institute of Physics, Jagiellonian University, Krakow, Poland
[39]The Henryk Niewodniczanski Institute of Nuclear Physics, Polish Academy of Sciences, Krakow, Poland
[40]Physics Department, Southern Methodist University, Dallas, Texas, USA
[41]Physics Department, University of Texas at Dallas, Richardson, Texas, USA
[42]DESY, Hamburg and Zeuthen, Germany
[43]Institut für Experimentelle Physik IV, Technische Universität Dortmund, Dortmund, Germany
[44]Institut für Kern- und Teilchenphysik, Technische Universität Dresden, Dresden, Germany
[45]Department of Physics, Duke University, Durham, North Carolina, USA
[46]SUPA - School of Physics and Astronomy, University of Edinburgh, Edinburgh, United Kingdom
[47]INFN Laboratori Nazionali di Frascati, Frascati, Italy
[48]Fakultät für Mathematik und Physik, Albert-Ludwigs-Universität, Freiburg, Germany
[49]Section de Physique, Université de Genève, Geneva, Switzerland
[50a]INFN Sezione di Genova, Italy
[50b]Dipartimento di Fisica, Università di Genova, Genova, Italy
[51a]E. Andronikashvili Institute of Physics, Iv. Javakhishvili Tbilisi State University, Tbilisi, Georgia
[51b]High Energy Physics Institute, Tbilisi State University, Tbilisi, Georgia
[52]II Physikalisches Institut, Justus-Liebig-Universität Giessen, Giessen, Germany
[53]SUPA - School of Physics and Astronomy, University of Glasgow, Glasgow, United Kingdom
[54]II Physikalisches Institut, Georg-August-Universität, Göttingen, Germany
[55]Laboratoire de Physique Subatomique et de Cosmologie, Université Grenoble-Alpes, CNRS/IN2P3, Grenoble, France
[56]Department of Physics, Hampton University, Hampton, Virginia, USA
[57]Laboratory for Particle Physics and Cosmology, Harvard University, Cambridge, Massachusetts, USA
[58a]Kirchhoff-Institut für Physik, Ruprecht-Karls-Universität Heidelberg, Heidelberg, Germany
[58b]Physikalisches Institut, Ruprecht-Karls-Universität Heidelberg, Heidelberg, Germany
[58c]ZITI Institut für technische Informatik, Ruprecht-Karls-Universität Heidelberg, Mannheim, Germany
[59]Faculty of Applied Information Science, Hiroshima Institute of Technology, Hiroshima, Japan
[60]Department of Physics, Indiana University, Bloomington, Indiana, USA
[61]Institut für Astro- und Teilchenphysik, Leopold-Franzens-Universität, Innsbruck, Austria
[62]University of Iowa, Iowa City, Iowa, USA
[63]Department of Physics and Astronomy, Iowa State University, Ames, Iowa, USA
[64]Joint Institute for Nuclear Research, JINR Dubna, Dubna, Russia
[65]KEK, High Energy Accelerator Research Organization, Tsukuba, Japan
[66]Graduate School of Science, Kobe University, Kobe, Japan
[67]Faculty of Science, Kyoto University, Kyoto, Japan
[68]Kyoto University of Education, Kyoto, Japan
[69]Department of Physics, Kyushu University, Fukuoka, Japan
[70]Instituto de Física La Plata, Universidad Nacional de La Plata and CONICET, La Plata, Argentina
[71]Physics Department, Lancaster University, Lancaster, United Kingdom
[72a]INFN Sezione di Lecce, Italy
[72b]Dipartimento di Matematica e Fisica, Università del Salento, Lecce, Italy
[73]Oliver Lodge Laboratory, University of Liverpool, Liverpool, United Kingdom
[74]Department of Physics, Jožef Stefan Institute and University of Ljubljana, Ljubljana, Slovenia
[75]School of Physics and Astronomy, Queen Mary University of London, London, United Kingdom
[76]Department of Physics, Royal Holloway University of London, Surrey, United Kingdom
[77]Department of Physics and Astronomy, University College London, London, United Kingdom
[78]Louisiana Tech University, Ruston, Louisiana, USA
[79]Laboratoire de Physique Nucléaire et de Hautes Energies, UPMC and Université Paris-Diderot and CNRS/IN2P3, Paris, France

[80]*Fysiska institutionen, Lunds universitet, Lund, Sweden*
[81]*Departamento de Fisica Teorica C-15, Universidad Autonoma de Madrid, Madrid, Spain*
[82]*Institut für Physik, Universität Mainz, Mainz, Germany*
[83]*School of Physics and Astronomy, University of Manchester, Manchester, United Kingdom*
[84]*CPPM, Aix-Marseille Université and CNRS/IN2P3, Marseille, France*
[85]*Department of Physics, University of Massachusetts, Amherst, Massachusetts, USA*
[86]*Department of Physics, McGill University, Montreal, Quebec, Canada*
[87]*School of Physics, University of Melbourne, Victoria, Australia*
[88]*Department of Physics, The University of Michigan, Ann Arbor, Michigan, USA*
[89]*Department of Physics and Astronomy, Michigan State University, East Lansing, Michigan, USA*
[90a]*INFN Sezione di Milano, Italy*
[90b]*Dipartimento di Fisica, Università di Milano, Milano, Italy*
[91]*B.I. Stepanov Institute of Physics, National Academy of Sciences of Belarus, Minsk, Republic of Belarus*
[92]*National Scientific and Educational Centre for Particle and High Energy Physics, Minsk, Republic of Belarus*
[93]*Department of Physics, Massachusetts Institute of Technology, Cambridge, Massachusetts, USA*
[94]*Group of Particle Physics, University of Montreal, Montreal, Quebec, Canada*
[95]*P.N. Lebedev Institute of Physics, Academy of Sciences, Moscow, Russia*
[96]*Institute for Theoretical and Experimental Physics (ITEP), Moscow, Russia*
[97]*Moscow Engineering and Physics Institute (MEPhI), Moscow, Russia*
[98]*D.V.Skobeltsyn Institute of Nuclear Physics, M.V. Lomonosov Moscow State University, Moscow, Russia*
[99]*Fakultät für Physik, Ludwig-Maximilians-Universität München, München, Germany*
[100]*Max-Planck-Institut für Physik (Werner-Heisenberg-Institut), München, Germany*
[101]*Nagasaki Institute of Applied Science, Nagasaki, Japan*
[102]*Graduate School of Science and Kobayashi-Maskawa Institute, Nagoya University, Nagoya, Japan*
[103a]*INFN Sezione di Napoli, Italy*
[103b]*Dipartimento di Fisica, Università di Napoli, Napoli, Italy*
[104]*Department of Physics and Astronomy, University of New Mexico, Albuquerque, New Mexico, USA*
[105]*Institute for Mathematics, Astrophysics and Particle Physics, Radboud University Nijmegen/Nikhef, Nijmegen, Netherlands*
[106]*Nikhef National Institute for Subatomic Physics and University of Amsterdam, Amsterdam, Netherlands*
[107]*Department of Physics, Northern Illinois University, DeKalb, Illinois, USA*
[108]*Budker Institute of Nuclear Physics, SB RAS, Novosibirsk, Russia*
[109]*Department of Physics, New York University, New York, New York, USA*
[110]*The Ohio State University, Columbus, Ohio, USA*
[111]*Faculty of Science, Okayama University, Okayama, Japan*
[112]*Homer L. Dodge Department of Physics and Astronomy, University of Oklahoma, Norman, Oklahoma, USA*
[113]*Department of Physics, Oklahoma State University, Stillwater, Oklahoma, USA*
[114]*Palacký University, RCPTM, Olomouc, Czech Republic*
[115]*Center for High Energy Physics, University of Oregon, Eugene, Oregon, USA*
[116]*LAL, Université Paris-Sud and CNRS/IN2P3, Orsay, France*
[117]*Graduate School of Science, Osaka University, Osaka, Japan*
[118]*Department of Physics, University of Oslo, Oslo, Norway*
[119]*Department of Physics, Oxford University, Oxford, United Kingdom*
[120a]*INFN Sezione di Pavia, Italy*
[120b]*Dipartimento di Fisica, Università di Pavia, Pavia, Italy*
[121]*Department of Physics, University of Pennsylvania, Philadelphia, Pennsylvania, USA*
[122]*Petersburg Nuclear Physics Institute, Gatchina, Russia*
[123a]*INFN Sezione di Pisa, Italy*
[123b]*Dipartimento di Fisica E. Fermi, Università di Pisa, Pisa, Italy*
[124]*Department of Physics and Astronomy, University of Pittsburgh, Pittsburgh, Pennsylvania, USA*
[125a]*Laboratorio de Instrumentacao e Fisica Experimental de Particulas - LIP, Lisboa, Portugal*
[125b]*Faculdade de Ciências, Universidade de Lisboa, Lisboa, Portugal*
[125c]*Department of Physics, University of Coimbra, Coimbra, Portugal*
[125d]*Centro de Física Nuclear da Universidade de Lisboa, Lisboa, Portugal*
[125e]*Departamento de Fisica, Universidade do Minho, Braga, Portugal*
[125f]*Departamento de Fisica Teorica y del Cosmos and CAFPE, Universidad de Granada, Granada, Portugal*

[125g]*Dep Fisica and CEFITEC of Faculdade de Ciencias e Tecnologia, Universidade Nova de Lisboa, Caparica, Portugal*
[126]*Institute of Physics, Academy of Sciences of the Czech Republic, Praha, Czech Republic*
[127]*Czech Technical University in Prague, Praha, Czech Republic*
[128]*Faculty of Mathematics and Physics, Charles University in Prague, Praha, Czech Republic*
[129]*State Research Center Institute for High Energy Physics, Protvino, Russia*
[130]*Particle Physics Department, Rutherford Appleton Laboratory, Didcot, United Kingdom*
[131]*Physics Department, University of Regina, Regina, Saskatchewan, Canada*
[132]*Ritsumeikan University, Kusatsu, Shiga, Japan*
[133a]*INFN Sezione di Roma, Italy*
[133b]*Dipartimento di Fisica, Sapienza Università di Roma, Roma, Italy*
[134a]*INFN Sezione di Roma Tor Vergata, Italy*
[134b]*Dipartimento di Fisica, Università di Roma Tor Vergata, Roma, Italy*
[135a]*INFN Sezione di Roma Tre, Italy*
[135b]*Dipartimento di Matematica e Fisica, Università Roma Tre, Roma, Italy*
[136a]*Faculté des Sciences Ain Chock, Réseau Universitaire de Physique des Hautes Energies - Université Hassan II, Casablanca, Morocco*
[136b]*Centre National de l'Energie des Sciences Techniques Nucleaires, Rabat, Morocco*
[136c]*Faculté des Sciences Semlalia, Université Cadi Ayyad, LPHEA-Marrakech, Morocco*
[136d]*Faculté des Sciences, Université Mohamed Premier and LPTPM, Oujda, Morocco*
[136e]*Faculté des sciences, Université Mohammed V-Agdal, Rabat, Morocco*
[137]*DSM/IRFU (Institut de Recherches sur les Lois Fondamentales de l'Univers), CEA Saclay (Commissariat à l'Energie Atomique et aux Energies Alternatives), Gif-sur-Yvette, France*
[138]*Santa Cruz Institute for Particle Physics, University of California Santa Cruz, Santa Cruz, California, USA*
[139]*Department of Physics, University of Washington, Seattle, Washington, USA*
[140]*Department of Physics and Astronomy, University of Sheffield, Sheffield, United Kingdom*
[141]*Department of Physics, Shinshu University, Nagano, Japan*
[142]*Fachbereich Physik, Universität Siegen, Siegen, Germany*
[143]*Department of Physics, Simon Fraser University, Burnaby, British Columbia, Canada*
[144]*SLAC National Accelerator Laboratory, Stanford, California, USA*
[145a]*Faculty of Mathematics, Physics & Informatics, Comenius University, Bratislava, Slovak Republic*
[145b]*Department of Subnuclear Physics, Institute of Experimental Physics of the Slovak Academy of Sciences, Kosice, Slovak Republic*
[146a]*Department of Physics, University of Cape Town, Cape Town, South Africa*
[146b]*Department of Physics, University of Johannesburg, Johannesburg, South Africa*
[146c]*School of Physics, University of the Witwatersrand, Johannesburg, South Africa*
[147a]*Department of Physics, Stockholm University, Sweden*
[147b]*The Oskar Klein Centre, Stockholm, Sweden*
[148]*Physics Department, Royal Institute of Technology, Stockholm, Sweden*
[149]*Departments of Physics & Astronomy and Chemistry, Stony Brook University, Stony Brook, New York, USA*
[150]*Department of Physics and Astronomy, University of Sussex, Brighton, United Kingdom*
[151]*School of Physics, University of Sydney, Sydney, Australia*
[152]*Institute of Physics, Academia Sinica, Taipei, Taiwan*
[153]*Department of Physics, Technion: Israel Institute of Technology, Haifa, Israel*
[154]*Raymond and Beverly Sackler School of Physics and Astronomy, Tel Aviv University, Tel Aviv, Israel*
[155]*Department of Physics, Aristotle University of Thessaloniki, Thessaloniki, Greece*
[156]*International Center for Elementary Particle Physics and Department of Physics, The University of Tokyo, Tokyo, Japan*
[157]*Graduate School of Science and Technology, Tokyo Metropolitan University, Tokyo, Japan*
[158]*Department of Physics, Tokyo Institute of Technology, Tokyo, Japan*
[159]*Department of Physics, University of Toronto, Toronto, Ontario, Canada*
[160a]*TRIUMF, Vancouver, British Columbia, Canada*
[160b]*Department of Physics and Astronomy, York University, Toronto, Ontario, Canada*
[161]*Faculty of Pure and Applied Sciences, University of Tsukuba, Tsukuba, Japan*
[162]*Department of Physics and Astronomy, Tufts University, Medford, Massachusetts, USA*
[163]*Centro de Investigaciones, Universidad Antonio Narino, Bogota, Colombia*
[164]*Department of Physics and Astronomy, University of California Irvine, Irvine, California, USA*
[165a]*INFN Gruppo Collegato di Udine, Sezione di Trieste, Udine, Italy*
[165b]*ICTP, Trieste, Italy*

[165c]*Dipartimento di Chimica, Fisica e Ambiente, Università di Udine, Udine, Italy*
[166]*Department of Physics, University of Illinois, Urbana, Illinois, USA*
[167]*Department of Physics and Astronomy, University of Uppsala, Uppsala, Sweden*
[168]*Instituto de Física Corpuscular (IFIC) and Departamento de Física Atómica, Molecular y Nuclear and Departamento de Ingeniería Electrónica and Instituto de Microelectrónica de Barcelona (IMB-CNM), University of Valencia and CSIC, Valencia, Spain*
[169]*Department of Physics, University of British Columbia, Vancouver, British Columbia, Canada*
[170]*Department of Physics and Astronomy, University of Victoria, Victoria, British Columbia, Canada*
[171]*Department of Physics, University of Warwick, Coventry, United Kingdom*
[172]*Waseda University, Tokyo, Japan*
[173]*Department of Particle Physics, The Weizmann Institute of Science, Rehovot, Israel*
[174]*Department of Physics, University of Wisconsin, Madison, Wisconsin, USA*
[175]*Fakultät für Physik und Astronomie, Julius-Maximilians-Universität, Würzburg, Germany*
[176]*Fachbereich C Physik, Bergische Universität Wuppertal, Wuppertal, Germany*
[177]*Department of Physics, Yale University, New Haven, Connecticut, USA*
[178]*Yerevan Physics Institute, Yerevan, Armenia*
[179]*Centre de Calcul de l'Institut National de Physique Nucléaire et de Physique des Particules (IN2P3), Villeurbanne, France*

[a]Deceased.
[b]Also at Department of Physics, King's College London, London, United Kingdom.
[c]Also at Institute of Physics, Azerbaijan Academy of Sciences, Baku, Azerbaijan.
[d]Also at Particle Physics Department, Rutherford Appleton Laboratory, Didcot, United Kingdom.
[e]Also at TRIUMF, Vancouver, British Columbia, Canada.
[f]Also at Department of Physics, California State University, Fresno, CA, USA.
[g]Also at Tomsk State University, Tomsk, Russia.
[h]Also at CPPM, Aix-Marseille Université and CNRS/IN2P3, Marseille, France.
[i]Also at Università di Napoli Parthenope, Napoli, Italy.
[j]Also at Institute of Particle Physics (IPP), Canada.
[k]Also at Department of Physics, St. Petersburg State Polytechnical University, St. Petersburg, Russia.
[l]Also at Chinese University of Hong Kong, China.
[m]Also at Department of Financial and Management Engineering, University of the Aegean, Chios, Greece.
[n]Also at Louisiana Tech University, Ruston, LA, USA.
[o]Also at Institucio Catalana de Recerca i Estudis Avancats, ICREA, Barcelona, Spain.
[p]Also at CERN, Geneva, Switzerland.
[q]Also at Ochadai Academic Production, Ochanomizu University, Tokyo, Japan.
[r]Also at Manhattan College, New York, NY, USA.
[s]Also at Novosibirsk State University, Novosibirsk, Russia.
[t]Also at Institute of Physics, Academia Sinica, Taipei, Taiwan.
[u]Also at LAL, Université Paris-Sud and CNRS/IN2P3, Orsay, France.
[v]Also at School of Physics and Engineering, Sun Yat-sen University, Guangzhou, China.
[w]Also at Academia Sinica Grid Computing, Institute of Physics, Academia Sinica, Taipei, Taiwan.
[x]Also at Laboratoire de Physique Nucléaire et de Hautes Energies, UPMC and Université Paris-Diderot and CNRS/IN2P3, Paris, France.
[y]Also at School of Physical Sciences, National Institute of Science Education and Research, Bhubaneswar, India.
[z]Also at Dipartimento di Fisica, Sapienza Università di Roma, Roma, Italy.
[aa]Also at Moscow Institute of Physics and Technology State University, Dolgoprudny, Russia.
[bb]Also at Section de Physique, Université de Genève, Geneva, Switzerland.
[cc]Also at Department of Physics, The University of Texas at Austin, Austin, TX, USA.
[dd]Also at Institute for Particle and Nuclear Physics, Wigner Research Centre for Physics, Budapest, Hungary.
[ee]Also at International School for Advanced Studies (SISSA), Trieste, Italy.
[ff]Also at Department of Physics and Astronomy, University of South Carolina, Columbia SC, USA.
[gg]Also at Faculty of Physics, M. V. Lomonosov Moscow State University, Moscow, Russia.
[hh]Also at Physics Department, Brookhaven National Laboratory, Upton, NY, USA.
[ii]Also at Moscow Engineering and Physics Institute (MEPhI), Moscow, Russia.
[jj]Also at Department of Physics, Oxford University, Oxford, United Kingdom.
[kk]Also at Department of Physics, Nanjing University, Jiangsu, China.
[ll]Also at Institut für Experimentalphysik, Universität Hamburg, Hamburg, Germany.
[mm]Also at Department of Physics, The University of Michigan, Ann Arbor, MI, USA.
[nn]Also at Discipline of Physics, University of KwaZulu-Natal, Durban, South Africa.